A NEW WIDEBAND, FULLY STEERABLE, DECAMETRIC ARRAY AT CLARK LAKE

William C. Erickson and J. Richard Fisher*

CLARK LAKE RADIO OBSERVATORY

ASTRONOMY PROGRAM

UNIVERSITY OF MARYLAND

COLLEGE PARK, MARYLAND

Clark Lake Radio Observatory is owned and operated by the University of Maryland. Correspondence relating to the observatory should be addressed to

Clark Lake Radio Observatory
Post Office Box
Borrego Springs, Calif. 92004

Requests for reprints, preprints, and data should be sent to

Clark Lake Radio Observatory
Astronomy Program
University of Maryland
College Park, Md. 20742

The Astronomy Program would appreciate receiving preprints and reprints related to Astronomy.

A NEW WIDEBAND, FULLY STEERABLE, DECAMETRIC ARRAY AT CLARK LAKE

William C. Erickson and J. Richard Fisher*

Astronomy Program
University of Maryland. College Park, Maryland 20742

Received _____

* Present address: National Radio Astronomy Observatory, Green Bank, West Virginia 24944.

A NEW WIDEBAND, FULLY STEERABLE, DECAMETRIC ARRAY AT CLARK LAKE

William C. Erickson and J. Richard Fisher*
Astronomy Program
University of Maryland, College Park, Maryland 20742

ABSTRACT

A new, fully steerable, decametric array for radio astronomy is under construction at the Clark Lake Radio Observatory near Borrego Springs, California. This array will be a "T" of 720 conical spiral antennas (teepee-shaped antennas, hence the array is called the TPT), 3.0 km by 1.8 km capable of operating between 15 and 125 MHz. Both its operating frequency and beam position will be adjustable in less than one millisecond, and the TPT will provide a 49-element picture around the central beam position for extended-source observations.

Considerable experience has been gained in the operation of completed portions of the array, and successful operation of the final array is assured. This paper describes the results of the tests which have been conducted with the conical spirals and outlines the planned electronics and data processing system.

---

* Present address: National Radio Astronomy Observatory, Green Bank, West Virginia 24944

Introduction

Most of the radio astronomical observations below 100 MHz have been the result of considerable effort on the part of a relatively small number of astronomers and engineers. The size of the instruments required has precluded the construction of more than a few in the world, and, until three or four years ago, technology had not allowed the design of a large decametric array which would operate over more than a limited frequency range and be steerable in two coordinates with reasonable speed. Consequently, this part of the radio spectrum has attracted very few astronomers even though much information about the physics of celestial objects may be found from the study of radiation at these wavelengths.

Recent advances have been made in the technology of decade bandwidth antennas (Rumsey, 1966), and reliable wideband, solid state devices have reached a price where it is practical to use hundreds or thousands of units in a large system. Around these developments, a design for a fully steerable decametric array has evolved. It is operable anywhere between 15 and 125 MHz with nearly instantaneous frequency and beam positioning capability.

The instrument has been designed with both solar and sidereal programs in mind. The spacing of the phase centers of the banks of elements has been arranged to provide a "field of view" clear of grating responses which is several solar diameters across. One of the first uses of the instrument will be as a multifrequency radioheliograph, similar to the Culgoora instrument. The system has most of the flexibility of a huge paraboloidal antenna, but has a number of advantages and disadvantages. First of all, its resolving power is approximately that of a 3 km paraboloid. The ability to slew rapidly and to change frequency rapidly permit many modes of operation that are

impossible with paraboloids. On the other hand, the collecting area of the unfilled aperture is less than 1% that of a 3 km paraboloid, so the system is most useful for programs where high angular resolution and only modest sensitivity are required.

The system is adaptable to the study of dynamic sources such as the sun, Jupiter, or pulsars for it can be used in an adaptive sense with priority given to dynamic sources whenever they are active. The beam can be stepped around the sky to monitor the sun, flare stars, planets, or ionospheric scintillations. Spectral observations can be made on many thousands of sidereal radio sources. Sources can be followed across the sky and observed successively at different frequencies for spectral measurements. Observations of calibration sources can be interspresed with observations of unknown sources on a second-to-second basis. At our sensitivity level, lunar occultations of radio sources will occur every few hours.

The instrument, called the TPT because of its geometry and antenna design, is a "T" of 720 conical spiral antennas under construction at the University of Maryland's Clark Lake Radio Observatory near Borrego Springs, California. Elements of the array have been in operation for about 3 years for test purposes and for some limited observations. Experience gained with portions of the array assures the success of the design and allows some definitive statements to be made about the properties of the individual elements and the overall phasing scheme. It is the purpose of this paper to describe the system, to outline the measured parameters of the conical spirals, and to compare the calculated and observed array patterns with particular emphasis on an incremental phasing scheme not normally employed in radio astronomical instruments. The sidelobe structure of the system is complex and affects

the confusion limit of the system as estimated in Paper II (Fisher, 1973). A brief description of the proposed electronics is included to give a coherent picture of the final instrument.

Outline of Array and Electronics

The new array is a 3.0 x 1.8 km "T" with the direction of its legs being approximately east, west and south. The array is laid out in the plane of the Clark's Dry Lake which is not exactly tangential to the geoid. The south arm, which is perpendicular to the east-west arms. has been laid out 18 arc-seconds from the plane containing the earth's axis and the center of the array. The array's effective coordinates become Lat. 33°20'29", Long. 116°17'25". The signals from each arm are combined to form 7 fan beams and the E-W fan beam signals are multiplied by the N-S fan beam signals to produce pencil beams with the approximate resolution of a 3 km dish. The beam shape is equivalent to that obtained with a full cross but the collecting area of the fourth arm is lost with the "T". Phase tolerances between the orthogonal arms are more critical in the "T" array than in a full cross (Christiansen and Högbom, 1969).

The TPT consists of 720 conical log spirals (teepees). Each has a collecting area of about $\lambda^2/3$, and is designed to operate between 20 and 125 MHz. The low frequency limit has been extended to 15 MHz at reduced efficiency by terminating the base of the spiral with resistors. The teepees are fixed in a vertical direction at 6.25 meter intervals in the east-west arms and 7.5 meter intervals in the south arm. This spacing gives rise to grating responses above 50 MHz which will be discussed in a later section. Since the elements are fixed, beam positioning is accomplished purely through adjustment of the phase gradient across each arm. The gain of the system is modulated by the response pattern of the individual elements. For good zenith distance coverage, the

response pattern must be wide, and the gain of each element is correspondingly low.

As shown in Figures 1 and 2, phasing of the array is accomplished in two stages. The elements are divided into 48 banks of 15, and the signals from the 15 antennas in each bank are combined, then pre-amplified and sent to the central building on separate coaxial feed lines. Phasing within a bank is accomplished by electronically "rotating" each conical spiral antenna with a diode switch controlled from the central building.

The signals from the 48 banks are processed separately, in carefully matched amplifiers and digital networks. Figures 3 and 4 are block diagrams of the proposed electronics. The slope filter ahead of the postamplifier is a high pass filter with a cutoff of 100 MHz and is designed to approximately compensate for increase of sky noise and decrease of cable attenuation with decreasing frequency. It also reduces the dynamic range requirements on the following electronics particularly with respect to the strong man-made interference below 30 MHz. The remaining R.F. and I.F. components are relatively straightforward. Each R.F. signal goes through two frequency conversions. It is first converted up to an intermediate frequency (I.F.) of 170 MHz to provide good image rejection. Then the signal is converted to 10 MHz where bandwidths between 0.1 and 3 MHz can be selected. The first local oscillator (L.O.) is variable from 185 to 295 MHz to select the appropriate operating frequency. The second L.O. is fixed in frequency at 160 MHz.

The high-level outputs of the 10 MHz I.F. amplifiers are digitized in 2-bit levels and delayed in random access memories. All of the real-time delays are controlled by the memory combinations. Phase adjustment between the channels is accomplished by appropriate bit permutations.

Finally, the digital signals are converted to analog levels and combined in resistor networks to form 7 east-west and 7 north-south fan beams. All fan beams are cross-correlated to form 49 picture elements around the primary direction for which the array is phased.

The instruments specifications and capabilities are listed in Table 1.

For comparison, the total collecting area of the elements in this array is equivalent to the geometrical area of a 50-meter (165 ft.) dish at 100 MHz and a 250-meter (800 ft.) dish at 20 MHz. The conical spiral has a constant gain with respect to an isotropic radiator so its collecting area varies as the wavelength squared. At 80 MHz the total collecting area is half that of the Culgoora array. The resolution values given in Table 1 are approximate and depend on taper and digital processing of the correlated output and on the zenith distance of the observed sources.

Single Element Construction and Operation

The basic building block of the array is the conical log spiral antenna. Ideally this antenna would consist of two conducting sheets wound on the surface of a cone as shown in Figure 5. It is a self-conjugate antenna with a characteristic impedance of 189Ω and is fed by a balanced transmission line at its apex.

The electrical and radiative properties of this antenna are as follows: First, the low-frequency limit of the antenna is determined by the size of the base of the spiral (circumference $\approx \lambda_{lim}$, diameter $\approx \lambda_{lim}/\pi$), and the high frequency limit is set by the point at which the top of the spiral is truncated and the accuracy with which it is wound. The low-frequency limit of the antenna is extended by terminating the base of the spiral with a resistive load.

Power that would ordinarily be reflected from the base of the antenna is dissipated in the load, and the same impedance at the antenna terminals is then maintained to very low frequencies. At frequencies where $\lambda > \lambda_{lim}$ some of the power on the antenna is lost in the resistive loads before it can be launched into space. Therefore the limit on the operating frequency is set by the loss of efficiency one can tolerate. In principle, at least, the radiation pattern and the circularity of the polarization should not change at lower frequencies.

Second, the antenna is unidirectional toward the apex and the polarization is in the opposite sense from the opening direction of the spiral, i.e. a right hand (clockwise) opening spiral as viewed from the top radiates predominately a left circular wave. The far field radiation pattern is determined by the apex angle of the cone and the pitch angle of the conductors. Considerably more detail may be obtained from other sources (Rumsey, 1966; Dyson, 1965; Yeh and Mei, 1967-68).

In actual practice the use of conducting sheets is very difficult because of cost and wind resistance for large antennas. A good approximation to a conducting sheet can be made by using three wires, one at the location of each edge of the conductor and one in the center. Thus the elements in this array use six coaxially wound spiral wires; three connected to each side of the transmission line.

Each element in the array is phased by electrically rotating it in 45° increments. Antenna rotation is a practical phasing scheme in this array only if the polarization remains very nearly circular in all directions observed. The conical spiral antennas meet this requirement quite well between

half-power points of their radiation pattern. Antenna rotation is accomplished by winding the spirals with eight instead of six wires and a diode switch has been devised to select six of the wires at any given time.

With the simplicity of this phasing scheme comes the disadvantage of not having continuous rotation. The phase error of any element can be as much as 22 1/2° due to incremental phasing.

Figure 6 shows the appearance of the antennas after the supports and switch circuitry are added. The diode switch is inside the top of the central pipe; the signal passes through a balanced-to-unbalanced transformer and is brought down the center of the pipe with 75Ω coaxial cable.

Element Grouping and Phasing Scheme

The phasing within each bank is accomplished by rotating each element, so there is no real time delay added to the signals from individual elements. All time delays are added to the 48 signal paths in the central building.

The use of simple phasing as opposed to delays in the 15-element banks limits the size of banks due to coherence loss with wide receiver bandwidths. One bank is approximately 100 meters in length so the coherence loss with a bandwidth of 3 MHz at a zenith distance of 45° is 9%. It is normally much less with smaller bandwidths and zenith distances.

In actual operation a computer controlled set of power transistors now supplies the phasing signals. Every bank in each arm is identically phased so elements with the same position in each bank have their control wires connected in parallel. Also, the east and west arms are normally phased alike so only 120 independent control wires are needed for the full array (4 wires per element times 15 elements per bank times 2 independent arms).

Normally equal lengths of transmission line would be run to the 15 elements in each bank, but in this array the line lengths have been cut pseudo-randomly to reduce the array's response to unwanted right-circularly polarized radiation (Swenson and Lo, 1961). The basic idea is the following: Each element has a small response to right circular polarization (cross-polarization). When an element is rotated, the phase of the right hand polarized signal is changed in the opposite direction from that of the left circularly polarized signal, i.e. when the left-polarized phase is advanced the right polarized phase is retarded. The result for an array with equal feeder lengths is that a "ghost beam" is formed with cross-polarized radiation on the opposite side of the zenith from the main beam. This "ghost beam" can be substantially reduced by staggering the lengths of the cables feeding the elements in a bank of 15. Thus, if a feeder cable is shorter than normal, the antenna is rotated counterclockwise to retard the left polarized wave to bring it back into phase. In the process the cross-polarized wave gets advanced by the shorter cable and again by rotation and, in general, is out of phase with respect to similarly polarized waves from other elements. Also, after the signals from the 48 banks are delayed and combined, the chance of having a pencil beam fall in one of the cross-polarized "ghost beams" is quite small.

Once the signals from the 15 elements in each bank have been combined, the resulting signal is amplified approximately 36 db in a wideband amplifier. This preamplifier has a noise figure less than 4 db (400°K) and a bandpass extending from 10 to 140 MHz. It is particularly designed to handle large interfacing signals without producing spurious intermodulation products.

After amplification the combined signal enters an air-filled coaxial cable of 1500 meters length for transmission to the central building. The loss in this cable is proportional to the square root of the frequency and is about 25 db at 110 MHz. Even at the highest frequency the preamplifier has adequate gain so that noise produced by succeeding components has little effect on the system noise figure. After accounting for the loss in all the cable and transformers ahead of the preamplifier, the system noise temperature is 1800°K at 110 MHz. At this frequency the sky noise is about 1000°K so $T_{sys} + T_{sky} \approx 2800°K$. The galactic background radiation (T_{sky}) is approximately proportional to $\lambda^{2.6}$, and the losses ahead of the preamplifier decrease in proportion to the square root of the frequency, so below about 70 MHz the system noise is quite insignificant compared to sky noise.

Array Pattern Calculations

To the authors' knowledge, the use of incremental phasing in linear arrays for radio astronomy has not been treated in detail. A considerable number of fundamental pattern calculations had to be performed to assure the feasibility of the scheme. We had to determine the magnitude of the sidelobes generated by phase errors up to 22 1/2° and calculate the confusion limits due to these sidelobes. The confusion calculation is carried out in Paper II.

For pattern calculations the array is most conveniently divided into two levels. First, the electric field pattern of a bank of 15 elements is calculated using incremental element phases. Then the pattern of one bank is multiplied by the array factor generated by isotropic radiators at the phase center of each bank to obtain the total response pattern.

To illustrate incremental phasing effects, assume that the elements are fed with equal lengths of transmission line. Figure 7 shows two examples of calculated patterns resulting from incremental phasing (solid lines). Superimposed on each is a plot of a pattern with perfect phasing (dashed lines). The most important difference between perfect and incremental phasing in Figure 7 is that the zero crossings are not identical. Therefore, when the 32-element grating response is multiplied by the 15-element pattern, the grating lobes which ordinarily would fall on zeroes of the 15-element pattern will no longer be completely canceled. Another way of looking at this is that there will be a periodic phase error distribution in the array which repeats every 15 elements. This will create small grating responses with angular spacings of $(\lambda/15d)$ radians, where d is the distance between individual elements.

The slight degradation of the main beam is a quasi-random function of direction so there will be about a 3 percent peak to peak modulation of the response as the array tracks a source. This is also a result of the imperfect phasing.

Cross-polarization tests showed that it would be necessary to use unequal lengths of cable to feed the 15 elements. This does not introduce larger phase errors, but it does change the pattern obtained with a 15-element bank. Some of the patterns calculated using the feeder system actually incorporated in the array are shown in Figures 8a and b. Equal and unequal feeder systems give the same average sidelobe level so the sidelobe and confusion calculations given in Paper II are valid for the actual system although they were made for equal feeder lengths. Incremental phasing is not the only source of phase errors, but it is by far the most important.

Total Array Pattern

With unequal feeder lengths in the 15-element banks the element phases are not antisymmetric around the center element, #8, e.g. the incremental phasing error of element #7 is not necessarily equal in amplitude and opposite in sign to the phase error of element #9. As a result, the phase center of the 15-element banks can be displaced by as much as 0.02 wavelengths (7°) from the center element. Because all of the banks within an arm are identically phased, the phase center displacement produces no additional phase error between the banks in one arm. The south arm is phased differently from the east-west arms so there will be a variation in relative phase of the combined signal from the south arm with respect to the combined signal from the east-west arms. This phase error can be calculated in the controlling computer's phasing program and compensated by adding a small phase shift in the signal paths from the south arm.

Another consequence of the asymmetric phasing in the 15-element banks is that the amplitude of the voltage vector which is the resultant of the addition of the 15 signals does not go through zero between sidelobe maxima (see Figures 8a and b). This, and the phase center motion, are results of the incomplete cancellation of the imaginary part of the vector sum. In other words, the phase of the resultant vector varies continuously from 0° to 180° but, after the signals from the east-west and south arms are multiplied, the combined pattern in the cosine receiver output will have zero amplitude when the east-west and south arm signals are in phase-quadrature.

Note that the 15-element patterns are voltage patterns and the pattern resulting from the correlation of the east-west and south arm signals is a product of two voltages. At a given direction in the sky the array response

Above 50 MHz the spacing of the individual elements is greater than one wavelength, giving rise to primary grating responses equal in amplitude to the main beam. These will be treated as a third type of sidelobe (C). The only method for reducing types B and C is through the use of a receiver bandwidth large enough to reduce the coherence of the radiation at the position of these sidelobes. Bandwidths of a few percent are needed to lower these sidelobes to manageable levels for weak source observations.

It must be remembered that the above discussion is only for the one-dimensional case. When the east-west and south arms are combined, sidelobe responses occur wherever a main beam in one direction crosses a significant response from the orthogonal arm. Figure 10a is a projection of the celestial sphere onto the plane of the horizon and shows the positions of the various types of sidelobes at 70 MHz. Figure 10b is an expansion of the area around the main beam.

A discussion of the effects of these sidelobes on source confusion is given in Paper II.

Antenna Test Results

TP Impedance Characteristics

Because the conical spiral elements in this array incorporate several features which have not been tried with these antennas before, it was imperative that impedance and radiation characteristics be investigated before building 720 units. For practical reasons the antenna impedance could not be measured directly. There was a length of cable, a transformer, and the phase switch between the impedance bridge and the antenna terminals. Since we are interested in the operation of the total system, the standing wave ratio (VSWR) and impedance measured through these components are perfectly

valid provided the power loss in the individual components is not more than 20% or so.

Significant stray reactances in the feed system arise due to the physical layout of the diode switch inside the central support pipe. These reactances were measured and compensated with small inductors incorporated in the switch. The combination of stray and lumped reactances form a nearly symmetrical low pass filter with a cutoff frequency of about 250 MHz in series with each antenna wire.

Figure 11 is a Smith Chart plot of the antenna impedance as a function of frequency. The measurement was made at the base of the TP and corrected for delay in the 20-ft feeder cable. The maximum VSWR encountered is 1.4:1 which corresponds to a reflected power loss of 4%. Ohmic losses in the transformer and switch are less than 1 db (20%) and the loss in the 20-ft coaxial cable is 0.4 db (8%) at 110 MHz. When one takes the 75:200 impedance transformer into account it is evident that the characteristic impedance of the antenna is close to 189 Ω which is the theoretical value for a self-conjugate antenna.

Antenna Efficiency

Determination of the efficiency of a single element is very difficult because it requires an absolute measurement. There are no isolated radio sources with accurately known intensities which are strong enough to be measured with a single antenna. The next best alternative was to compare the noise output of the TP due to the galactic background with that of dipoles at two frequencies. This type of measurement does not give the gain of the antenna in any particular direction, but it should account for ohmic losses in the antenna and absorption of radiation by the ground. Since the galactic background is concentrated in the galactic plane, this measurement has to assume that the radiation patterns of the TP and dipole are approximately the

same and that the measurements are taken at the same sidereal time. A half-wave dipole, one quarter wavelength above a conducting plane, produces a power pattern not too different from that of the conical spiral antenna with which it is compared. Because the galactic background is randomly polarized, the difference in polarization of the two antennas should be of little consequence.

Half-wave folded dipoles were constructed for 110 and 33 MHz. The test procedure at 110 MHz was to record the total power from the TP for 24 hours and then repeat the observation using the dipole. The antenna temperature was calibrated by substituting a noise source for the antenna at the pre-amplifier input and recording a series of noise levels. The noise output from both antennas peaked at the same sidereal time and the ratio of their outputs was approximately the same throughout the sidereal day. This confirms the assumption that the two antennas have nearly the same radiation patterns.

The dipole antenna temperatures at similar sidereal times, corrected for cable losses, are plotted on Figure 12 as x's. The error bars represent outside limits on the uncertainty in reflection losses and calibration errors. Other points on the graph have approximately the same error estimate. The dipole measurements fit the expected background spectrum as shown by the straight line. The solid circles are the TP measurements which were directly compared to the dipole values. The 110 MHz TP antenna temperature is 20% $\pm$ 20% below the dipole value and the 33 MHz TP antenna temperature was 50% $\pm$ 20% below the dipole standard.

To get an estimate of the efficiency of the TP at other frequencies, its noise output was measured at discrete frequencies down to 14 MHz. After correction for losses between the antenna and the preamplifier, the antenna temperatures are plotted as open circles on Figure 12. These values were

normalized to agree with the TP/dipole ratios. Below 30 MHz the sky noise increases less rapidly with decreasing frequency, but the exact value of the integrated sky temperature in the antenna beam is not known because it is very difficult to take the effects of the ionosphere and ground reflections into account. The construction of a lower-frequency dipole at Clark Lake was impractical. As a result the conical spiral efficiency below 25 MHz is not well known.

It can be seen from Figure 12 that the antenna begins to lose efficiency rapidly below 25 MHz where a considerable fraction of the power is absorbed by the terminations. The system temperature is still dominated by sky noise down to about 12 MHz, however.

Element Power Patterns

Many components of the elements were too small to be scaled down in size by any significant factor, so all pattern measurements were made on full size antenna elements. The most convenient far-field sources for the measurements were natural ones and they were used for all of the pattern measurements.

The response of the antenna elements as a function of direction was determined in two stages. First, the azimuthal dependence of the power pattern was determined at several frequencies by observing a radio source at a given elevation on a series of nights with the antenna "rotated" to a different position each night with the phase switch. The zenith angle dependence was studied by comparing the apparent strength of two known radio sources at different elevations on the same interferometer fringe.

The two radio sources used in nearly all of the antenna tests were Cassiopeia A [$\alpha = 23^h\ 22^m$, $\delta = 58°41'$ (1970)] and Cygnus A [$\alpha = 19^h\ 58^m$, $\delta = 40°\ 36'$ (1970)]. Where the flux ratio of the two sources was needed,

the spectra compiled by Viner (1973) were used. Cas A is about 20 to 50% stronger than Cyg A depending on frequency.

The azimuthal pattern was measured at four frequencies and three zenith distances, and the results are shown in Table 2. With four independent samples at a given frequency and zenith distance, the azimuthal voltage pattern can be approximated by an ellipse. Table 2 gives the axial ratio of each ellipse (minor/major). The horizontal extent of the radiating region of this antenna is about λ/π so it should not produce structure in the azimuthal pattern with a scale size of less than a radian. Thus the 45° sampling interval should be adequate. Note that the values in Table 2 refer to the voltage pattern (not power) so they are a direct indication of how the illumination of one element will vary as it is rotated.

One drawback in this method for measuring the electric field pattern of the TP's is that the unwanted right-hand polarization response contributes to the fringe amplitude. This will cause very little error if the right-hand interferometer response remains constant in amplitude and phase as the antennas are rotated. The electric field pattern in the right-hand polarization probably does vary in amplitude in different azimuthal directions, however. This may cause an error in addition to those quoted in Table 2 of as much as $\pm$ 0.07 at 110 MHz and $\pm$ 0.04 at other frequencies.

Unless otherwise stated, the errors quoted for the measurements are outer limits on the possible range of each value. These limits, which take the signal-to-noise ratio into account, are mainly derived from the estimated reading error on the strip charts used to record the measurements and from experience with the calibration accuracies and reproducibility of the measurements.

As one might expect, the azimuthal pattern is more nearly circular at small zenith distances. Also, the pattern has a larger variation at 110 MHz where the antenna is operating near its design limit than it does at lower frequencies. Naturally, we would like to sample the pattern below 25 MHz where the antenna operates below its natural frequency limit, but man-made interference prohibits the use of bandwidths necessary to get a sufficient signal-to-noise ratio using only two antennas.

Measurement of the zenith-distance dependence of the electric field pattern was less straightforward. A method had to be devised to separate the observed intensity variation due to the antenna pattern from that due to coherence loss when using a wide bandwidth and antenna separation.

For this measurement, the two central east-west banks of elements were used as the two components of a phase-switched interferometer. This configuration produced several north-south fan beams which could be judiciously placed so that only one of the two test sources was in a beam at one time. The coherence loss factor was eliminated by comparing the response to Cas A and Cyg A in the same fan beam. Phasing combinations were chosen so that the eight phase positions were fairly evenly represented and the azimuthal antenna pattern tended to average out. The azimuthal dependence should only contribute an error of about $\pm$ 5% to an individual ratio in the worst case. Also, care was taken to be sure that a cross-polarization (right-hand) fan beam did not fall on one of the sources when a left-hand polarized fan beam measurement was taking place. Thus, the cross-polarized response caused no significant error in this part of the antenna pattern study.

Adopting the flux ratios of Cas A and Cyg A given by Viner (1973) at the several observed frequencies, the procedure was to use a bootstrap

technique to construct the zenith-distance dependence of the antenna pattern. Ratios of response to Cyg A and Cas A on the same fan beam were measured for five to seven fan beams at each of four different frequencies. The response to Cyg A nearest the zenith was assumed to be unity and the relative value for Cas A, corrected for its higher flux, was plotted at its larger zenith distance as in Figure 13. By interpolating between the first two points, the next largest zenith-distance value for Cyg A could be normalized and the power pattern extended to larger Z with the corresponding Cas A value, and so forth.

As a point of interest, the above method for measuring antenna patterns will work for any linear array of elements which have a pattern which is a surface of rotation whose axis is perpendicular to the array axis; e.g. an east-west array of north-south dipoles.

Figure 13a shows the zenith distance dependence of the TP power pattern at four frequencies. In each graph similar symbols refer to measurements of Cas A and Cyg A on the same fan beam. Cyg A is always at the lesser zenith distance. The assumed flux ratio, α, of Cas A to Cyg A is given on each graph.

The errors in the curves measured in Figure 13a are rather complicated in that they tend to accumulate at higher zenith distances. The initial response ratio has an estimated error limit of $\pm$ 5% and the point at largest zenith distance may be in error by $\pm$ 10%. The small scatter at large zenith distance indicates a fairly small error.

In interpreting the graphs in Figure 13, it should be remembered that they show an average zenith distance dependence, and a plot of the power pattern at a fixed azimuth will differ slightly from the average curve. The most important result of these curves is that they give the zenith distance to which the array is useful. It appears that the half-power point falls

at about Z = 50°. At all but 110 MHz the zenith distance dependence is fairly smooth. At 110 MHz there is a roughly sinusoidal component with a 25% peak to peak amplitude superimposed on a smooth curve with a half-power width of about 55°. This sinusoid could be explained by a ground reflection 20 db below the direct wave (10% in electric field) from a ground plane 7 meters below the phase center of the antenna. This would mean the effective ground is about 1 meter below the surface of the dry lake. There may be a weak ground-reflected wave at the other frequencies, but it is not possible to distinguish its effect from the direct-wave power pattern features.

In summary, the half-power beamwidth of the conical spiral antenna used in the TPT is about 100° except near 110 MHz where the pattern is apparently distorted by a ground-reflected wave. This ground reflection causes a secondary peak in the zenith-distance dependence of the power pattern at Z $\approx$ 30°. The variation of the antenna pattern in the azimuthal direction at a constant zenith distance ranges from $\pm$ 1 db at 110 MHz and Z = 45° to practically no variation at 45 MHz and Z = 20°. In no case is the modulation of the pattern in azimuth large enough to cause unacceptable irregularities in the array illumination.

Cross-polarization Response

The cross-polarization response (response of the antennas to right-hand circular polarization) was measured with the same observations which were used to determine the zenith-distance dependence of the antenna power pattern. As was explained in an earlier section, the cross-polarized wave forms a "ghost" beam on the opposite side of the zenith from the properly polarized beam.

The amplitude of the right-hand polarized fan beam was measured for at least four different positions in the sky for each frequency. Its amplitude, relative to the left-hand polarized beam, was somewhat dependent on the beam

position. All of the measurements were within 25° of the meridian, so coherence and antenna pattern effects were unimportant. Table 3 gives the range or upper limit on the relative amplitudes of the cross-polarized responses with respect to the left-hand polarized fan beam. The detection limit of about 5% was set by confusion with the minor sidelobes of the properly polarized response.

As would be expected, the cross-polarization response is highest at 110 MHz where the antenna is working near its design limit. The wires from the phasing switch to the spiral are no doubt radiating a significant amount of power which is linearly polarized. Possibly, at the other design limit below 20 MHz the cross-polarization response will also be fairly high, but it could not be measured because of strong broadcast interference.

In a previous section the method for reducing the cross-polarization response of a bank of elements using staggered lengths of feed cables was outlined. With unequal feeder lengths in both banks, all of the cross-polarized fan-beams were below a 4% detection limit at all four frequencies. On the average, the staggering of phases in the right-hand waves should reduce the unwanted fan beams by a factor of $\sqrt{15}$ provided the phase difference between the shortest and longest cables is more than 2 radians. This appears to be confirmed by the measurements.

The difference in electrical length between the shortest and longest cables is about 11.5 meters, so there is not quite enough phase scrambling below 20 MHz to realize the full potential of the cross-polarization reduction. If the difference were made larger, the loss differential in the cables at 110 MHz would cause excessive illumination irregularities across the banks of elements, creating sidelobes more difficult to eliminate than the cross-

polarization responses. It should also be noted that a further reduction in the unwanted polarization is realized in the phasing of the full array because the chance of having the overall phasing correct for both the main beam direction and the cross-polarized beam direction is very small. The right-hand polarized wave should cause very few confusion problems.

Phase Measurements

To confirm that the 45° phase-stepping system on the conical spiral antennas does indeed provide the proper phase increments, a pair of TP's were connected in a phase-switched interferometer as in the azimuthal pattern measurements. The fringe phase of this interferometer was measured on successive nights with one of the antennas rotated in steps of 45°.

This technique was not completely definitive, however. There was no practical way to eliminate the response of the antenna to right-hand polarized radiation. The cross-polarized interferometer pattern will cause an apparent phase shift in the fringes measured with the above technique when the oppositely polarized patterns are near phase-quadrature. A 20% cross-polarized response will produce an apparent phase error of up to 20°. The values given in Table 3 then set upper limits on the accuracy of the phase measurements.

Table 4 lists the limits on the phase errors in the conical spiral antennas as derived from these measurements. The signal-to-noise ratio and ionospheric seeing set a detection limit of about 5° on the phase errors, and the higher upper limits were due to the cross-polarization response. It can be stated that no phase errors were measured which would not be consistent with the errors expected from the cross-polarization response given in Table 3.

Thus far, all of the discussion of phase errors has concerned itself with those produced by the individual elements. There are further phase errors introduced by the transmission lines and amplifiers which are summarized in Table 5. Because the signals are combined in two stages, the phase errors are divided into two groups; those associated with the 15-element banks and those occurring in the 48 signal paths from the 48 banks.

Two values are given in Table 5, the larger of which is the outside limit on the phase deviation due to each component. In practice the phase deviations are considerably smaller than the specification limits as is indicated by the rms values. Also, the phase errors on items 2 through 6 are given for an operating frequency of 110 MHz with these errors decreasing with decreasing frequency. It can be seen that the largest phase error is due to incremental phasing as was assumed in the sidelobe calculations.

Prototype "T" Operation

An initial check on the full "T" performance indicated the central three banks of elements were combined as a prototype "T". This formed a small telescope of about 200 m effective aperture which includes the central region where the arms may interact. A few beam positions were tried at each of the four test frequencies, and the results were as expected. The pointing accuracy was within limits set by the incremental phasing and the sidelobe level was no higher than expected.

A more detailed analysis was done at 70 MHz where the best signal-to-noise ratio was obtained with moderate to low ionospheric scintillation levels. Figure 14 shows 7 drift scans of Cyg A at different beam positions. No attempt was made to maintain receiver gain calibrations over the 7 nights so the

intensities should not be compared directly. The expected beam positions as indicated by the tick marks in Figure 14 coincided with the measured values within the timing accuracy that could be obtained. Some examples of ionospheric intensity scintillations are seen in the drift scans. Observations 4 and 5 are virtually unaffected by the ionosphere while peak-to-peak scintillations of up to 20% are seen on other nights. The agreement between calculated and observed patterns is excellent.

Operational Tests of the Full Aperture

The 48 coaxial feed lines, preamplifiers, slope filters, and post amplifiers were next installed. The cables were buried at a depth of about 1 m, but were brought above ground at every splice. They are pressurized with dry air. The relative attenuations and electrical lengths of each of the 1500 m cables were found to remain identical at all frequencies and outdoor temperatures within the accuracy of our measurements, about $\pm$ 0.2 db and $\pm$ 0.3 cm, respectively. The absolute attenuation of the cables varies with underground temperature, as expected, and in the calibration of observed intensities it will be necessary to correct for this effect. The cables and other components appear to operate within the error budget given in Table 5 so we should expect the full aperture to operate in accordance with theory.

The center element of each bank was constructed and each was connected to a preamplifier and feed line. E-W and N-S grating arrays were thus formed. They yield the full angular resolution of the final system, but have large grating responses and only 1/15 of the final array's collecting area. As accurately as we can measure, these arrays produce the expected response of a uniformly illuminated aperture. Below 50 MHz, these response pattern

measurements are accurate to a few percent; above 50 MHz, all of the stronger radio sources are partly resolved by the arrays and the interpretation of the observed profiles is complicated. In fact, the arrays are being used for some measurements of the angular structure of strong sources.

The E-W grating array has also been correlated with the completed E-W banks of elements. This process eliminates all grating responses except the one that falls within the pattern of the banks of elements. The element banks are pointed under computer control and their response pattern can be placed on any of the grating lobes to form single N-S fan beams. By taking successive drift scans across a given source at many zenith distances, the data shown in Figure 13 has been checked. Pattern measurements have also been taken at frequencies intermediate between those shown in Figure 14. In all cases, these patterns represent reasonable interpolations between those shown in the figure.

The E-W arm of the instrument is now complete and in full operation. The N-S arm is nearly finished and the electronics system will next be completed. The grating arrays mentioned above are being used for studies of solar bursts, while the E-W arm is being employed in multifrequency observations of the quiet sun, X-ray sources, supernova remnants, and other objects.

All data indicate that the completed system will operate as planned, so its construction is proceeding as rapidly as funds will permit. During the next few months, as the system comes into operation, a powerful new instrument will be available to the astronomical community. We will welcome visitor usage of the system.

Acknowledgements

The authors wish to acknowledge the work of Mr. John Hubbard, Mr. Stig Johansson and Mr. Kenneth Barbier. They have all devoted a significant fraction of their professional careers to the design and construction of this instrument. Many other temporary staff and students have devoted themselves tirelessly to this effort. The work is supported by the National Science Foundation under grant GP-19401 and by the National Aeronautics and Space Administration under grant NGR 21-002-367.

REFERENCES

Christiansen, W. N. and Hogbom, J. A. (1969), Radiotelescopes, Cambridge Press, Cambridge, England.

Dyson, J. D. (1965), The characteristics and design of the conical log-spiral antenna, IEEE Trans. on Antennas and Propagation, AP-13, no. 4. 488-499.

Fisher, J. R. (1973), this issue (Paper II).

Perini, J. (1964), Sidelobe reduction by beam shifting, IEEE Trans. on Antennas and Propagation, AP-12, no. 6, 791-792.

Rumsey, V. H. (1966), Frequency independent antennas, Academic Press, New York.

Swenson, G. W., Jr., and Lo, Y. T. (1961), The University of Illinois radio telescope, IRE Trans. Antennas and Propagation, AP-9, no. 1.

Viner, M. R. (1973), A discrete source survey at 26.3 MHz with an absolute flux basis, Ph.D. Thesis, University of Maryland.

Yek, Y. S., and Mei, K. K. (1967), Theory of conical equiangular-spiral antennas, IEEE Trans. Antennas and Propagation, AP-15, no. 5, 634-639, and (1968) AP-16, no. 1, 14-21.

TABLE 1

TPT Specifications

Frequency range	15-125 MHz
Instantaneous bandwidth	0.10 to 3 MHz
Total collecting area	250 λ^2
Resolution 20 MHz	20 arcminutes
100 MHz	4 arcminutes
Steering and frequency changing time	<< 1 millisecond
Sky coverage	< 45° zenith distance
Sensitivity ($\tau = 10^s$. BW = 2 MHz)	$\sim$ 1 f.u.* at all frequencies
Confusion limit	$\sim$ 1 f.u. at all frequencies
Polarization	Left circular

* 1 f.u. (flux unit) = 10^{-26} watts/m^2/Hz.

TABLE 2

Axial Ratios of Azimuthal Voltage Patterns

Zenith Distances

Frequency	20°	32°	42°	Estimated errors
28 MHz	0.86	0.95	0.87	± 0.07
45 MHz	0.97	0.93	0.86	± 0.05
70 MHz	0.94	0.95	0.77	± 0.04
110 MHz	0.91	0.83	0.79	± 0.07

TABLE 3

Right-hand Polarized Response Relative
to the Left-hand Polarized Response

Frequency	110 MHz	70 MHz	40 MHz	20 MHz
Response	10 to 20%	<5 to 10%	<5 to 8%	<6%

TABLE 4

TP Phase Error Upper Limits

Frequency	110 MHz	70 MHz	40 MHz	20 MHz
Error	<20°	<10°	<5°	<7°

TABLE 5

Phase Error Budget. Items 2 through 6 assume a frequency of 110 MHz.

	Limit	RMS
15-element bank		
1. Incremental Phasing	±22°.5	±13°.9
2. Cable, switch and transformer	± 5°	± 2°
3. Power combiner	± 5°	± 2°
RMS total		±14°.1
48 signal paths		
4. Preamps	± 5°	± 2°
5. High pass filters	± 5°	± 2°
6. Cables	± 2°	± 1°
7. R.F. and I.F. electronics	± 5°	± 2°
8. Digital delays	± 5°	± 2°
RMS total		± 5°.8

FIGURE CAPTIONS

Figure 1. Array layout.

Figure 2. One bank of 15 conical spiral elements.

Figure 3. Block diagram of one of 48 channels in which signals from the 15-element banks are processed.

Figure 4. Block diagram of digital delay and correlation system.

Figure 5. Basic form of conical log spiral antenna.

Figure 6. The working version of the TP antenna in the array.

Figure 7. Fifteen element array patterns with incremental phasing (solid lines) compared to perfectly phased array pattern (dashed lines).

Figure 8. Representative voltage pattern of incrementally phased 15-element banks using staggered feeder cable lengths (solid lines) compared to perfect phasing patterns (sinc X, dashed lines). Only the amplitude of the resultant voltage vector is plotted (see text).

Figure 9. Total one-dimensional array voltage pattern (solid line). The dashed envelope is the 15-element pattern.

Figure 10a. Projection of the 70 MHz TPT array pattern onto the plane of the horizon. Beam sizes are not to scale.

Figure 10b. Expansion of Figure 10a around the main beam. Beam sizes are approximately to scale.

Figure 11. Impedance characteristics of the production version of the TP antenna corrected for delay in the feeder cable.

Figure 12. Spectrum of noise output from a single TP (circles and curved line). The crosses are dipole measurements, and the straight line represents a background spectrum of $T \propto f^{-2.6}$.

FIGURE CAPTIONS (continued):

Figure 13a. Zenith-distance dependence of the TP power pattern at four frequencies measured with the central banks of elements. α is the ratio of the flux of Cas A to Cyg A at the given frequency.

Figure 13b. Zenith-distance dependence of the TP power pattern at various frequencies measured using the full E-W arm.

Figure 14. Drift scans of Cygnus A through the prototype "T" beam at several beam positions. Points on 4 and 6 are calculated values.

Figure 15. Swept frequency records of solar radio emission using 32 elements spanning the full east-west aperture.

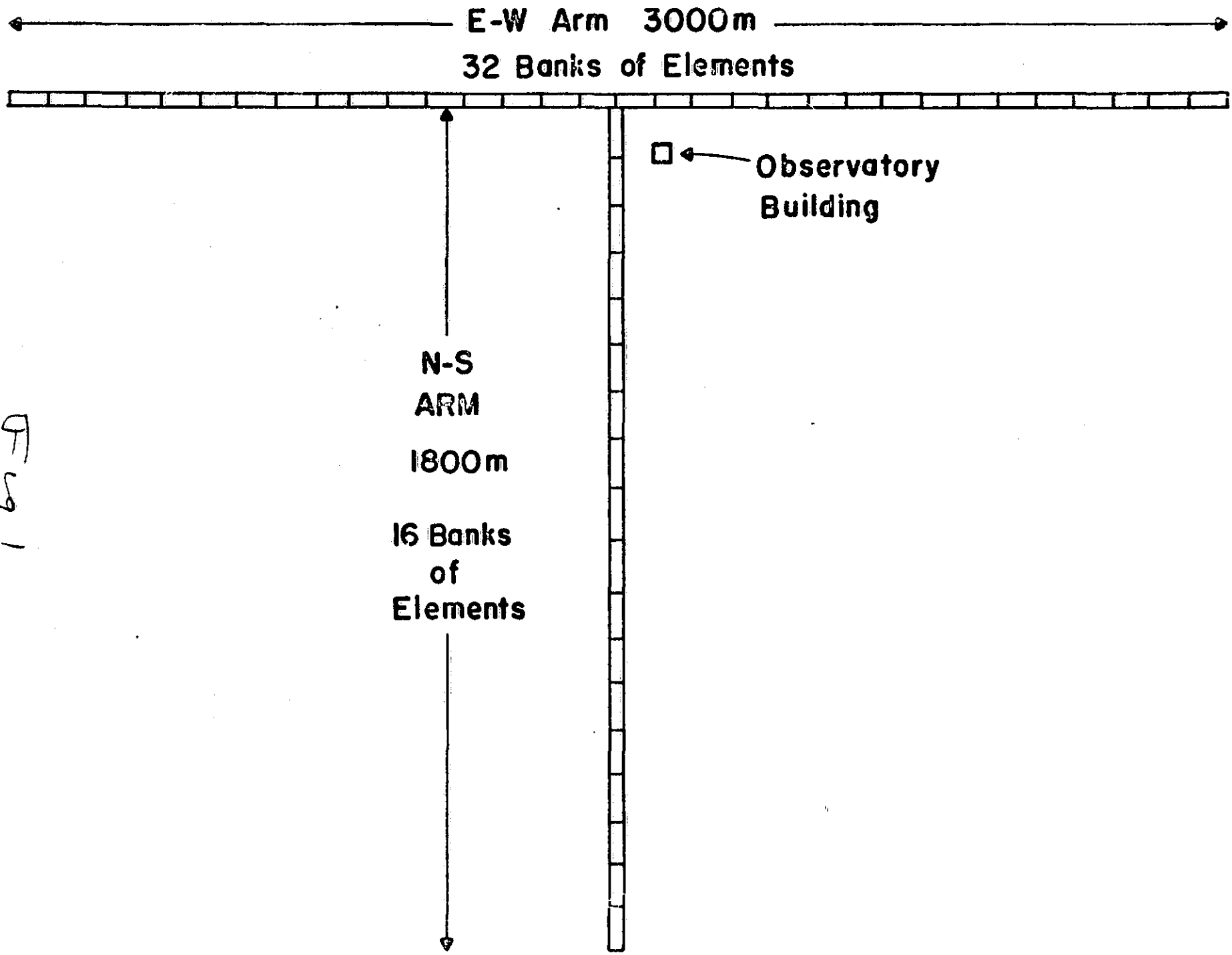
E-W Arm 3000m
32 Banks of Elements
Observatory Building
N-S ARM
1800m
16 Banks of Elements

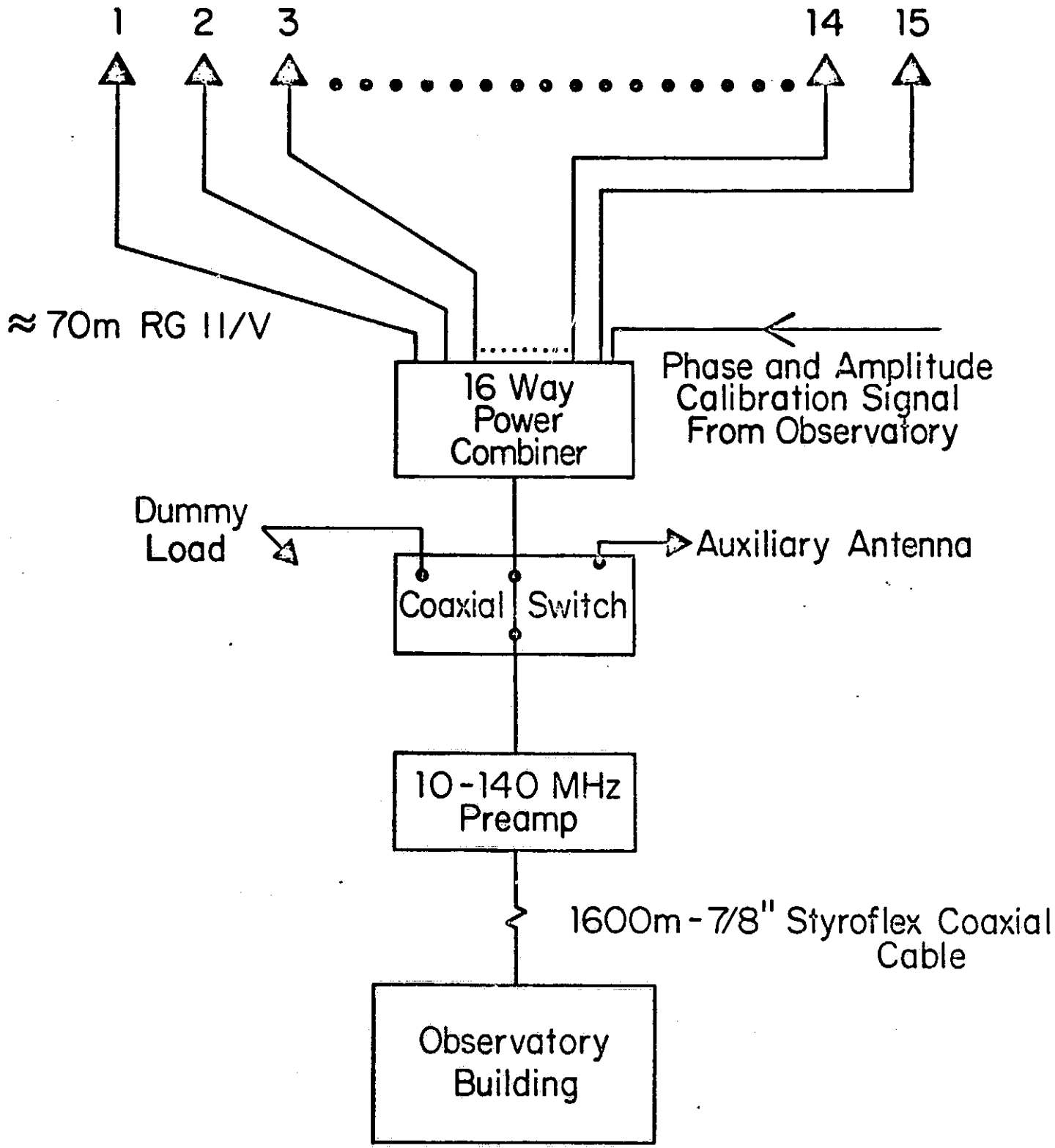
1
2
3
14
15
≈ 70m RG 11/V
16 Way
Power
Combiner
Phase and Amplitude
Calibration Signal
From Observatory
Dummy
Load
Auxiliary Antenna
Coaxial Switch
10-140 MHz
Preamp
1600m - 7/8" Styroflex Coaxial
Cable
Observatory
Building

Fig 2

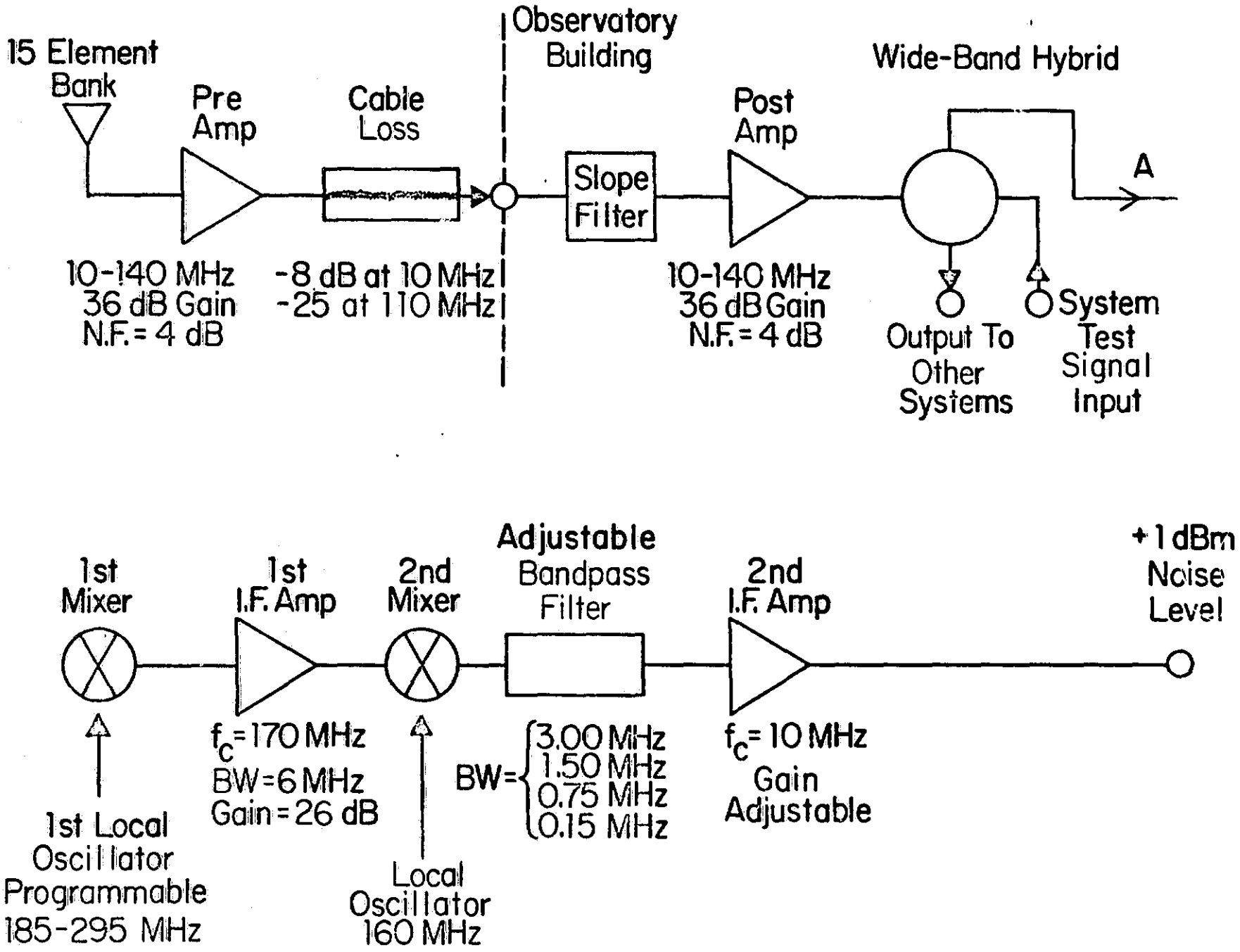
15 Element Bank
Pre Amp
Cable Loss
Observatory Building
Slope Filter
Post Amp
Wide-Band Hybrid
A
10-140 MHz
36 dB Gain
N.F. = 4 dB
-8 dB at 10 MHz
-25 at 110 MHz
10-140 MHz
36 dB Gain
N.F. = 4 dB
Output To Other Systems
System Test Signal Input
1st Mixer
1st I.F. Amp
2nd Mixer
Adjustable Bandpass Filter
2nd I.F. Amp
+1 dBm Noise Level
1st Local Oscillator Programmable 185-295 MHz
f_c = 170 MHz
BW = 6 MHz
Gain = 26 dB
Local Oscillator 160 MHz
BW = 3.00 MHz / 1.50 MHz / 0.75 MHz / 0.15 MHz
f_c = 10 MHz
Gain Adjustable

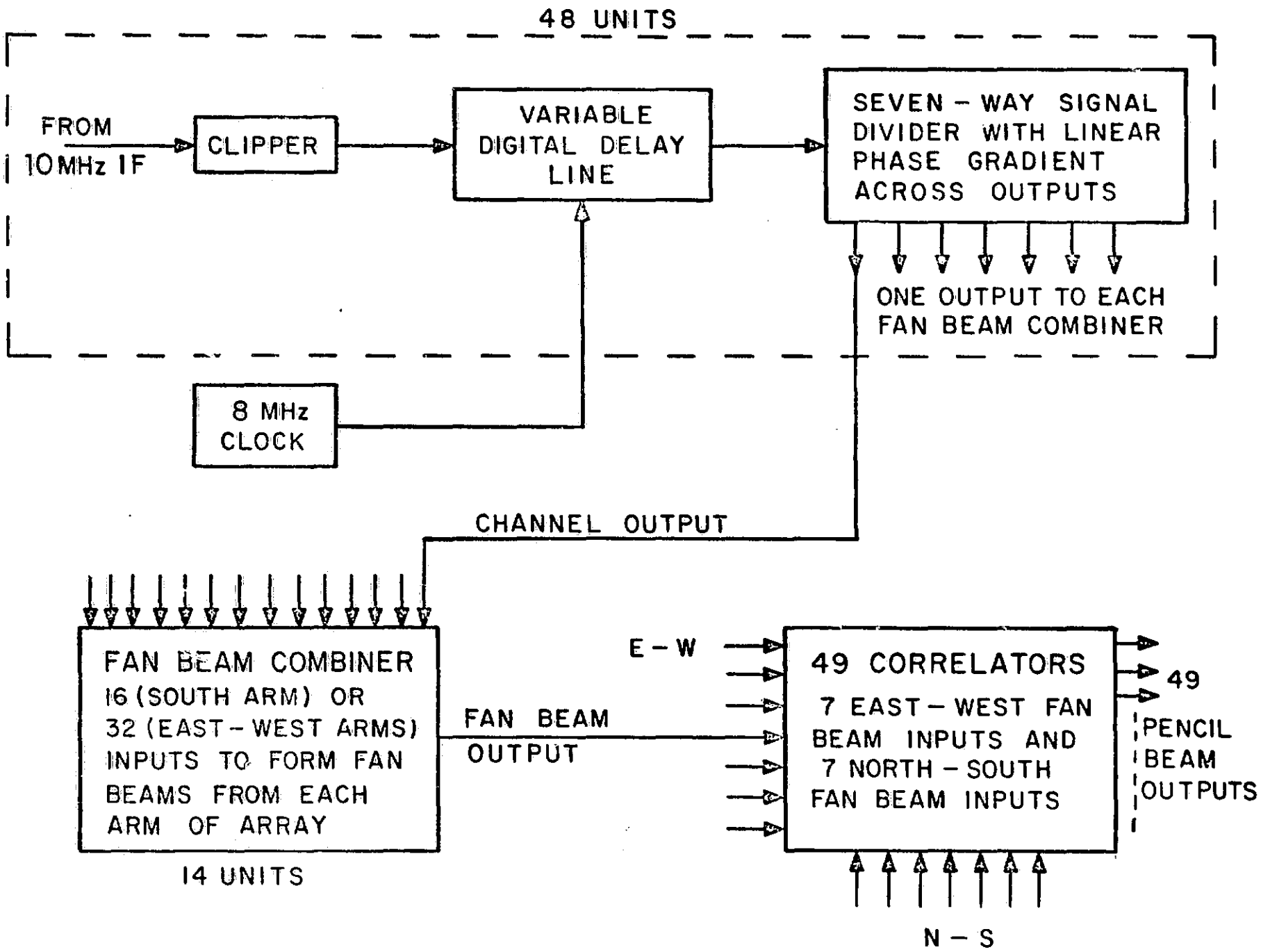
48 UNITS
FROM
10MHz IF
CLIPPER
VARIABLE
DIGITAL DELAY
LINE
SEVEN - WAY SIGNAL
DIVIDER WITH LINEAR
PHASE GRADIENT
ACROSS OUTPUTS
ONE OUTPUT TO EACH
FAN BEAM COMBINER
8 MHz
CLOCK
CHANNEL OUTPUT
FAN BEAM COMBINER
16 (SOUTH ARM) OR
32 (EAST - WEST ARMS)
INPUTS TO FORM FAN
BEAMS FROM EACH
ARM OF ARRAY
14 UNITS
FAN BEAM
OUTPUT
E - W
49 CORRELATORS
7 EAST - WEST FAN
BEAM INPUTS AND
7 NORTH - SOUTH
FAN BEAM INPUTS
49
PENCIL
BEAM
OUTPUTS
N - S

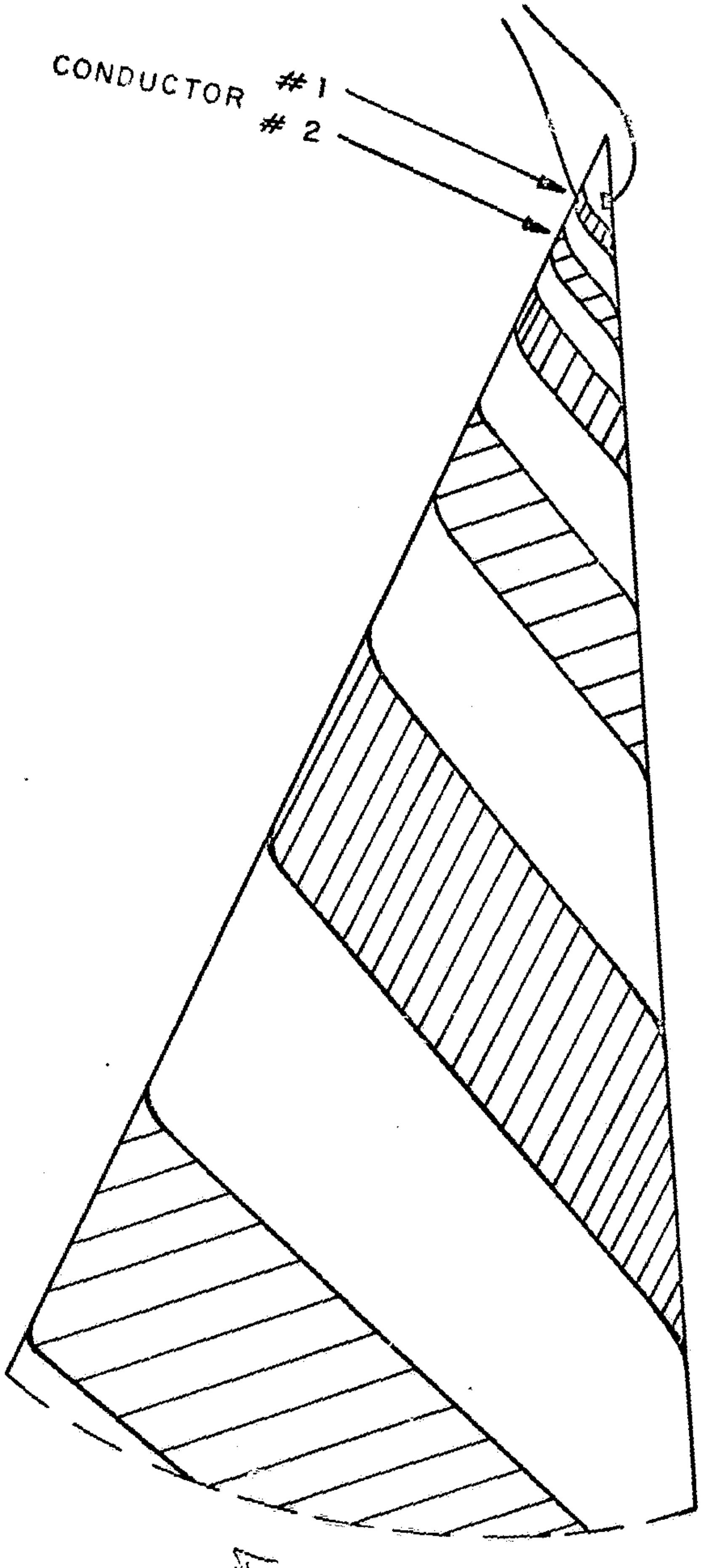

Fig 5

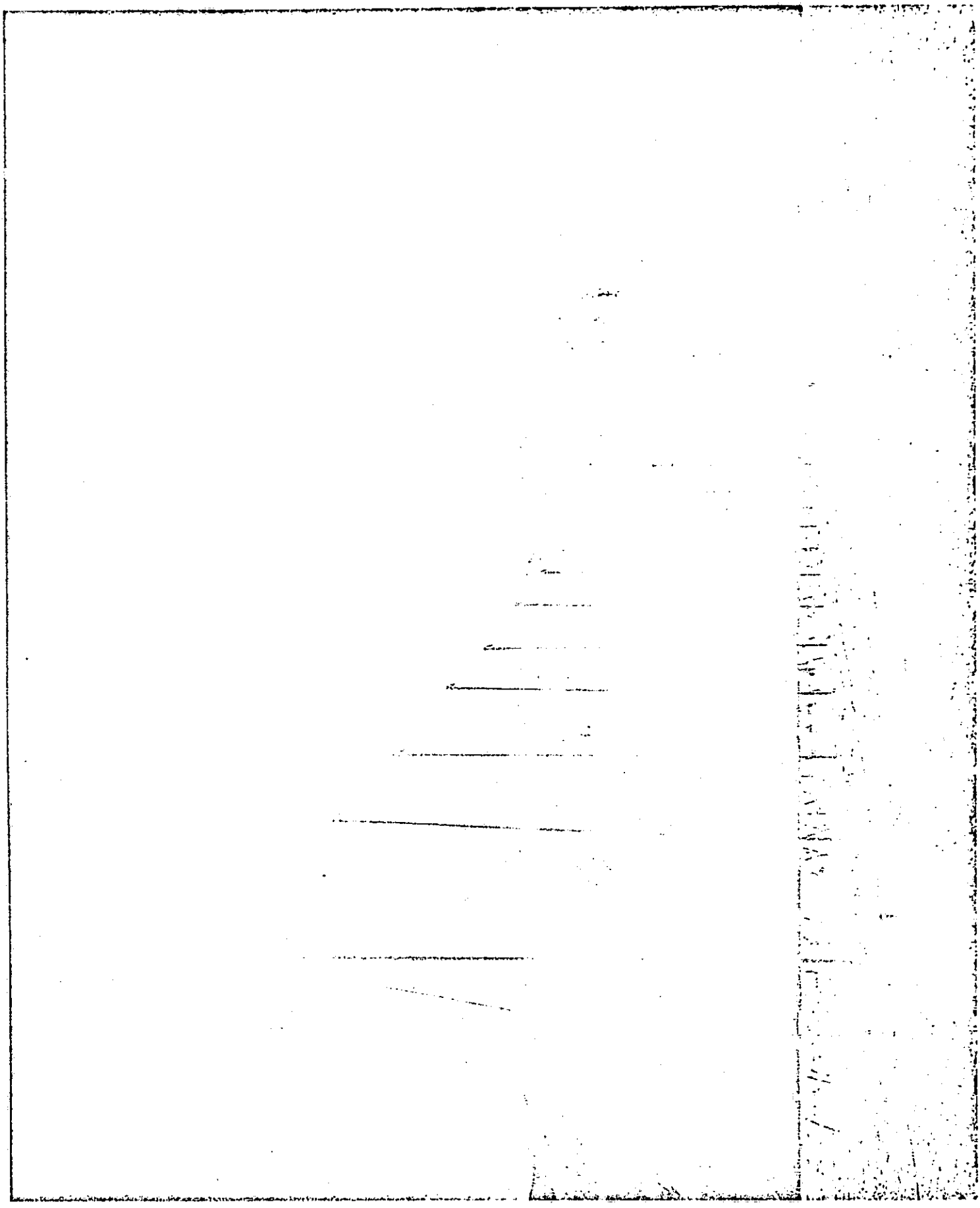

Fig 6

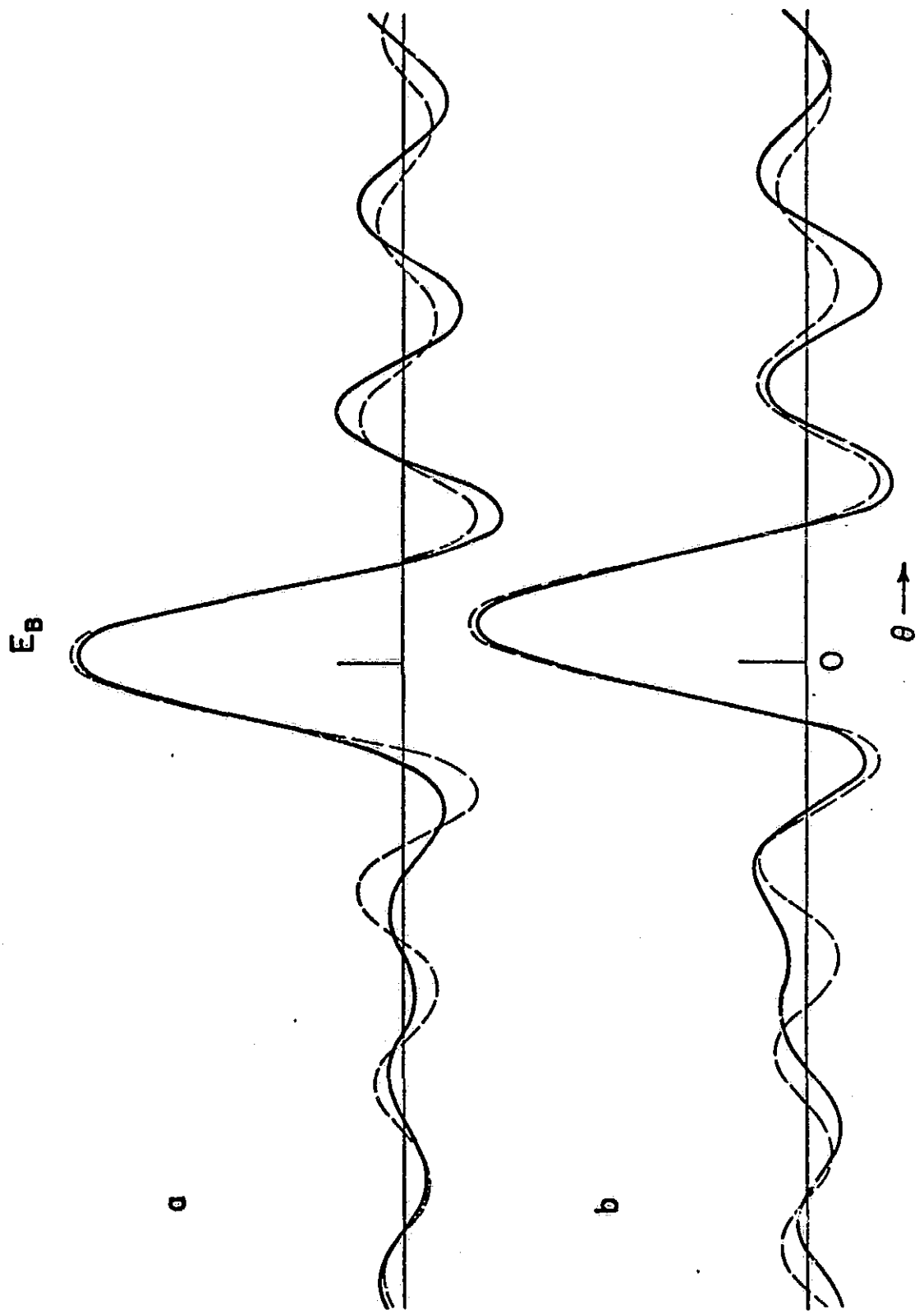

Fig 7

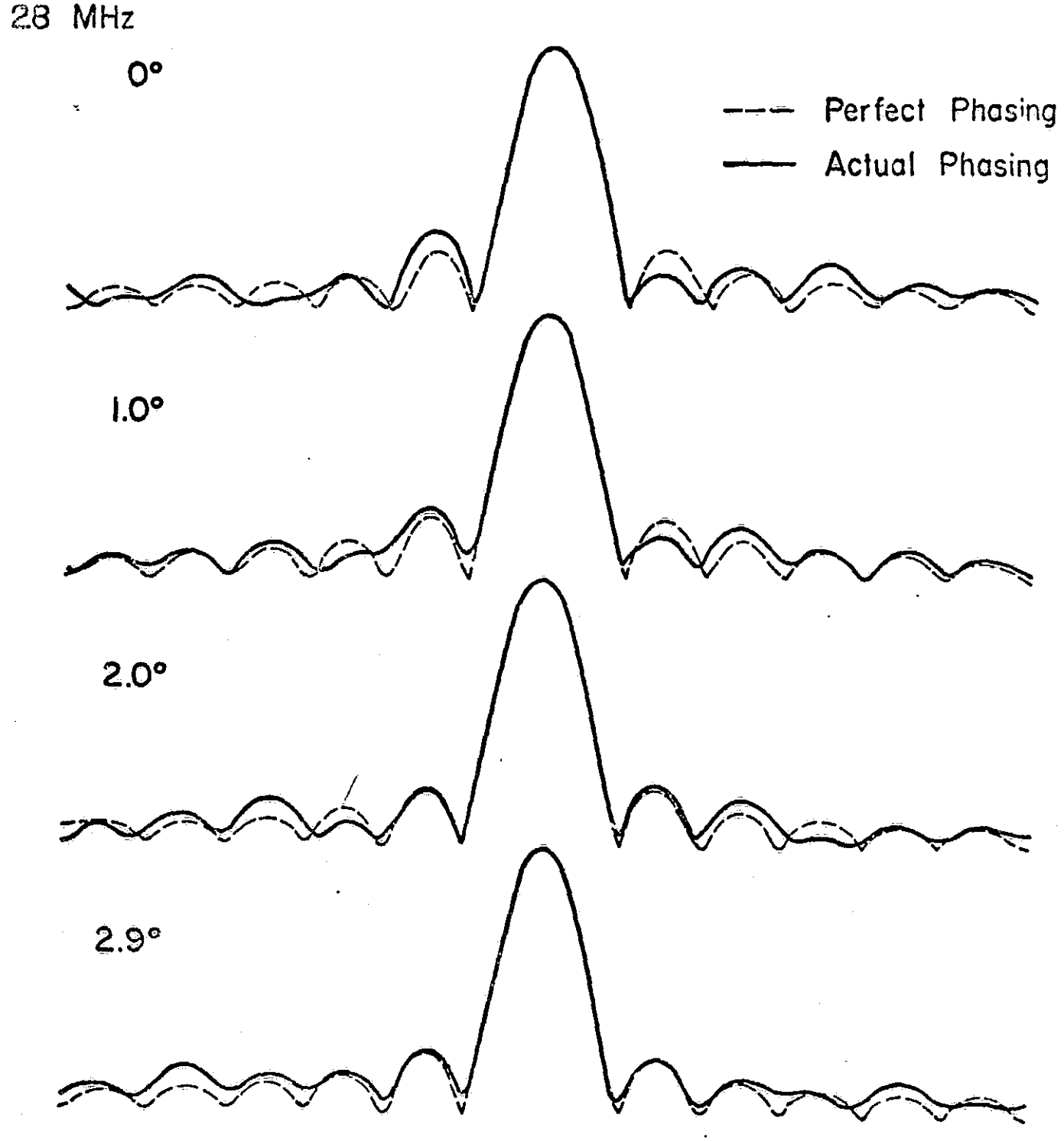

Fig 8a

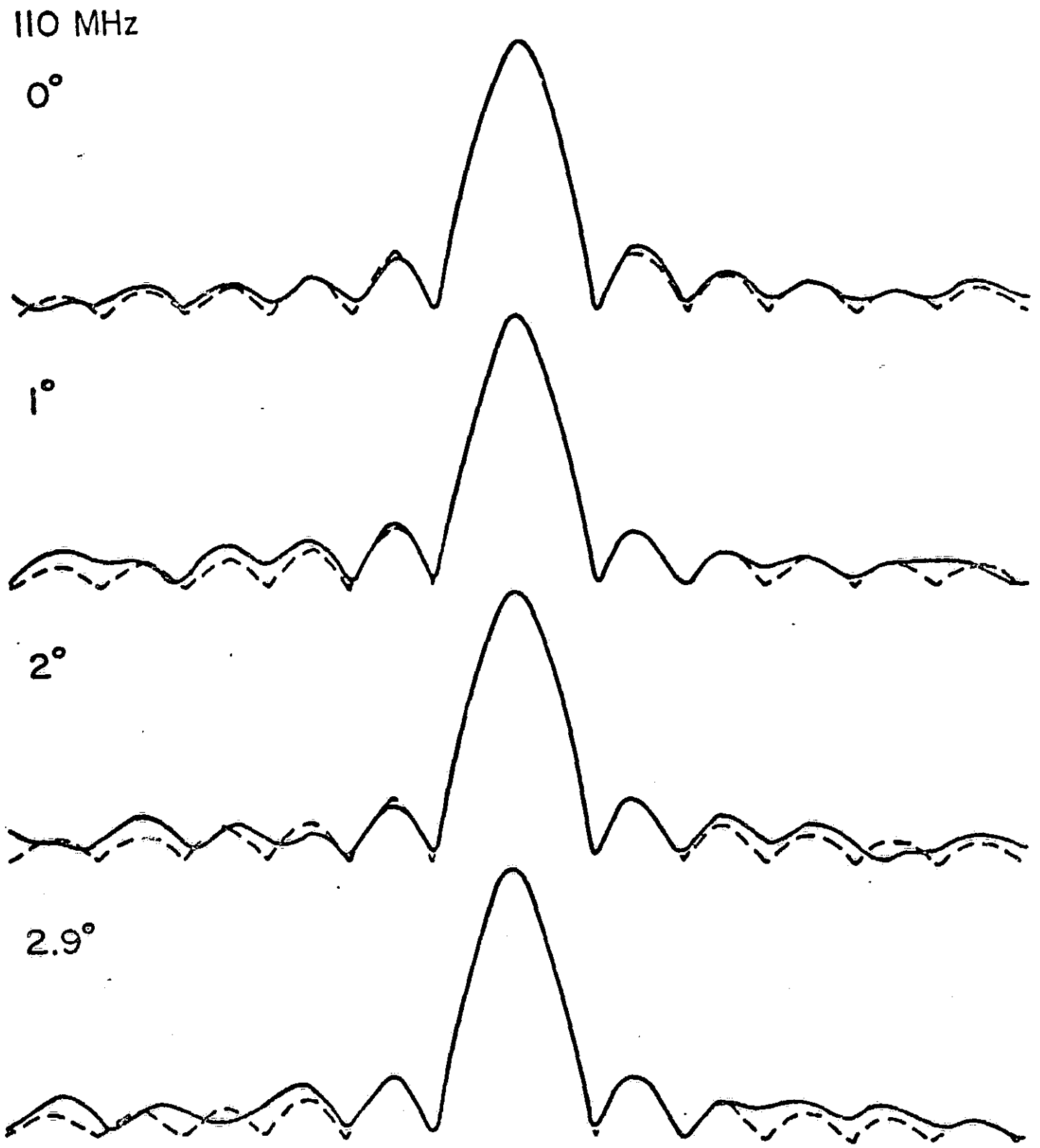

Fig 8b

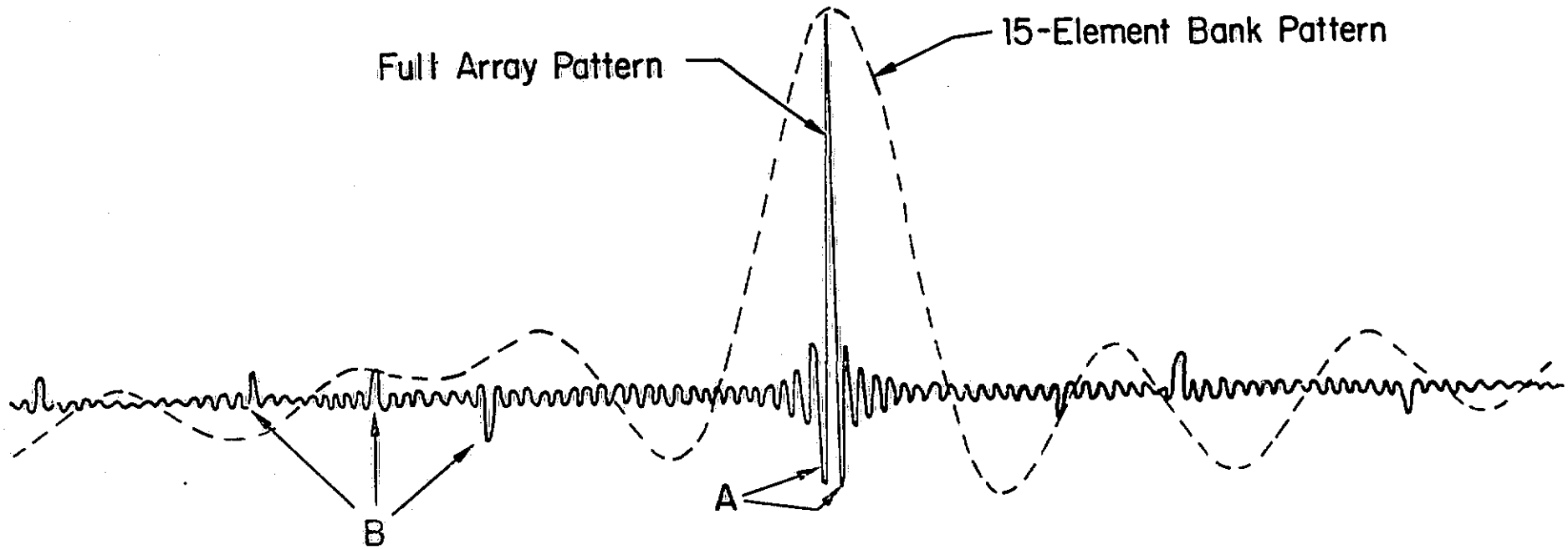

Fig 9

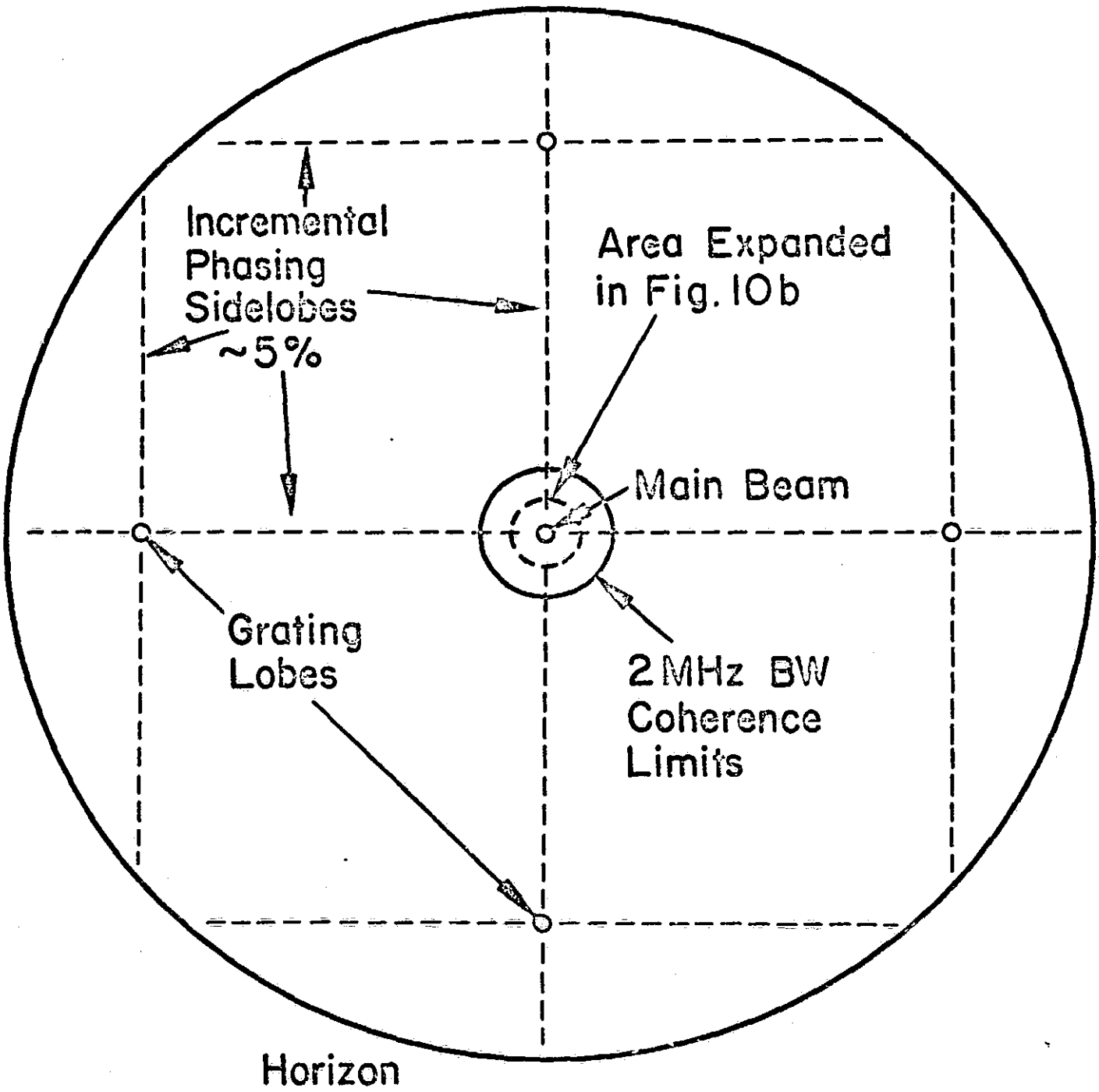
Incremental
Phasing
Sidelobes
~5%
Area Expanded
in Fig. 10b
Main Beam
Grating
Lobes
2 MHz BW
Coherence
Limits
Horizon

Fig 10a

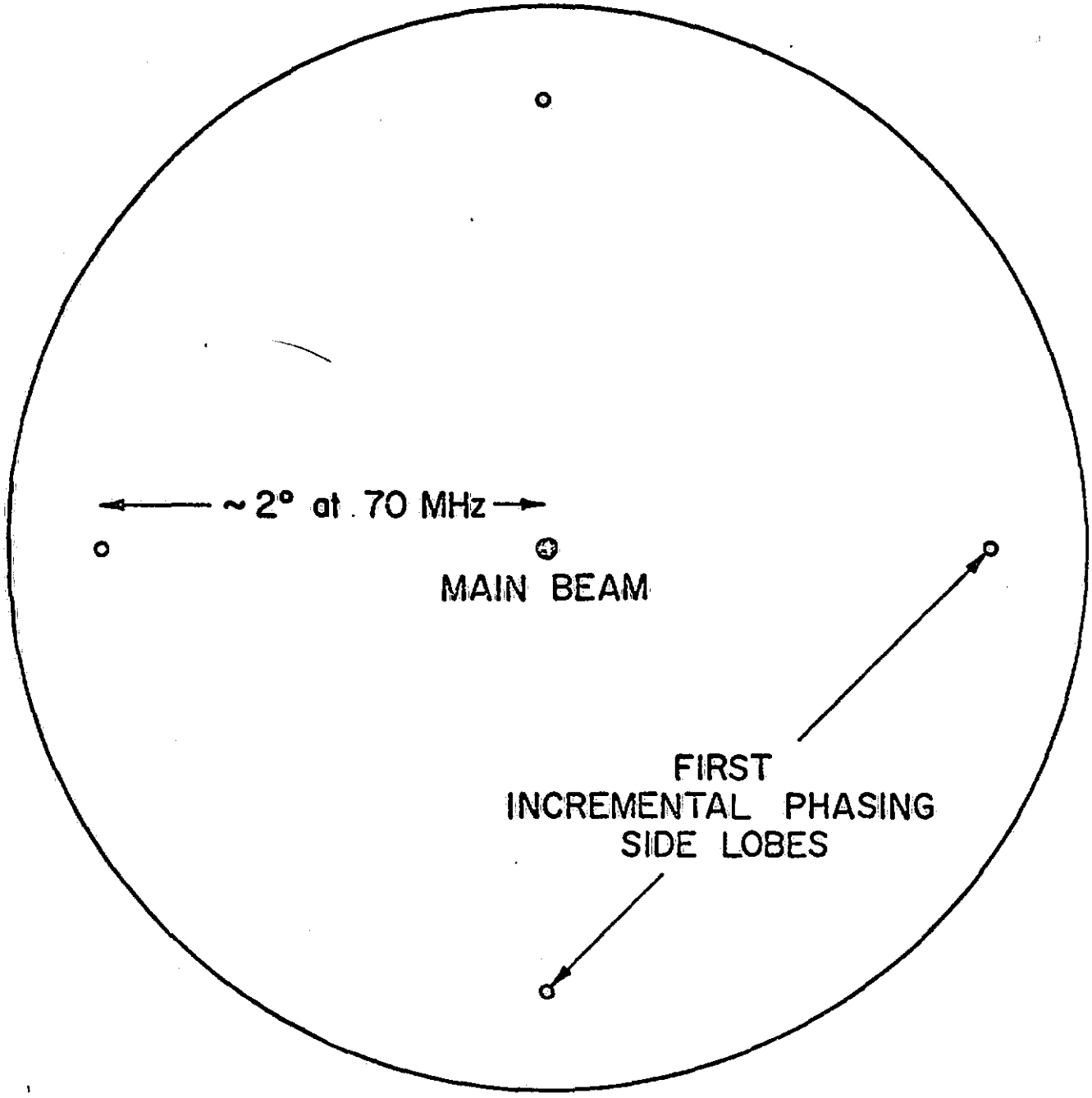
~ 2° at 70 MHz
MAIN BEAM
FIRST
INCREMENTAL PHASING
SIDE LOBES

0
0.1
0.1
0.7
0.2
0.2
0.3
0.8
0.3
73
55
37
0.9
109
91
0.4
19
VSWR = 1.4:1
0.4
1.0
FREQUENCY IN MHz
1.1
1.2
1.3
1.4
1.5

Fig 11

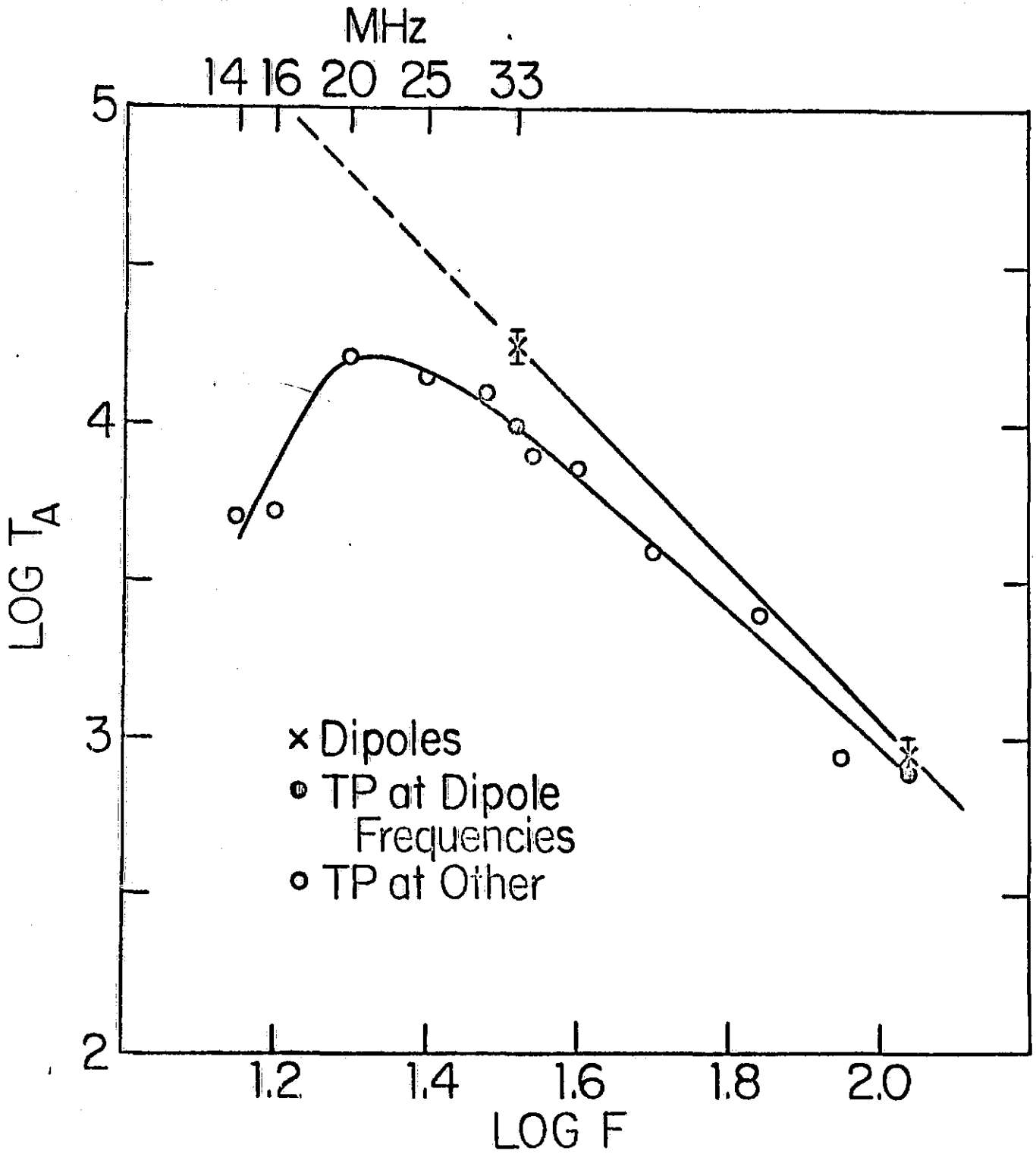
MHz
14 16 20 25 33
5
4
3
2
LOG T_A
× Dipoles
• TP at Dipole Frequencies
o TP at Other
1.2
1.4
1.6
1.8
2.0
LOG F

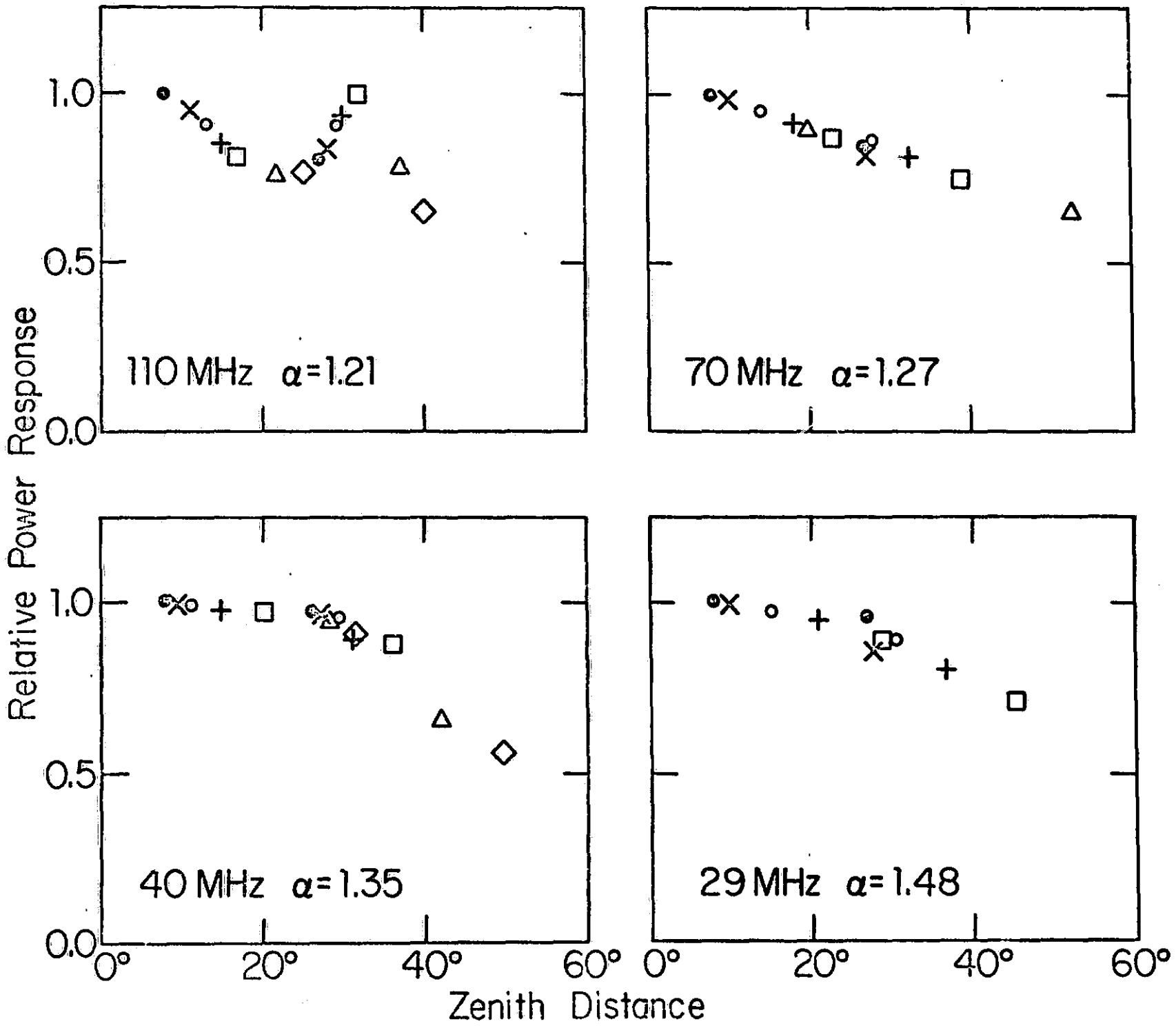
110 MHz α=1.21
70 MHz α=1.27
40 MHz α=1.35
29 MHz α=1.48
Relative Power Response
Zenith Distance
0.0
0.5
1.0
0°
20°
40°
60°

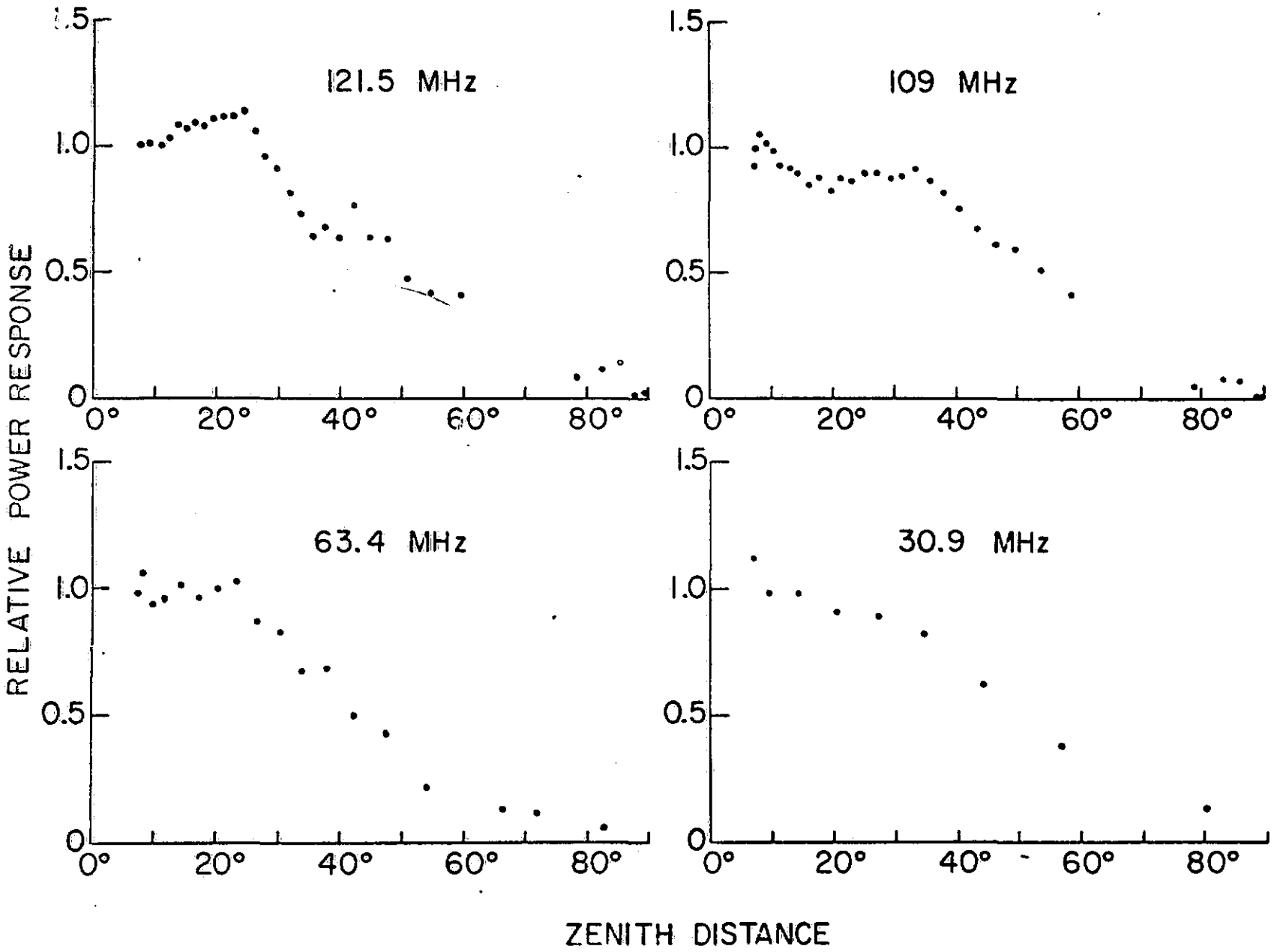
121.5 MHz
109 MHz
63.4 MHz
30.9 MHz
RELATIVE POWER RESPONSE
ZENITH DISTANCE
1.5
1.0
0.5
0
0°
20°
40°
60°
80°

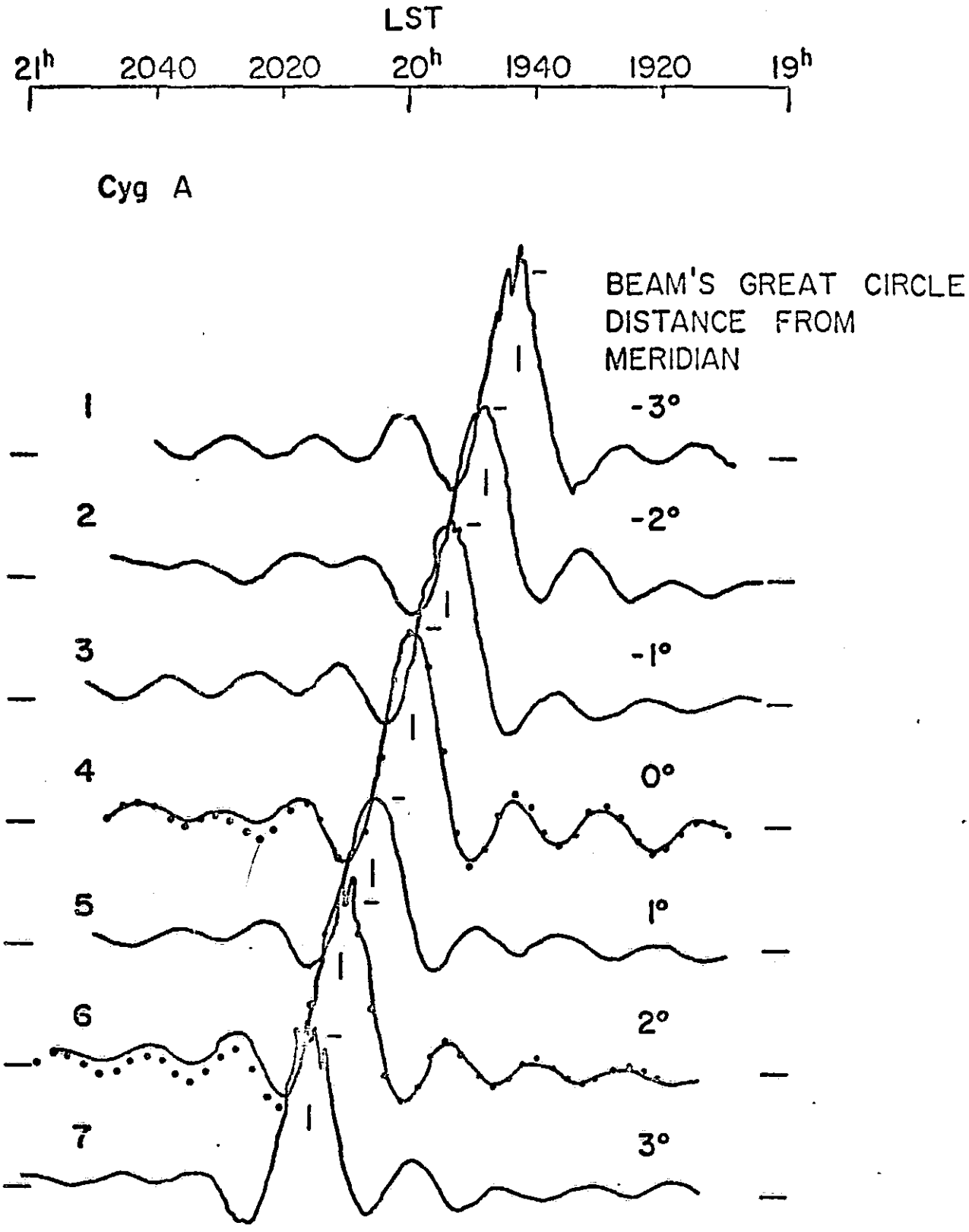
LST
21h
2040
2020
20h
1940
1920
19h
Cyg A
BEAM'S GREAT CIRCLE DISTANCE FROM MERIDIAN
1
-3°
2
-2°
3
-1°
4
0°
5
1°
6
2°
7
3°

Fig 14

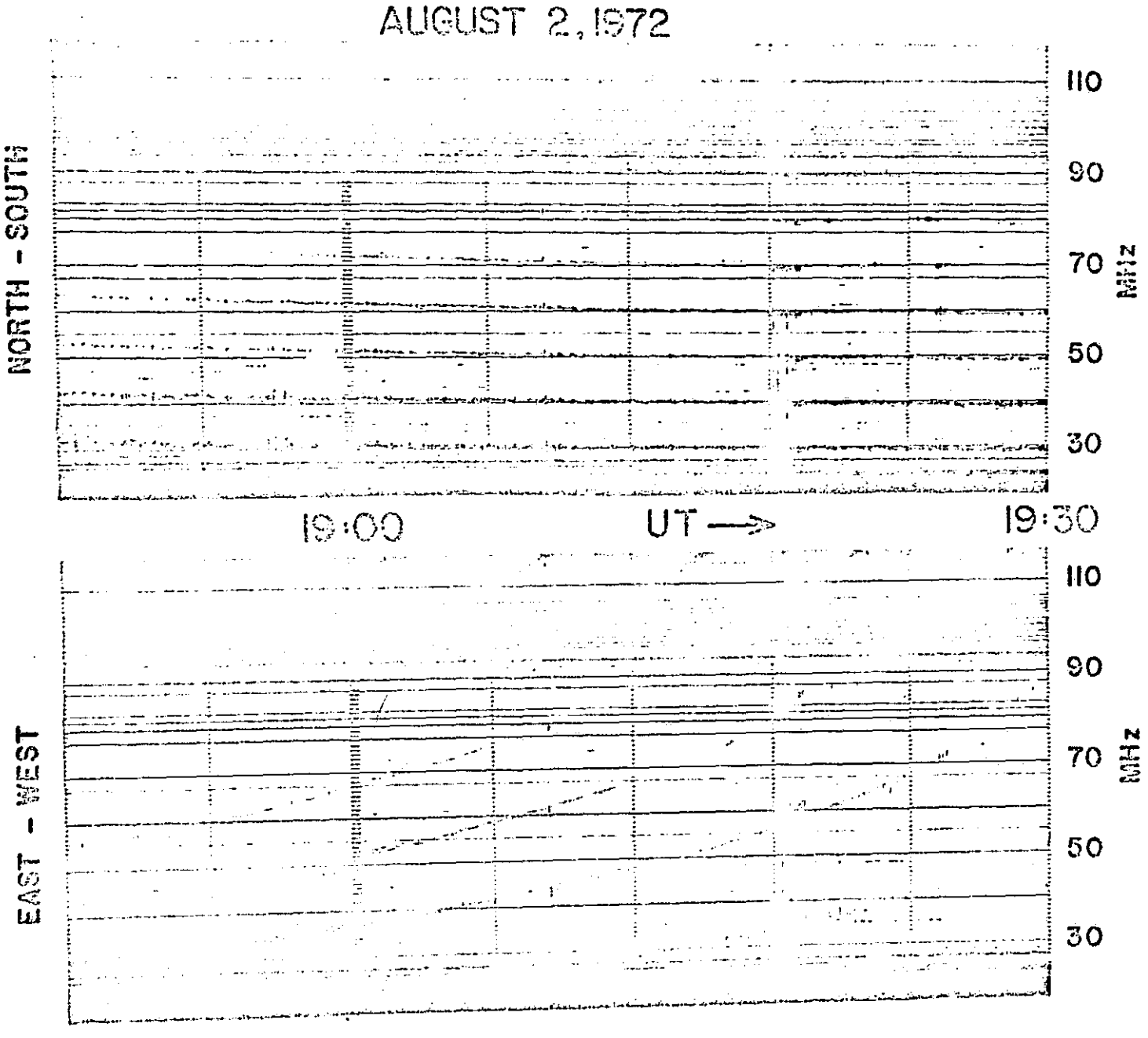

3 May 1974

Grant NGR 21-002-029 - Final Report

This is a final report on grant NGR 21-002-029. The work carried out under this grant is best detailed by the publications in the following list. Any of these publications are available upon request, and only few examples are enclosed. They are,

1. "Positions and Motions of Solar Bursts at Decameter Wavelengths," M. R. Kundu, W. C. Erickson, P. D. Jackson and J. Fainberg, Solar Physics, 14, 394, 1970. - A71-12764

2. "Meter and Decameter Wavelength Positions of Solar Bursts of July 3[illegible] August 7, 1972," M. R. Kundu and W. C. Erickson, Solar Phys. (in press).

3. "Detailed Correlation of Type III [illegible] Bursts with Hα Activity, I: Active Region of May 22, 1970," T.B.H. Kuiper, Solar Phys., 28, 187, 1973. A73-25950

4. "Detailed Comparison of Type III Radio Bursts with Hα Activity, II: The Isolated Type III Activity of March and April, 1971," T.B.H. Kuiper, Solar Phys., 33, 461, 1973.

5. "VLBI Interferometer Observations of Tau A and Other Sources at 121.6 MHz," W. C. Erickson, T.B.H. Kuiper, T. A. Clark, S. H. Knowles and J. J. Broderick, Astrophys. J., 177, 101, 1972. A71-12933

6. "Long Wavelength VLBI," T. A. Clark and W. C. Erickson, Proc. IEEE, 61 1230, 1973. - A73-43355

7. "The Log Periodic Array at the Clark Lake Radio Observatory," P. C. Jackson and T.B.H. Kuiper, Radio Science, 8, 845, 1973.

8. "The Clark Lake Array," W. C. Erickson, Proc. IEEE, 61, 1276, 1973.

9. "A New Wideband, Fully Steerable, Decametric Array at Clark Lake," W. C. Erickson and J. R. Fisher, 9, 387, 1974.

Many of the other publications are so bulky (200-300 pages) that it would be impractical to enclose them.

In some cases, the effort was begun under NGR 21-002-029 and completed under NGR 21-002-367.

This grant supported approximately five years of solar radio observations in the frequency range of 20-60 MHz with only the log periodic array discussed in paper 7. Since mid-1972 two dimensional observations in the 10-120 MHz range have also been conducted with the new TPT antenna (paper 9). All of the data are recorded on magnetic tape and stored at Goddard Space Flight Center. For the investigations reported above, the University of Maryland group have employed facimile reproductions of these data.

POSITIONS AND MOTIONS OF SOLAR BURSTS AT DECAMETER WAVELENGTHS

M. R. KUNDU, W. C. ERICKSON, P. D. JACKSON
Astronomy Program, University of Maryland, College Park, Md., U.S.A.

and

J. FAINBERG
NASA-Goddard Space Flight Center, Greenbelt, Md., U.S.A.

(Received 6 May, 1970)

Abstract. The positions and motions of solar bursts in the range 20 to 60 MHz have been measured by the means of a sweep-frequency grating interferometer with angular resolution of 5′ arc at 60 MHz decreasing to 15′ arc at 20 MHz. The positional characteristics of the decameter wavelength bursts are discussed in terms of the commonly accepted theories of the origin of radio bursts from plasma and synchrotron radiations.

1. Introduction

One of the most interesting problems of solar radio astronomy is the study of the generating mechanisms of radio bursts. The most relevant observations for such studies are the measurements of dynamic spectra and positions of burst sources as a function of frequency and time. At meter and decameter wavelengths, the phenomena of most interest, bursts and storms, vary rapidly from second to second, and therefore the measurements must be made almost instantaneously over the entire frequency range of interest. A sweep frequency grating interferometer capable of measuring the dynamic spectra as well as instantaneous positions of burst sources simultaneously over all frequencies in the range 20–60 MHz was recently constructed jointly by the University of Maryland and Goddard Space Flight Center. The solar array (Erickson and Fainberg, in preparation) at the Clark Lake Radio Observatory consists of 16 log periodic antennas equally spaced on a two mile east-west baseline. The array beam spacing and width are such that only one narrow beam is on the sun at one time. The angular resolution is about 5′ arc at 60 MHz decreasing to 15′ arc at 20 MHz. The array is swept in frequency over the range 20–60 MHz at a rate of 4 sweeps per second. This system gives the one-dimensional position and angular size of emissive regions on the sun nearly simultaneously at all frequencies over the range 20–60 MHz for studies of evolution of these regions as a function of time. We discuss below some preliminary results obtained with this instrument.

Irregular ionospheric refraction may cause considerable error in the positional determination of bursts. A test of ionospheric effects is provided by occasional observation of long lasting continuum events in which the position deviates by as much as 10–15 min arc, the amount of deviation being greater at lower frequencies. When such conditions prevail, determination of positions of bursts may be seriously

Solar Physics **14** (1970) 394–403.

in error, and so we have not used such data in our analysis. The seriousness of ionospheric effects on position determinations was first pointed out by Wild *et al.* (1959).

2. Type III and Type V Bursts

In the radio spectrum in which we are interested, the most commonly occurring phenomena are the type III bursts. It is now generally accepted that each individual type III burst is radiation from streams of electrons moving outwards through the corona and exciting plasma oscillations of progressively diminishing frequency as the stream passes through coronal plasma of diminishing electron density. Their properties at decameter wavelengths are similar to those at meter wavelengths – their sudden rise to peak intensity occurs in a period of about 1 sec, and their subsequent decay is governed mainly by collisional damping of plasma oscillations by the coronal gas. However, a new kind of burst resembling the type III has been observed with our instrument, especially during periods of quietness in an otherwise active period. These bursts start and decay within 1 scan period or 1 sec at 30 MHz. This implies a very rapid acceleration process, and a rapid damping mechanism. In a two-million degree

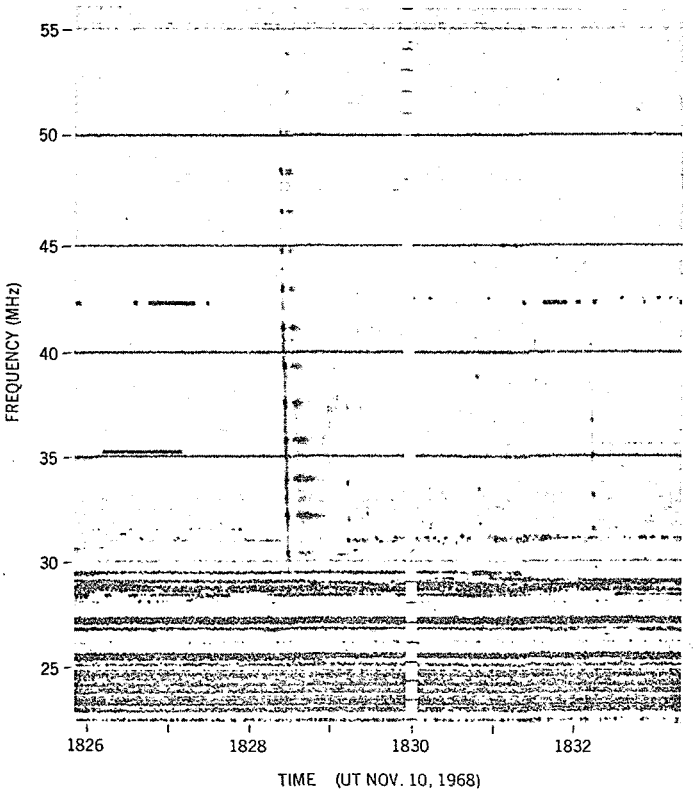

Fig. 1a. Interferometer record of a harmonic type III burst observed on Nov. 10, 1968.

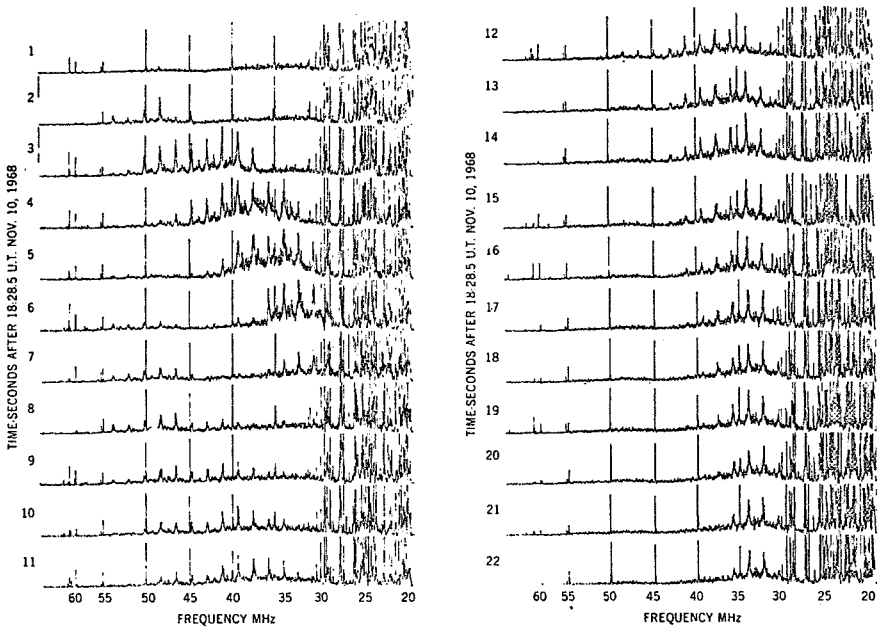

Fig. 1b. Successive one-second scans of the harmonic type III burst of Nov. 10, 1968. The harmonic structure can be recognized easily from the intensity-frequency profiles.

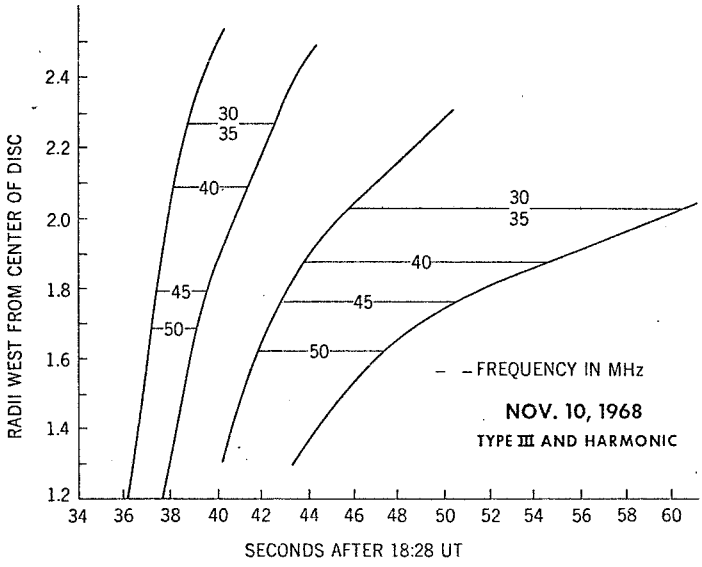

Fig. 1c. Positions of the type III and its harmonic as a function of frequency and time.

corona, typical decay times due to collisional damping are about 1.5 sec and 5 sec at 60 and 30 MHz respectively (see for example Kundu, 1965). It is not unlikely that these short bursts are produced by the same generating mechanism as the type I burst, although their bandwidth is much larger than the type I.

The positional data of type III bursts indicate a systematic dispersion with frequency, the lower frequencies occurring higher in the corona than the higher frequencies, consistent with the interpretation of type III bursts in terms of plasma radiation. When type III bursts occur in a group, the individual members of the group seem to originate at the same position, with some scatter probably attributable to instrumental errors. From the position-measurements of type III bursts occurring near the limb, and assuming that the disturbance (the stream of electrons) originating from the flare moves radially outwards producing the plasma oscillations responsible for type III bursts, one can compute the electron density as a function of height. The average electron density distribution determined in this manner is consistent with that found by others from earlier measurements. It should be noted that since the measurements are made with a swept-frequency grating interferometer rather than a two-element interfero-

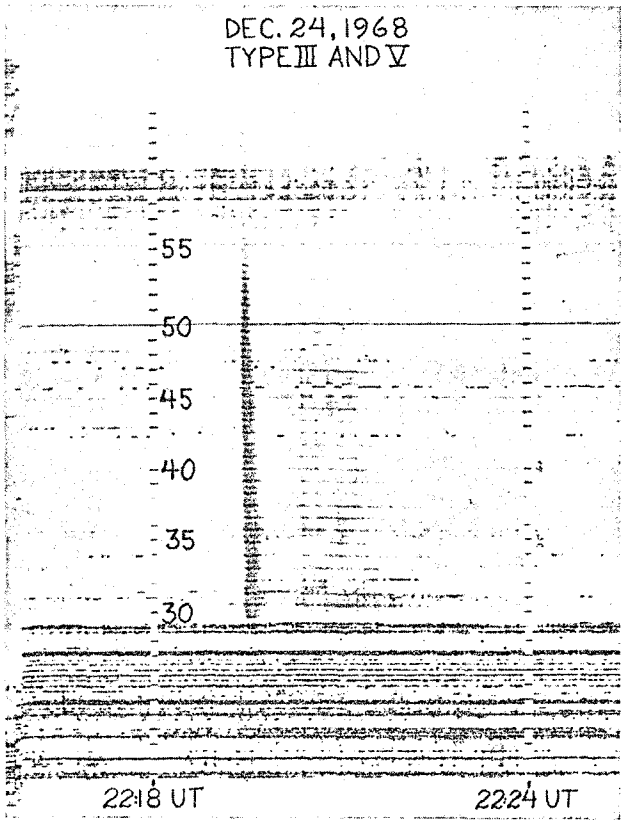

Fig. 2a. Interferometer record of a type III-type V burst observed on Dec. 24, 1968.

meter, the recognition of the fringe order essential for position determination is much less ambiguous. Consequently, the whole procedure of determining the electron density distribution is considerably simplified. From the width of the fringes, one can determine the angular extent of the emitting regions. In most cases, the fringe width is essentially unchanged, that is, the burst sources appear as point sources with respect to the angular resolutions of the array. In some cases, however, the fringes are broadened, which means that the burst sources have angular sizes larger than the angular resolutions of the array.

So far, we have been able to identify unambiguously one type III burst having both fundamental and second harmonic of the plasma frequency. This burst record is illustrated in Figure 1a. The harmonic feature is also clear from the intensity-frequency profiles shown in Figure 1b. We find that the harmonic position is situated systematically lower than the fundamental [Figure 1c]. This result is consistent with the hypothesis of combination scattering by which the plasma waves are converted into electromagnetic radiation.

In a few cases where we have observed type V in association with type III, the position determinations indicate that the type V source is 'detached' from that of type III by several arc minutes, although they both show similar dispersion in position with frequency. In the example shown in Figure 2, the type V source is located higher than that of type III. Such displacement in position is consistent with the type V emission being caused by electrons trapped between mirror points of arched magnetic field lines, whereas the type III is caused by electron streams escaping along neutral sheets into the interplanetary medium (Weiss and Stewart, 1965).

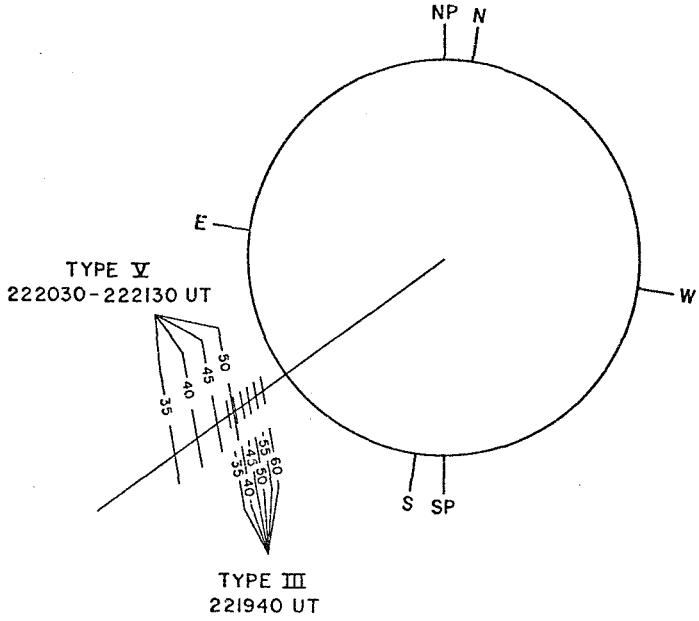

Fig. 2b. Positions of type III and associated type V as a function of frequency. The positions have been averaged over the durations of the type III and type V bursts.

3. Type IV Bursts

During and following large flares, type IV continuum radiation is observed – almost always associated with type IV at meter wavelengths. Even in our restricted frequency range, type IV is occasionally observed to occur in association with a type II which usually precedes it. Position determinations usually indicates a dispersion in frequency. Occasionally near the beginning of the type IV event, the radiation at all frequencies seems to come from the same region. This result is consistent with the commonly accepted interpretation of meter-wave type IV in the initial and late phases of the event. We shall illustrate the positional characteristics of the large events by describing the event of March 12, 1969.

The event of March 12, 1969: This event (Figure 3) is interesting in many respects. A flare occurred at 1735 UT near N10W80, Imp 2B. The flare reached its maximum at 1742 UT with erupting filaments. The prominence reached a height of 0.5 R_0 around 1743.5 UT when the radio event started with a type II. No harmonic has been reported for this type II, although there is a suggestion on our records that a harmonic might have been present. The type II source position (Figure 3b) shows the characteristic dispersion in frequency: however, it moves to a lower position toward the end of the burst (around 1754 UT). If the harmonic is present, then the lower position at later times at the same frequency is quite consistent with the interpretation that the harmonic is due to combination scattering (Smerd *et al.*, 1962). In the absence of a harmonic, one has to interpret this movement as tangential to the surfaces of constant electron density (Weiss, 1963). It is also possible that the type II burst was caused by multiple shocks, the later burst at lower altitude being the result of a different shock travelling on a path inclined to that of a first shock with slower speed. Indeed, the careful analysis by McCabe (private communication) of Hα prominences indicate the existence of multiple trajectories along which the prominence material travelled. The type IV emission at our wavelengths started at 1759 UT. The position determinations indicate a frequency dispersion which is similar to, but smaller than, that observed for type II. The initial 'synchrotron' source which would be indicated by all frequencies coming from the same region, does not seem to be present on our records. It is quite possible, however, that a synchrotron source exists simultaneously with, but is swamped by, the source of plasma radiation which is much stronger. At a later time, at $\sim$1830 UT, such a source tends to show up when the 'plasma' source is weak. The source of type IV remains more or less stable within a height range of 2.3 to 3.1 R_0. It is interesting to note that the prominence which started at 1744 UT developed into a looped structure (Figure 4) at a height of approximately $1R_0$ where it was visible until about 2112 UT.

Although the characteristic dispersion of position with frequency is nicely seen in many large continuum events such as that of March 12, 1969, the positional measurements of large complex events are often difficult to interpret, particularly if there are two or more sources simultaneously present on the Sun. In general, in decameter-wave type IV associated with flares, we mostly see a smooth continuum; only occasio-

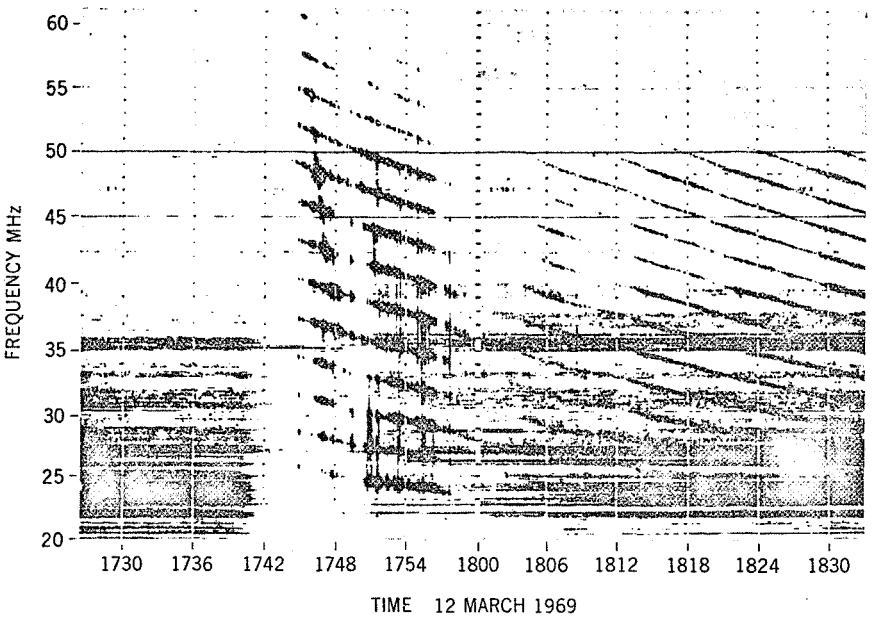

Fig. 3a. Interferometer record of a type II-type IV event observed on March 12, 1969.

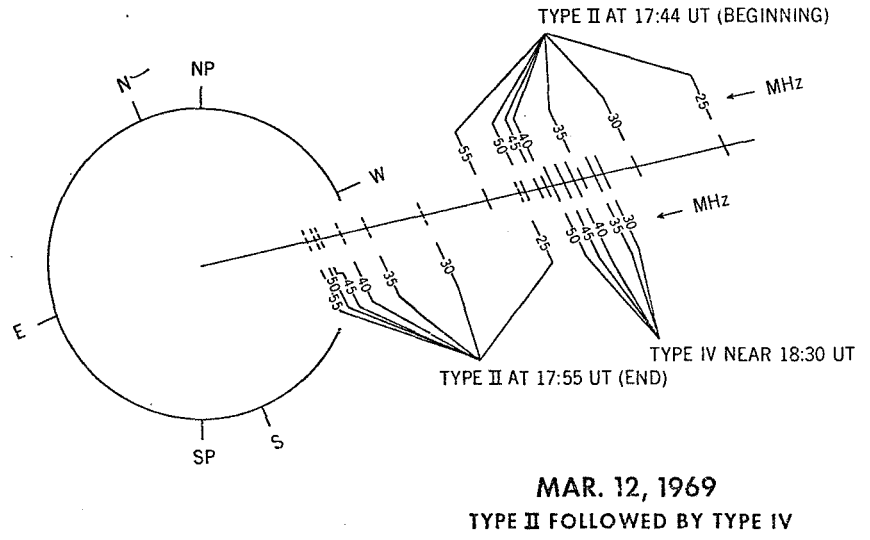

Fig. 3b. Positions of type II and type IV bursts as a function of frequency at some representative times in course of the event.

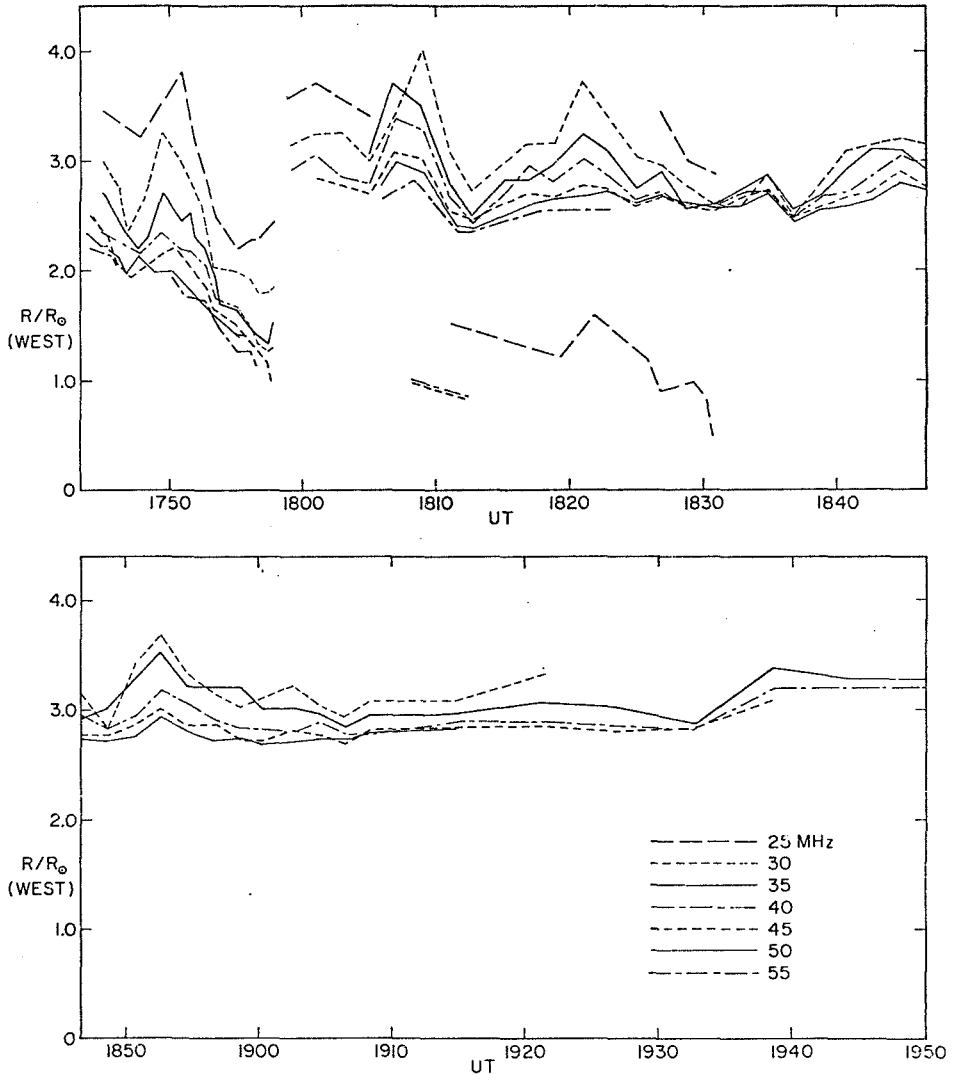

Fig. 3c. Positions of the composite type II-type IV event as a function of frequency and time.

nally we see structure resembling a continuous series of type III. Regarding the type IV power spectra at decameter wavelengths, we do not observe any decrease in intensity with decreasing frequency. On the contrary, sometimes we observe a continuum at 20–30 MHz but not at higher frequencies. This observation is not consistent with the Razin-Tsytovich Effect of the plasma on the synchrotron radiation. This effect predicts that if the plasma in which the synchrotron radiation is generated is dense enough to influence the refractive index of the medium, then the intensity should decrease very steeply with decreasing frequency (Ramaty and Lingenfelter, 1967). However, this kind of power spectrum may be quite consistent with the origin of

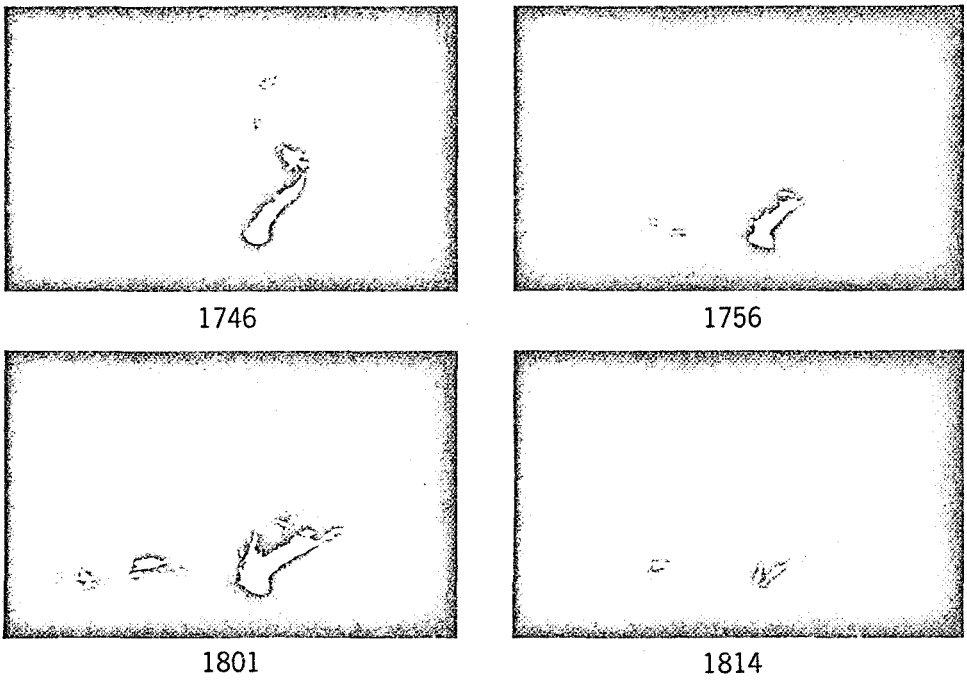

Fig. 4. Hα coronagraph pictures of the prominence observed during the type II-type IV event of March 12, 1969 at some representative times. The times are in UT.
(Courtesy: Institute for Astronomy, University of Hawaii.)

type IV in plasma radiation. Since we see the 'synchrotron part' of the source only occasionally at the beginning of a type IV, we can conclude that the Razin effect probably plays an important role in suppressing the decameter wavelength type IV of synchrotron origin.

4. Discussion

The positions of type III bursts at decameter wavelengths show the same characteristic dispersion with frequency as that observed at meter wavelengths. The second harmonic of type III is situated systematically at a lower level than the fundamental. Both these results are consistent with the currently accepted interpretation of type III generation, namely the excitation of plasma waves by electron streams and subsequent conversion of longitudinal plasma waves into transverse electromagnetic waves by scattering on density and charge fluctuations. When a type V burst follows a type III, it is found that the type V position is displaced from that of type III, but shows similar dispersion with frequency. This is consistent with the interpretation that, like type III, the type V is due to plasma radiation, but it is excited by an electron stream different from that producing the type III. It is possible that type V is caused by electrons trapped between mirror points of arched magnetic fields, whereas type III is caused by electron streams escaping along neutral sheets into the interplanetary medium (Weiss and Stewart, 1965; Zheleznyakov and Zaitsev, 1968). However, the

higher position as well as higher dispersion of type V relative to those of type III found in one case is not necessarily consistent with the interpretation of Zheleznyakov and Zaitsev (1968) that the type V, like type III, is generated primarily at twice the electron plasma frequency. It is obvious that we need further positional data in order to better understand the generating mechanism of type V.

Two conclusions emerge from studies of large events with the present equipment. First, the type IV burst at decameter wavelengths shows the same kind of complexity as that observed at meter wavelengths, probably being made of two parts, a 'synchrotron' one and a 'plasma wave' one. The first seems to be less frequent than on meter wavelengths, probably due to the Razin effect. The source of type IV at 20–60 MHz is, on the average, much higher in the solar atmosphere than at meter wavelengths, the height increasing with decreasing frequency. One can conclude that the source of decameter continuum is quite distinct from that of meter-wave continuum. This is consistent with the plasma origin of decameter continuum. Secondly, in large complex events when there are several sources at the same time on the sun, the one-dimensional positional measurements do not lead to easy and meaningful interpretation. The only way this difficulty can be overcome is by making fast two-dimensional maps of the sun at decameter wavelengths.

Acknowledgement

The University of Maryland's participation in this work was supported by the National Aeronautics and Space Administration under grant NGR 21 002 029. The operation of the Clark Lake Radio Observatory is also supported by the National Science Foundation under grant GP-12537.

References

Kundu, M. R.: 1965, *Solar Radio Astronomy*, John Wiley-Interscience Publishers, p. 329.
Ramaty, R. and Lingenfelter, R. E.: 1967, *J. Geophys. Res.* **72**, 879.
Smerd, S. F., Wild, J. P. and Sheridan, K. V.: 1962, *Australian J. Phys.* **15**, 180.
Weiss, A. A.: 1963, *Australian J. Phys.* **16**, 526.
Weiss, A. A. and Stewart, R. T.: 1965, *Australian J. Phys.* **18**, 143.
Wild, J. P., Sheridan, K. V., and Neylan, A. A.: 1959, *Australian J. Phys.* **12**, 369.
Zheleznyakov, V. V. and Zaitsev, V. V.; 1968, *Soviet Astron.-AJ* **12**, 14.

METER AND DECAMETER WAVELENGTH POSITIONS OF SOLAR BURSTS OF JULY 31–AUGUST 7, 1972

M. R. KUNDU and W. C. ERICKSON

Astronomy Program, University of Maryland, College Park, Md., U.S.A.

(Received 24 August, 1973; revised 30 January, 1974)

Abstract. The positional analysis of solar bursts at meter and decameter wavelengths observed during the period July 31–August 7, 1972 is presented. Most of the activity during this period was associated with the active regions McMath 11976 and 11970. Except near the CMP of region 11976, two regions of continuum emission were observed – one a relatively smooth continuum and the other a continuum superimposed with many type III's and other fine structure. It seems possible to interpret these continua in terms of plasma waves originating from two sources located at different heights or with different electron density gradients. The angular size of type III sources seems to increase with decreasing frequency. This implies that the open field lines along which the type III electrons travel have larger angular extent at greater heights.

1. Introduction

During July 30–August 7, 1972, a series of solar radio storms occurred. These storms produced intense type III bursts and continuum storms in the frequency range 10–120 MHz. Studies of these bursts and other associated electromagnetic radiation, including the Hα flares, have appeared in a number of published papers. In the present paper we present the results of positional analysis of burst sources in the range 10–120 MHz during this period of spectacular solar flare activity.

The observations were taken with two arrays – a log periodic array of 16 elements situated on an E–W base line of 3.3 km (Erickson and Kuiper, 1973) and portions of the new Clark Lake array in the form of a Tee (an E–W arm of 32 log spiral antennas and a N–S arm of 16 similar antennas). The new array (Erickson, 1973) operates over the frequency range 10–120 MHz and has angular resolutions of approx. 3'.5 at 100 MHz and 8'.5 at 40 MHz in the E–W direction. In the N–S direction the instrument has a resolution of 6' at 100 MHz and 15' at 40 MHz.

During this period the activity was often so complex that we represent it only by 'snapshots' taken at representative times. We then note the times when significant changes appear to occur. Positions will be given for the apparent center of activity. No corrections have been made for ionospheric refraction and the positions are most reliable within about 2 hr of solar transit (~1945 UT). In assessing the significance of the positions that we give, the limited angular resolution of the instrument and the large angular size of some of the emissive regions must be borne in mind.

A photograph of some of the original data is presented in Figure 1. In Figures 2 to 5 we diagramatically represent the data. We generally give three positions, a high frequency position in the 90–110 MHz range, an intermediate frequency in the 60–80 MHz range and a low frequency in the 30–50 MHz range. The lower frequencies

Solar Physics 28 (1974) 477–485.

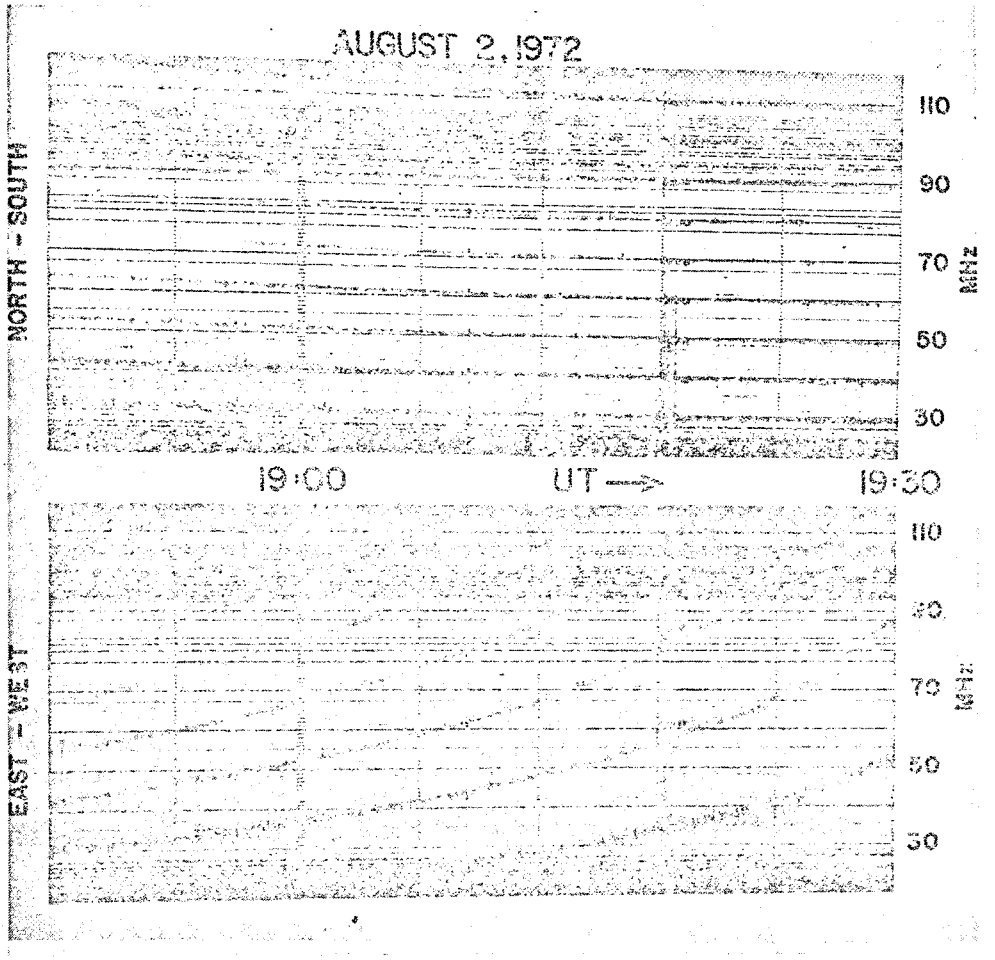

Fig. 1. Radio spectrograms of solar continuum obtained during the period 1848–1930 UT on August 2, 1972. These recordings were taken with swept frequency receivers attached to the output of and E–W grating arrays. The receivers sweep the 20 to 120 MHz spectrum twice per second; as they sweep, lobes of the grating array's response cross the Sun. Determination of time and frequency gives the position of the source. The rather steady sloping bands of continuum originate in regions Ca and Cb as shown in Figure 2. The type III bursts at 1918–1920 UT originate in a region in the S–W (see Figure 2). Interference below 30 MHz and FM transmissions in the 88 to 108 MHz are plainly visible.

are omitted when the Sun is far from transit, since they would be seriously disturbed by ionospheric refraction. The exact choice of frequencies for each measurement depends upon the frequency range of the emission, the positions of the antenna lobes and freedom from terrestrial interference.

If two identical sources are scanned with the perpendicular fan beams of our system, the data are generally ambiguous because the two fan beams intersect at four points where the sources could be located. However when we observe double regions

of solar emission this ambiguity practically never arises because we can easily correlate the intensity variations observed with the E–W and N–S arrays to uniquely determine the position of each source.

2. Observations

The activity in the frequency range 20–120 MHz during the period July 31–August 7, 1972 was mostly in the form of type III and continuum events. The type III's appeared to be associated with two regions McMath 11976 and 11970, and after August 3, possibly also with the region 11977. The source of continuum emission which was sometimes double in structure was associated only with the region 11976. In what follows we give a brief description of important features of the 20–120 MHz activity by means of selected 'snapshots' (Figures 2 to 5).

Several type III bursts observed on July 31 between 1833 and 2014 UT were apparently associated with the region 11976. The burst source (only E–W position available) was situated about 1.3 R_0 E from the center of the Sun. On August 1, a strong group of III's observed between 2118.5 and 2120.5 UT was most likely associated with the region 11970. The burst position showed considerable dispersion in frequency (Figure 2). On August 2, a continuum source apparently associated with the region 11976 existed from the start of the observations. Type III bursts were occurring frequently on this day and until 1907 UT were all located near the S–W limb, apparently associated with the region 11970. A type V was observed at 1801.5–1803 UT below 65 MHz and was considerably displaced in position from the accompanying type III. Around 45 MHz the type V was distinguished from type III by its narrow angular size (Figure 2). The large impulsive flare that occurred in region 11976 at ~1840 UT produced no radio emission in the 20–120 MHz range. However, at about 1900 UT a second continuum appeared at ~0.2 R_0 E of the first continuum in the 70 MHz frequency range, also apparently associated with region 11976. It was smooth and of small angular size. At 1907.5 the first type III occurred in the N–E quadrant (Figure 2) – possibly associated with the activity in McMath 11976. At 1918 UT there was another strong type III group in the S–W quadrant (Figure 2). Dodge (1973) placed this type III group in the N–E quadrant but a glance at Figure 1 shows that the lobes of this group are clearly to the high frequency (western) side of the continuum source. About 1920 UT the second continuum intensified in the 80 to 110 MHz range and by 1924 UT the two continuum sources were clearly resolved at 110 MHz (Figure 2) and the second one became bursty. At 70 MHz the two continuum sources were unresolved in the E–W direction and barely resolved in the N–S direction. At 40 MHz the continuum source was of large angular size and was centered S–E. At 2018 UT a type IIIg occurred at high frequencies (~100 MHz) at the N–E limb. This region developed into a continuum which started to increase in intensity after 2018 UT below 50 MHz. By 2033 UT the emission spread over the entire frequency range 20–120 MHz and saturated the receiver. This extremely intense emission was associated with the second large flare in region 11976

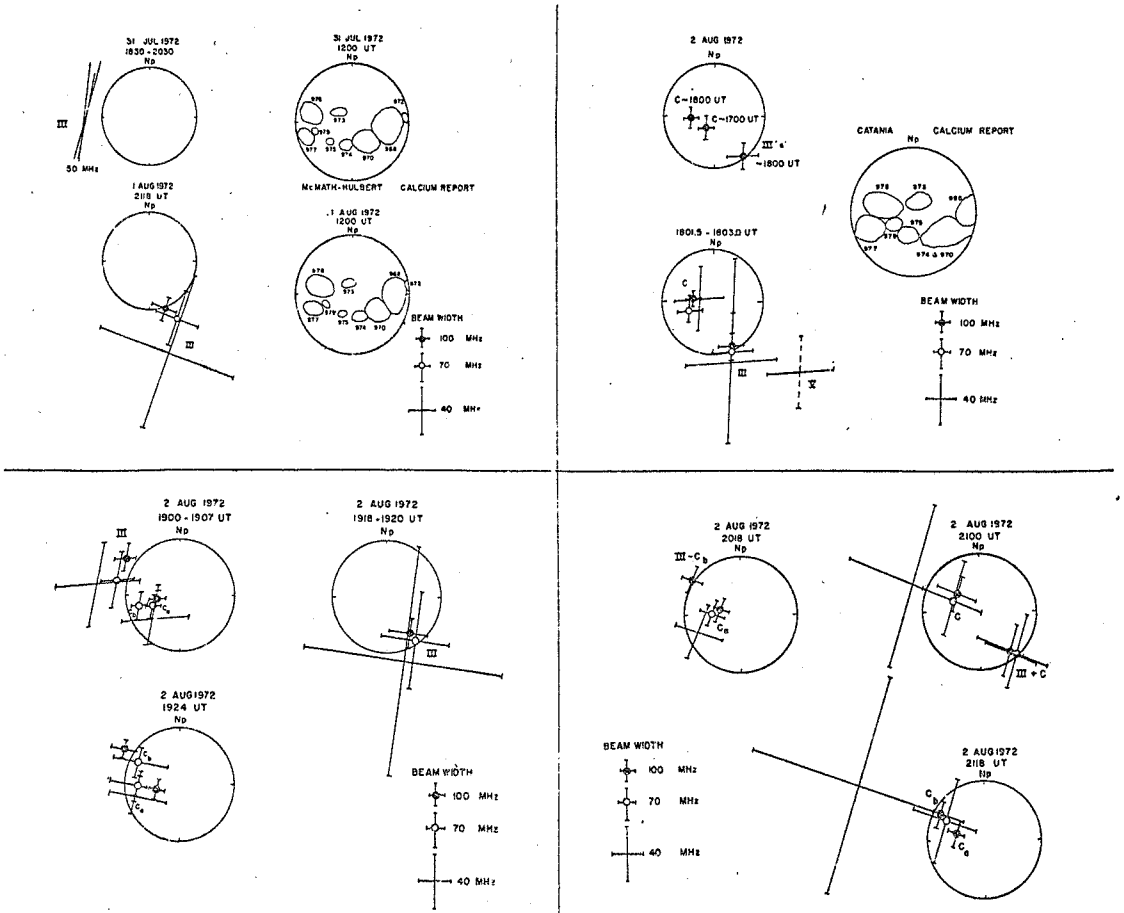

Fig. 2. Positions of the solar bursts for July 31, August 1 and August 2 (1900–2118 UT) along with McMath-Hulbert Calcium reports. For July 31, the positions are indicated by the fringe lines of the E–W array. The big circle represents the optical disk. For August 1 and 2, the positions were obtained from a combination of both E–W and N–S data. The E–W and N–S sizes of the burst sources are indicated by the lengths of the lines aligned with the appropriate fringe angle. Also included is the Catania Calcium report for August 2.

at 2000–2030 UT. It is remarkable that this second flare which was very similar in structure to the one that occurred at ~1840 UT produced strong radio emission whereas the first one did not produce any obvious effect. At 2100 UT the continuum was in the N–E quadrant; it was strong in intensity and so large in angular size that its possible double structure could not be discerned. The 40 MHz position appears to be displaced to the east (by about 1 R_0) from the 100 and 70 MHz position. This shift is possibly due to the ionospheric refraction. About 2118 UT there were two reasonably smooth and distinct continua at higher frequencies of 100 MHz (Figure 2). At lower frequencies of 70 and 40 MHz we could recognize only one continuum which appears to have been disturbed by the ionospheric effects (Figure 2). Often the distinction between bursty and smooth continua is quite arbitrary. On many occasions a source will appear relatively smooth in the 100 MHz region while it is bursty at lower frequencies and appears as though it were the result of the superposition of many type III's or type I's. This is illustrated quite clearly in Figure 1 between 1848 and 1906 UT. On the other hand, there do exist definite type III's which are usually displaced from the continuum (e.g. at 1919 UT in Figure 1).

On August 3, smooth continuum existed all day – situated about 0.4 R_0 E from the center (Figure 3). There was only small dispersion in position with frequency. Around 1742 UT, starting at higher frequencies and spreading gradually to lower frequencies there appeared groups of short duration (~1 s) narrowband (2–3 MHz wide) type I-like bursts. But about 1745 UT these bursts occurred at random over the entire frequency range and continued throughout the day.

The smooth continuum continued through the first part of the next day (August 4). During the period 1600–1800 UT the continuum at 110 MHz was located ~0.2 R_0 S from the center (Figure 3). The angular size of the continuum was large (~1.2 R_0) at 60 MHz and smaller at 30 MHz. Below about 50 MHz the emission consisted mostly of type III's superimposed on a weak continuum. The type III's were located in the same position as the continuum (on-band), between the regions McMath 11976 and 11977. At 2030 UT the continuum position at frequencies above 70 MHz remained near the center but it was shifted by 0.8 R_0 to the SE at lower frequencies where the emission was mostly type III's.

On August 5, both continuum and type III's were still observed. At 1830 UT, the continuum at 110 MHz was barely resolved, indicating possible double structure. The two components (both narrow in size) were located at the center and 0.2 R_0 W. At 1900 UT the continuum source was definitely double at both 100 and 70 MHz and was located in the N–W quadrant at 0.3 R_0 and 0.8 R_0 from the center. At lower frequencies the emission consisted mostly of type III's located at the W-limb. At 1924 UT the continuum located near the center became bursty at 100 and 70 MHz; at 40 MHz only one bursty continuum appeared at 0.7 R_0 W from the center. Later the continuum at 40 MHz showed double structure and the easterly one was bursty as shown in Figure 4 for 2018 UT. By 2100 UT the previously observed smooth continuum source at 100 MHz had almost died and the bursty continuum became

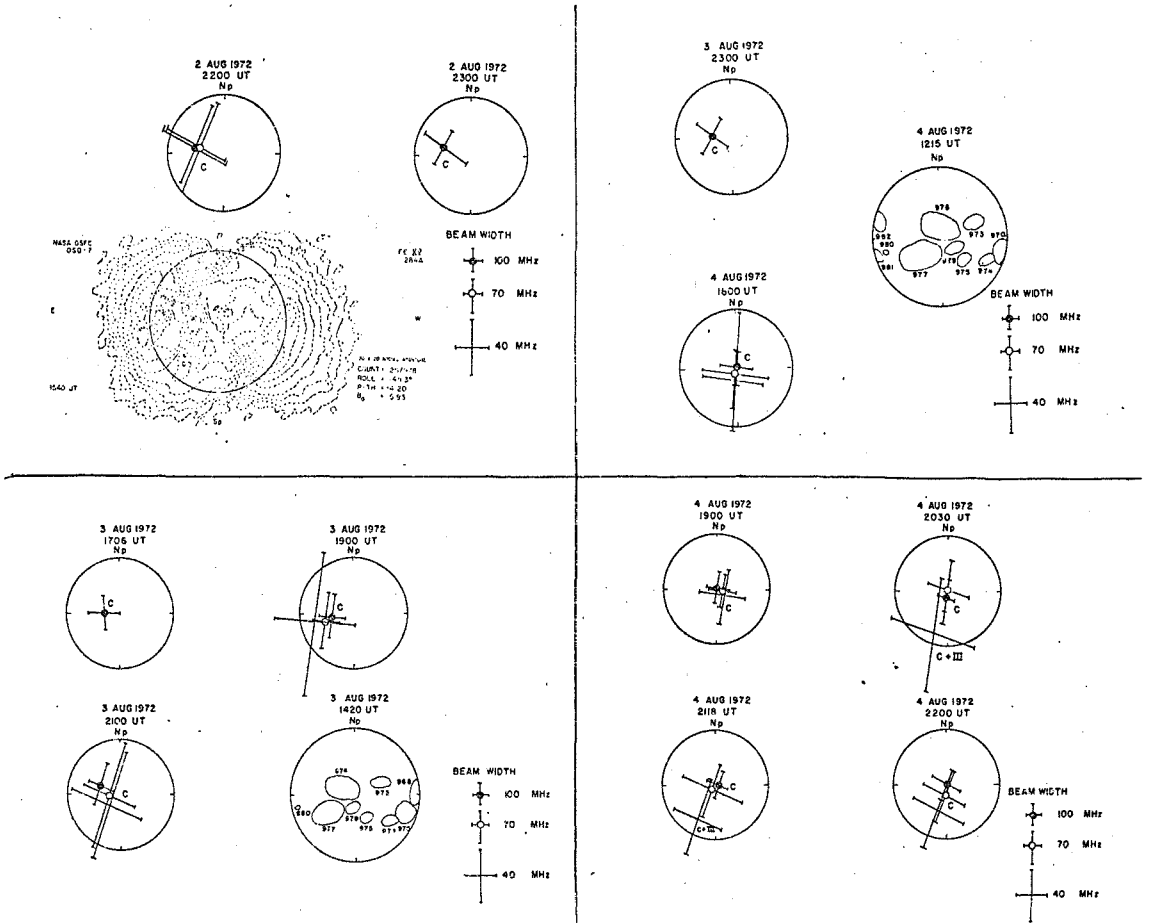

Fig. 3. Positions of bursts observed on August 2 (2200–2300 UT), August 3 and August 4, along with the Fe xv line (284 Å) map for August 2 obtained by NASA-GSFC OSO-7. The radio positions are indicated in the same way as in Figure2. Also included are the McMath-HulbertCalcium reports for August 3 and 4.

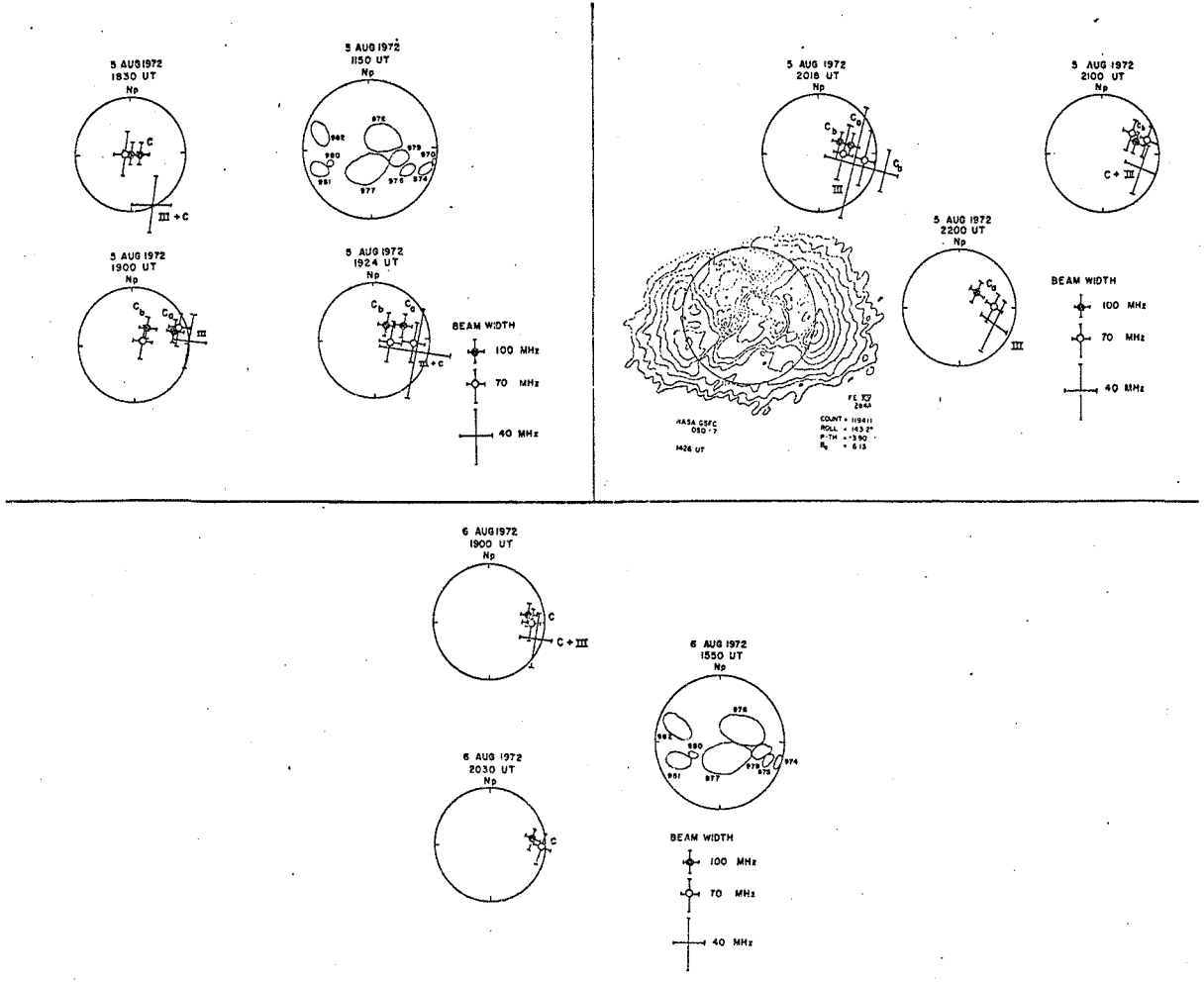

Fig. 4. Positions of bursts for August 5 and 6, together with the McMath-Hulbert Calcium reports. Also included is the Fe XV line (284 Å) map for August 5, obtained by NASA-GSFC OSO-7. The radio positions are indicated in the same way as in Figure 2.

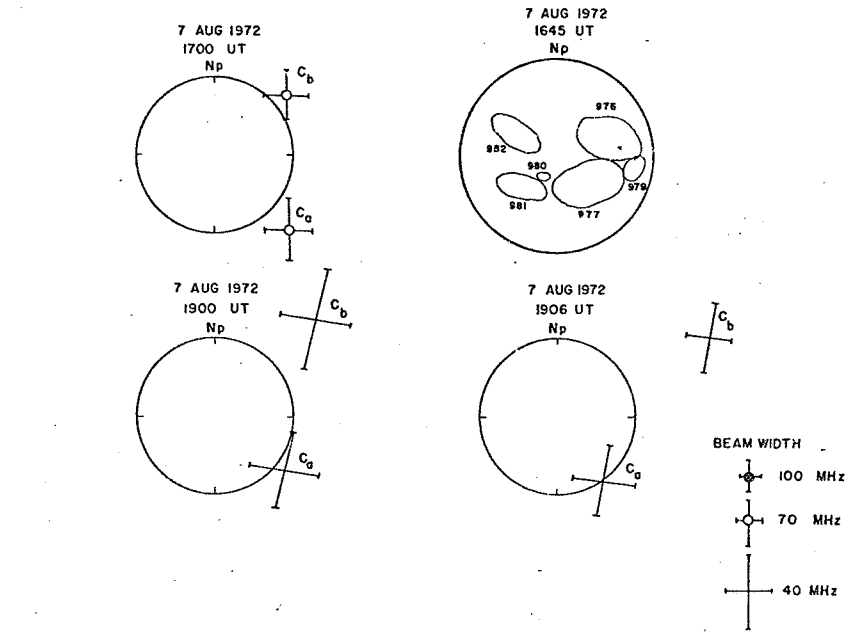

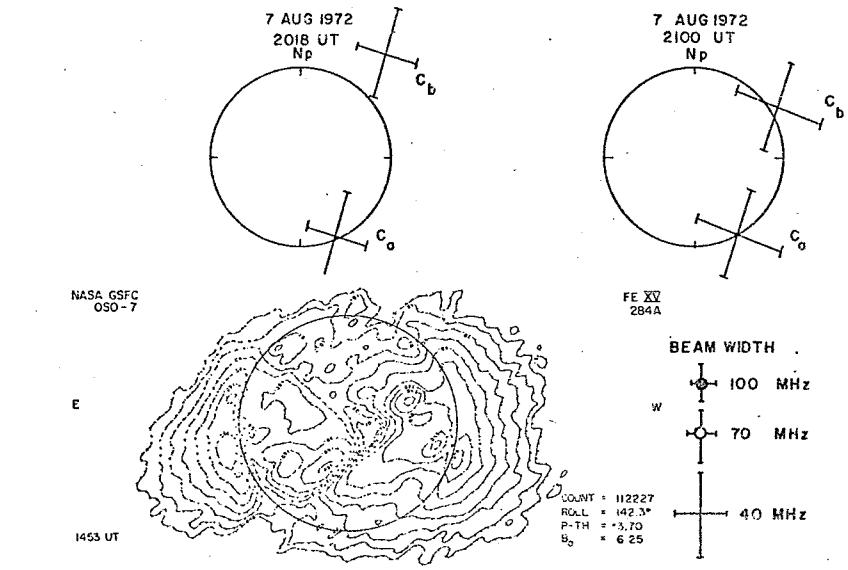

Fig. 5. Positions of bursts for August 7, together with the McMath-Hulbert Calcium report and the Fe XV line (284 Å) map obtained by the NASA-GSFC OSO-7. The positions are indicated in the same way as in Figure 2.

smooth and stronger (Figure 4). At 70 MHz a part of the smooth continuum was still visible, the two positions being in the N–W quadrant at 0.4 R_0 W and 0.7 R_0 W. At 40 MHz the continuum source with type III's was of large angular size and was located at a position intermediate between those of the two continua observed earlier.

On August 6, the emission was mostly smooth continuum except that there were some on-band type III's randomly distributed around 1700 UT. The intensity was stronger at higher frequencies. The source was located about 0.8 R_0 N–W, with some dispersion in position (Figure 4). At 40 MHz the emission consisted mostly of type III's plus a very weak continuum.

On August 7, a great flare occurred around 1510 UT in the region McMath 11976, with its maximum at 1530 UT. Our observations began at 1600 UT in the post-maximum phase of the flare. Initially, the continuum was smooth; very strong at lower frequencies and weak at the high frequency end. At 70 MHz it was located at an apparent position of 2.5 R_0 S–W. At this time of the day there may have been considerable ionospheric refraction effects at 70 MHz. At 1700 UT the source was double – 1.3 R_0 S–W and 1.2 R_0 N–W at 70 MHz (Figure 5). The northern source was bursty. Both continuum sources were weak at higher frequencies. Groups of type III's continued to occur between the two continuum sources as well as on both continuum sources. By 1900 UT the continuum was very weak at higher frequencies. At 35 MHz the source was double – located at 1.1 R_0 S–W and 1.8 R_0 N–W (Figure 5). At 1905–08 UT the northern bursty continuum source became smooth and moved to the west (Figure 5) from 1.8 R_0 at 1900 UT to 2.2 R_0 at 1906 UT. This motion corresponds to a velocity of 1400 ± 400 km s^{-1}. This moving source appears to be an ejection from the continuum source 'C_b' and by 1909 UT it had disappeared completely. By 2018 UT both continuum sources appeared at lower frequencies; they were fairly smooth and were located at 1.0 R_0 S–W and 1.4 R_0 N–W (Figure 5). At 2100 UT the source had the same appearance.

3. Discussion

Most of the activity during the period July 31–August 7, 1972 was associated with the regions McMath 11970 and 11976; another region McMath 11977 possibly became active after August 3. One important characteristic of the region 970 was that no continuum was observed in association with it; only type III's and a type V were observed from this region. The radio emissive activity in region 970 generally intensified during the period of strong activity in region 976. Indeed, the strong type IIIg that occurred at 2100 UT on August 2, followed the maximum of the flare that occurred in region 976.

The continuum emission during this period appears to be associated mostly with the region 976. Frequently, the source was double with one component a relatively smooth continuum and the other a continuum with superimposed type III's and other fine structure. It is interesting to note that the double structure of the source disappeared around the central meridan passage (CMP) of the region (August 3–4) and

appeared again on August 5. On August 6 we also observed only one component but the intensity of the emission had decreased considerably and one of the components may have been too weak to be observed.

The sources at decameter wavelengths (40 MHz), whether they produce continuum or type III's appear to be very well associated with corresponding regions on the OSO-7 maps of Fe XV line at 284 Å (see Figures 3, 4 and 5). This close correspondence between the two possibly indicates that the decametric emissive regions originate in about the same level of the Sun's corona as the Fe XV line.

In general, there appears to be some dispersion of continuum position with frequency. This is true for observations near local transit and when the source is away from the disk-center. For observations at large hour angles, ionospheric effects may be important and the frequency dispersion is not always apparent. We might remark that the continuum sources are narrower in angular size at higher frequencies than at lower frequencies. In general, the sources appear very broad at 40 MHz, especially when the continuum is strong. The size at low frequencies also appears broad when there are type III's superimposed on the continuum. The continuum source at both meter and decameter wavelengths appears to be stationary and it shows some dispersion in position with the frequency. It is generally accepted that such stationary continuum radiation can be produced by Čerenkov plasma waves.

The observed double structure of the continuum source is obviously related to the existence of two separate component sources. If the two component sources were displaced laterally, there would be greater separation between them near the CMP of the region. The fact that the double structure appears only when the region is away from the CMP may imply that the two component sources are situated at different heights. A consequence of this displacement in height is that the higher source should appear farther from the center on either side of CMP. This seems to have been observed, although we cannot unambiguously distinguish between two components, since both contain bursty structure.

As we know, the continuum emission results from plasma radiation propagating in the ordinary mode in a strong magnetic field (Takakura, 1963). Therefore, it is conceivable that the two component sources are situated either along two streamers with different densities or more likely, one along a streamer with open field lines and the other in the strong magnetic field lines above an active region, somewhat similar to the model proposed by Stewart and Labrum (1972). Open field lines provide a path for the type III electrons; the electrons seem to be ejected continuously from the continuum which therefore appears bursty. The relatively smooth continuum source is situated in the closed field lines. In our frequency range, we see very few type I's on the continuum; sometimes at the lower frequencies we see type I – like bursts constituting and superimposed on the continuum. In this context, we might consider the mechanism proposed by Gordon (1971), in which the low phase-velocity plasma waves (responsible for type I bursts) are scattered to high phase velocities (0.1–0.6 c). These waves are ultimately responsible for the acceleration of type III electrons. One consequence of such a mechanism is that it may produce

type I and type III bursts from the same source; this seems to have been observed to some extent. This simple interpretation seems to be borne out by the result that the continuum systematically appears at a lower height than the type III's. The only exception to this appears in the case of the flare associated continuum observed on August 7, 1900 UT. We believe that in this case we were dealing with a continuum at decametric wavelengths, that had been ejected from the parent smooth continuum. In the Stewart and Labrum model one distinguishes between the type I and type III sources. However, at decameter wavelengths ($\sim$40 MHz) we often see continuum with superimposed fine structure which resemble type III's rather than type I's. Indeed, it is often extremely difficult to distinguish continuum from almost continuously occurring sources of type III's at decameter wavelengths. In their model, Stewart and Labrum postulated that the type III electrons are accelerated near the observed 80 MHz source position and that the required energy is released by the triggering of a magnetic instability at this point by a magnetohydrodynamic disturbance propagating from the type I source region. We often observe a relatively smooth continuum in the 90–120 MHz region; this continuum source, situated in the strong field lines above an active region, is a likely source of mhd waves. When sufficiently energetic mhd waves reach the top of closed field lines and trigger an instability at the cusp of a helmet magnetic structure, type III bursts begin to be observed. Our observations indicate that this height, where type III bursts start, is situated around 50–60 MHz plasma level.

We would like to draw attention to another property of type III bursts. The angular size of strong type III increases with decreasing frequency and sometimes reaches up to 4–5 R_0 at 40 MHz. However, we should point out that these intense low frequency bursts saturated the records and accurate angular size measurements were difficult. We do not believe that this large size can be fully accounted for by coronal scattering. Consequently, this result would imply that the open field lines along which type III electrons travel has a rather large lateral extent.

Acknowledgements

This work was supported by NSF grant GP-19401 and NASA grant NGR 21-002-367. The computer time for this project was supported by National Areonautics and Space Administration Grant NSG-398 to the Computer Science Center of the University of Maryland.

References

Dodge, J. C.: 1973, preprint, Solar System Radio Observations, SN-1, of the University of Colorado.
Erickson, W. C.: 1973, *Proc. IEEE* **61**, 1276.
Erickson, W. C. and Kuiper, T. B. H.: 1973, *Radio Sci.* **8**, 845.
Gordon, I. M.: 1971, *Astrophys. Letters* **5**, 251.
Stewart, R. T. and Labrum, N. R.: 1972, *Solar Phys.* **27**, 192.
Takakura, T.: 1963, *Publ. Astron. Soc. Japan* **15**, 462.

DETAILED CORRELATION OF TYPE III RADIO BURSTS WITH Hα ACTIVITY

I: *Active Region of 22 May 1970*

T. B. H. KUIPER

Clark Lake Radio Observatory, Astronomy Program, University of Maryland, College Park, Md. 20742, U.S.A.

and

JAY M. PASACHOFF*

Big Bear Solar Observatory, Hale Observatories, Carnegie Institution of Washington California Institute of Technology, Pasadena, Calif. 91109, U.S.A.

(Received 14 August, 1972)

Abstract. We compare observations of type III impulsive radio bursts made at the Clark Lake Radio Observatory with high-spatial-resolution cinematographic observations taken at the Big Bear Solar Observatory. Use of the log-periodic radio interferometer allows us to localize the radio emission uniquely. This study concentrates on the particularly active region close to the limb on 22 May 1970. Sixteen of the 17 groups were associated with some Hα activity, 11 of them with the start of such activity.

1. Introduction

Statistical studies of the correlation of type III bursts with flares showed that, at the maximum of solar cycle 19, 60% of these bursts occurred during the life of a flare (Swarup *et al.*, 1960). Only half of this number were truly associated with the flare, however, the remainder representing chance occurrences. It had also been noted that flares occurring in certain active regions showed a high degree of correlation with bursts, while those in other regions showed little or no correlation (Loughhead *et al.*, 1957). Zirin and Werner (1967) reported that Hα brightenings could usually be found at the times of strong type III bursts. Our more complete time coverage of both Hα structure and radio events justifies a re-examination of this correlation. Further, use of an interferometer allows us to localize the radio emission correlation. As a first step, we wish to report the detailed analysis of the activity in McMath 10743, a region showing inverted polarity, between 1700 and 2230 UT on 22 May 1970. This region was particularly well-suited for study as it was near the limb and especially active.

On that day, a series of spectacular surges occurred, including the one shown in Figure 1a (Zirin, 1971; Pasachoff, 1972). We have identified the various active parts of this activity center in Figure 1b. The most impressive surges appeared to be emitted out of region 5, streaming along 1. Streaming also followed 2 and 3, the latter being the more important. Surges along 3 generally appeared in 'mid-air' and then moved outwards. Surges along 2 appeared to come from the southern part of loop 4. Loop 4

* as of September 1972: Williams College-Hopkins Observatory, Williamstown, Massachusetts 01267.

Solar Physics **28** (1973) 187–196.

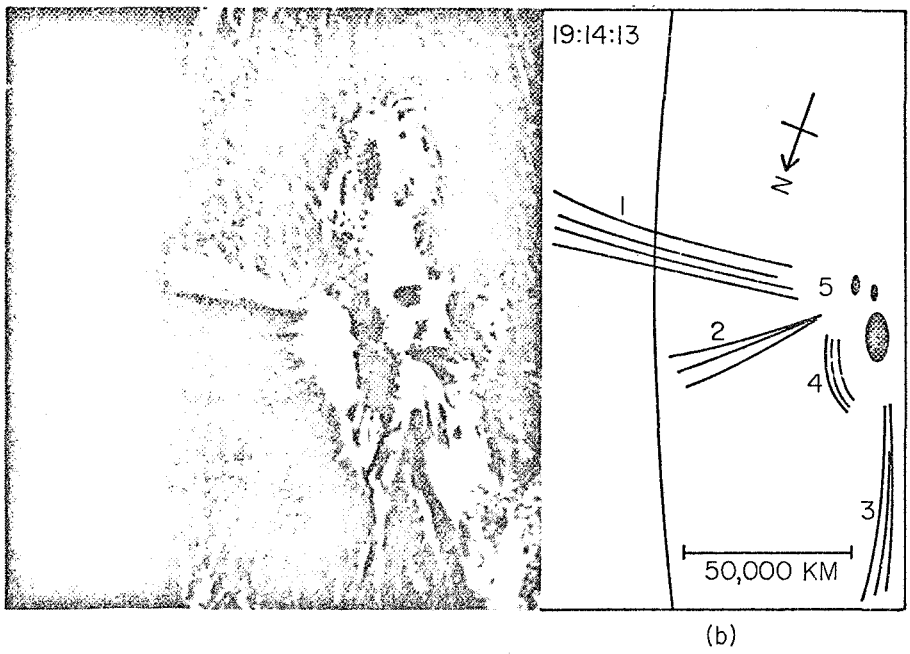

Fig. 1. (a) The spectacular surge of 19:05 UT on 22 May 1970 achieved its maximum extent at 19:14:13. This and all subsequent photographs have north to the bottom. (b) The active elements of the region. 1, 2 and 3 are trajectories along which material appeared to be ejected. 4 appears occasionally to be a closed set of field lines, though this feature is not apparent here due to the brightness of the flare. 5 is a plage region of complex structure in which the major flares occurred. (Big Bear Solar Observatory photograph.)

is not apparent in Figure 1 because of the bright flare. Figure 7 shows the best example of the loop structure in 4. The loop itself also showed activity, generally bulging outwards and then subsiding again. Within each group the flares seemed homologous. These events were photographed with a ten-inch refractor at the Big Bear Solar Observatory through a $\frac{1}{2}$ Å filter centered in the Hα line center. Exposures were made every fifteen seconds.

At the same time, a series of type III (impulsive) bursts were observed at the Clark Lake Radio Observatory on the log-periodic array. This instrument is a sixteen-element swept-frequency interferometer, having an east–west extent of 3.3 km. It scans from 65 to 20 MHz once per second. The principle of operation has been described by Sheridan (1963). Some early results were reported by Kundu *et al.* (1970).

2. Positions of the Radio Bursts

Since the Big Bear Hα cinematograph covers only one activity center at a time, any type III bursts without corresponding Hα activity could be attributed to centers not in the field. For this reason, it is important to observe the positions of the radio bursts.

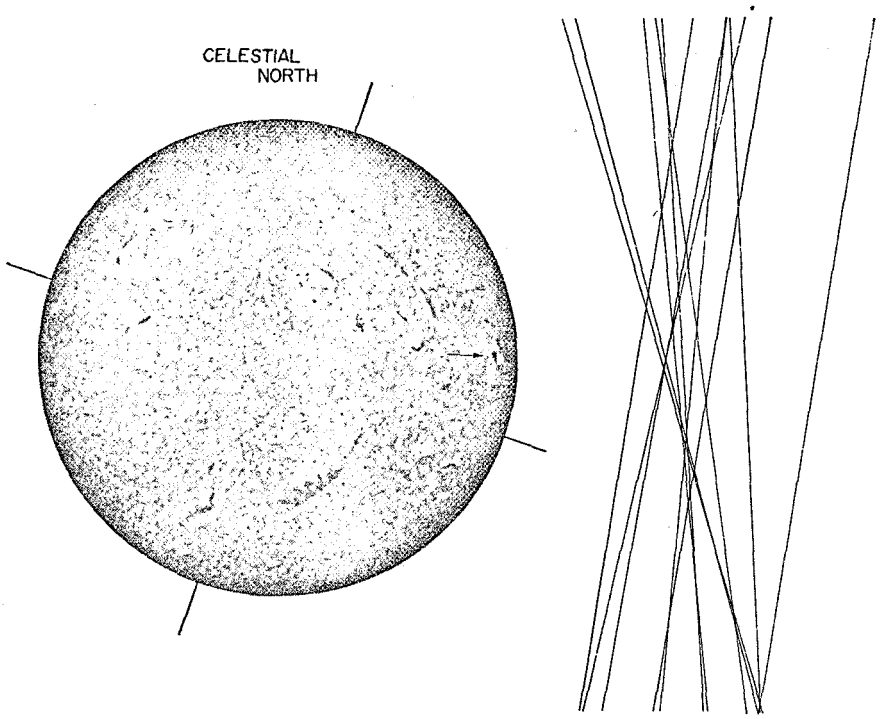

Fig. 2. The positions of the type III burst groups relative to the active region. The interferometer has only east-west resolution, so that the bursts may have occurred anywhere along the position lines plotted. The position lines have various tilts because the orientation of the interferometer baseline varies as the Earth rotates. (Lockheed Solar Observatory photograph.)

Figure 2 shows the 60 MHz position lines for the groups of bursts observed between 1700 and 2230. In this context, 'group' may mean either a single, isolated burst, or any collection of bursts separated by less than a minute. Since the array does not resolve in the north–south direction, we can only give a position line for each group; the bursts could have occurred anywhere along this line. As the Earth rotates, however, the orientation of the telescope changes relative to the Sun, just as the solar image reflected from a heliostat rotates. The intersection of the position lines observed at different times gives some measure of the north-south position, assuming that all bursts have about the same position. The source of radio bursts at 60 MHz appears to have been located above McMath 10743 on an extension of the lines of force implied by the structure seen in Hα in region 1. We note that the bursts lie considerably above the expected 60 MHz plasma level. If we assume that the bursts occur more or less radially above the active region, then they are at an apparent height of 1 solar radius. Ionospheric refraction effects are calculated not to exceed 0.2 radius. Because of the difficulties of propagation in a non-uniform corona and our lack of knowledge about whether the bursts represent fundamentals or harmonics, we cannot more properly assess the height of the bursts and hence infer coronal densities.

3. Detailed Description of the Correlation

In the description which follows, times are given to the nearest second, the resolution used at Clark Lake. It should be borne in mind, however, that the Big Bear frames were taken every quarter minute. In addition, there was a one-minute ambiguity in reading the minute hand of the Big Bear clock. It is thus possible that the times for the Hα events are one minute later, although we believe the stated times to be correct. The times of the type III events refer to a frequency of 60 MHz. At lower frequencies, times were a few seconds later because of the frequency drift of the bursts. The reader must also allow for a possible systematic error of a few seconds in the Clark Lake times.

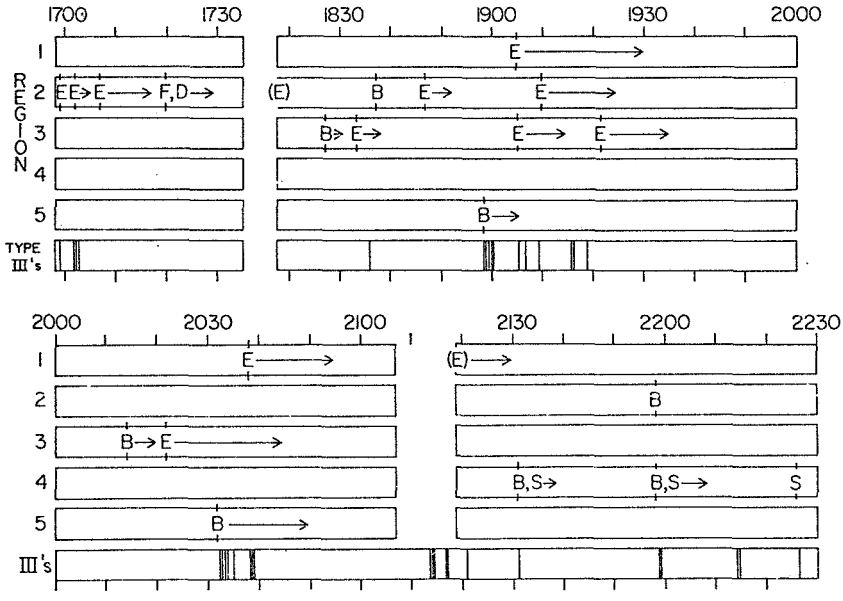

Fig. 3. A schematic representation of the activity in McMath 10743. The regions labeled 1 through 5 are identified in Figure 1. We use the following codes: B – brightening, D – diminishing, E – ejection, F – fan-like structure, S – stretching or bulging, ( ) – in progress, → – continuing.

Figure 3 is a schematic representation of the activity, and is useful for seeing the general correlation between type III bursts and Hα events. A detailed description of the correlation is given in semi-tabular form below. It is based on a study of the film sequence, part of which has been included in the 'show film' available from the Big Bear Solar Observatory (1971). For purposes of demonstration, certain details are represented in Figures 4 through 7.

The first event described was reported in *Solar Geophysical Data* as an unconfirmed subflare with several brilliant points, which lasted from 16:58 to 17:15.

'16:59:04–16:59:13 type II burst.

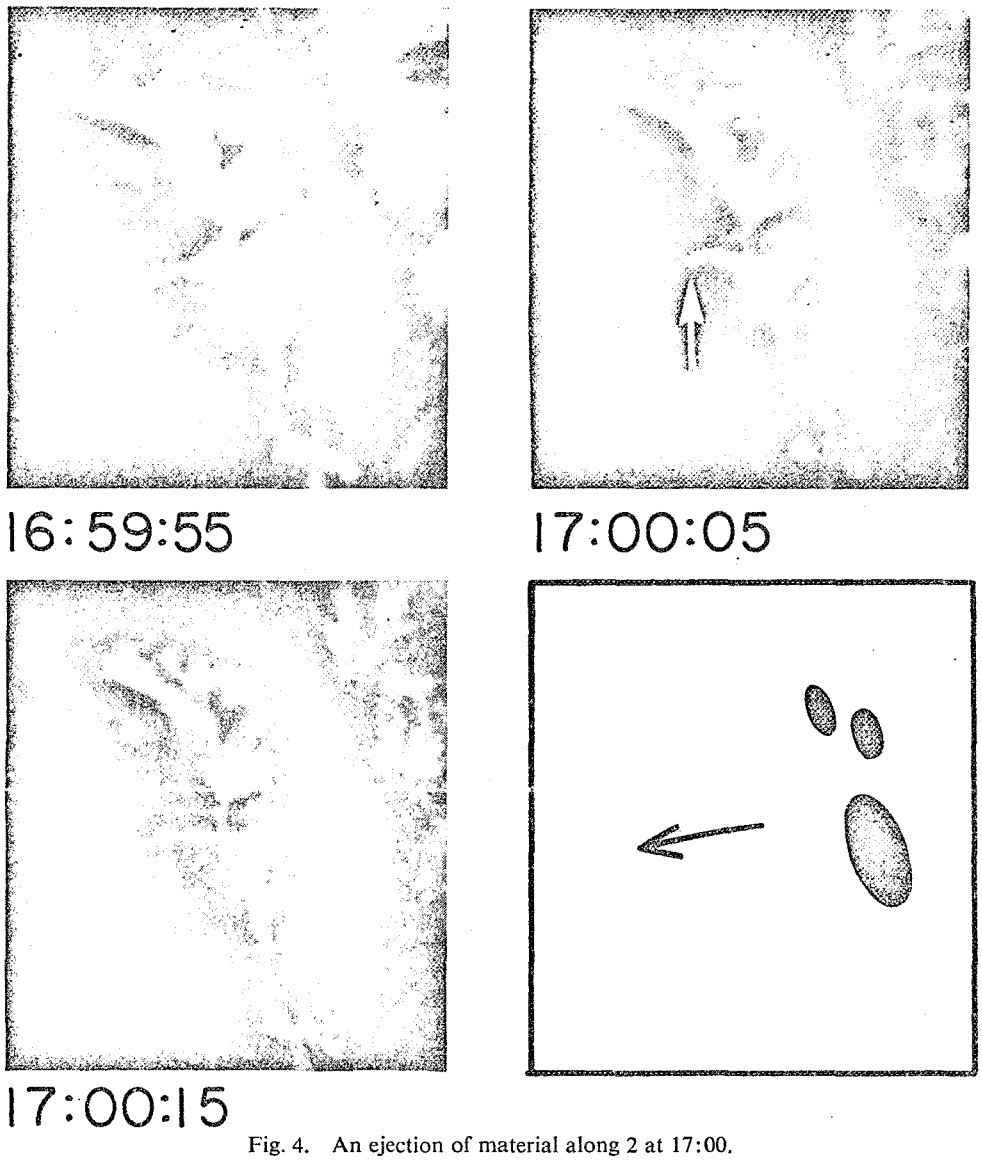

Fig. 4. An ejection of material along 2 at 17:00.

16:59:55 bright spot appeared at the base of 2 and was ejected (Figure 2).
17:02:02–17:02:10 type III burst.
17:02:05 some more bright material began to move along 2.
17:02:23–17:02:35 a pair of type III bursts.

17:06:55–17:20 a whole sequence of ejections along 2.
17:20 a dark fan-like structure became apparent at 2, and then gradually faded away.

The next series of events described were not reported in *Solar Geophysical Data*.
18:17:50 a small ejection of material along 2. No type III burst was recorded at Clark

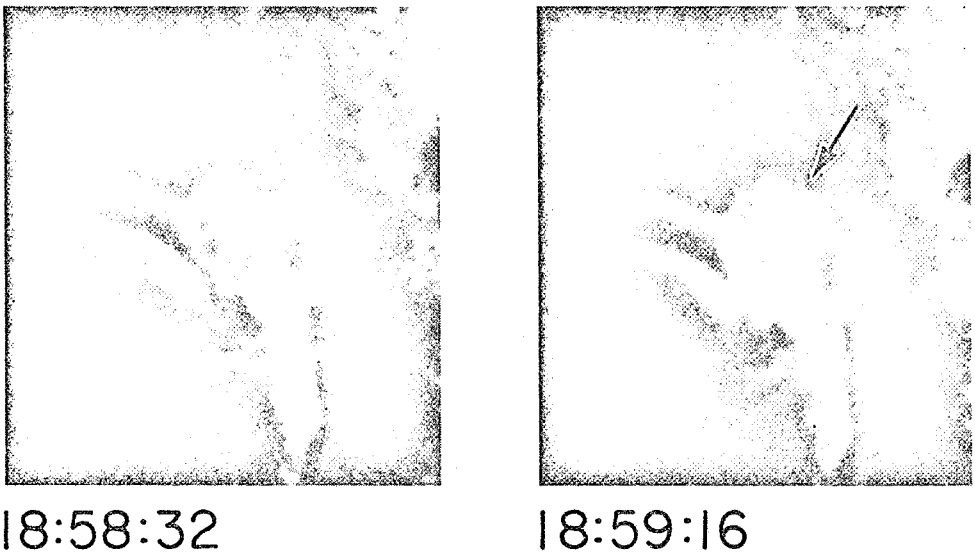

Fig. 5. The flare in region 5 at 18:59.

Lake, although Uccle Observatory in Belgium reported a small burst at 18:17, lasting half a minute, at 600 MHz.

18:27:25 a bright region at the base of 3 began to develop a small tail outwards along 3.

18:33:25–18:38:25 a faint ejection of material along 3.
18:36:01–18:36:11 faint type III burst.
18:37:40 the region at the base of 2 showed a brief brightening.

18:40:20 very faint type III burst.
18:46:50–18:53 a small spray in 2. No bursts were seen at Clark Lake but Uccle reported bursts at 18:43 and 18:51.

The main event of our mutual observing period was reported in *Solar Geophysical Data* as a confirmed bright subflare (Grp 30106) with several bright points and a high velocity dark surge, and lasted from 18:58 to 19:17, with a maximum at 19:01.

18:58:46 a sudden flare in 5 (Figure 5).
18:58:45–19:00:35 a strong, complex group of type III bursts.

19:04:45 material began to stream out of 1.
19:05:15 streaming along 3 became apparent (Figure 6).
19:05:19–19:05:29 type III burst of moderate intensity.
19:06:31 a weak type III burst.

19:09:19–19:09:50 a faint group of type III bursts.
19:10:00 streaming started along 2, while streaming along 3 had stopped.

19:15:20 a very faint type III burst.
19:15:51–19:16:01 a type III burst of moderate intensity.
19:16:17 a weak type III burst.

19:19:00 a very faint type III burst.
19:21:40 streaming appeared again in 3. Since this material appeared to condense out along the stream at this time, it seems likely that the ejection started at an

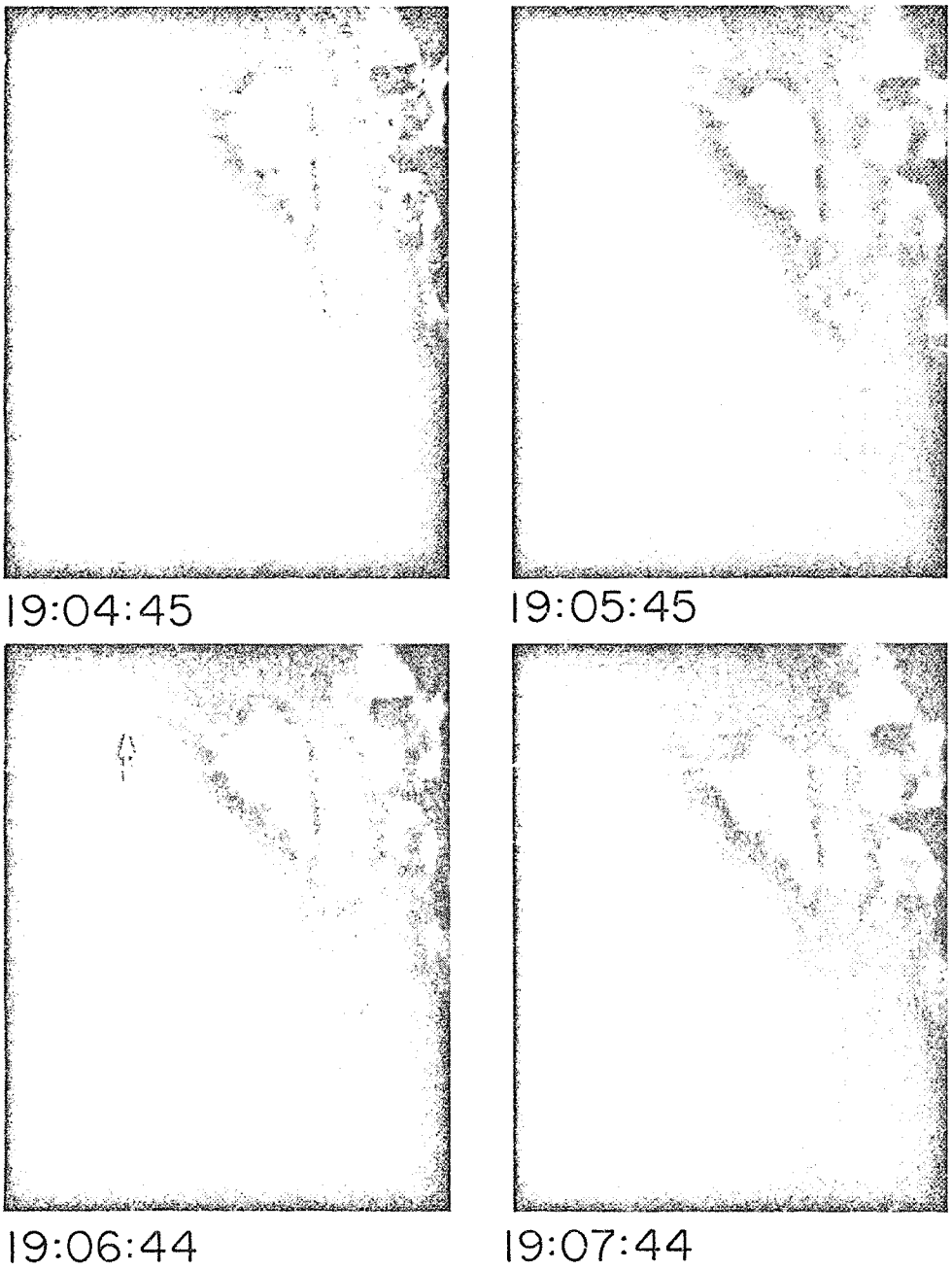

Fig. 6. Expulsion of material along 1 and 3 following the 18:59 flare.

earlier time nearer the active center, and may have been associated with the type III burst 3 min earlier.

19:35 activity ceased.

The next event was also reported as a confirmed subflare (Grp 30107) with several bright points, a

Fig. 7. Region 4 brightens and then develops a small hook attached to the southern foot. This may be similar to an outward 'bulge' of 4, but with bright material along only part of the bulging region.

high velocity dark surge, an extensive active region, and marked intensity variations in the active plage. It reportedly began at 20:27, reached a maximum at 20:38, and ended at 20:51.

20:14:10	brightening occurred at the base of 3.
20:21:50	streaming along 3 became noticeable.
20:32:05	region 5 began to brighten as streaming along 3 reached a maximum intensity.
20:32:34–20:34:08	an intense group of type III bursts.
20:34:45	brightening in 5 achieved its maximum.
20:35:14–20:35:19	type III burst.

20:38:00 faint streaming along 1 began.
20:38:38–20:39:02 faint group of type III's.

20:45 streaming along 3 stopped.
20:55 streaming along 1 stopped.
An unconfirmed subflare with an extensive active region was reported from 21:06 to 21:20, with a maximum at 21:10. There was no Big Bear coverage until 21:19:05.
21:13:55–21:14:42 a group of type III bursts of moderate intensity.
21:16:56–21:17:21 a pair of type III bursts.
21:19:05 Big Bear coverage resumed. Streaming along 1 was in progress.
21:21:01–21:21:07 type III burst.

21:31:00 the streaming along 1 had subsided when loop 4 suddenly brightened and bulged outward.
21:31:15 loop 4 achieved its maximum extension.
21:31:16 type III burst of moderate intensity.

21:35:30 outward motion along 1 became briefly apparent.
21:37 loop 4 returned to its normal configuration.
There was an unconfirmed subflare in progress at 21:57 which lasted until 22:12, according to *Solar Geophysical Data.*
21:58:25 a small bright spot appeared at the base of 2 and 4.
21:59:10–21:59:35 a group of type III bursts.
21:59:55 loop 4 began to bulge.
22:01:40 loop 4 achieved its maximum extension.

22:14:33–22:14:50 a pair of type III bursts.
22:15 a possible brightening in loop 4, weak enough to be attributed to seeing effects.
The last event described was not reported in *Solar Geophysical Data.*
22:25:30 loop 4 showed a faint brightening.
22:26:00 a small hook appeared to come out of the southern end of loop 4 (Figure 7).
22:26:13–22:26:23 type III burst.

4. Conclusions

We have found a very high degree of correlation of type III bursts with Hα activity. Of a total of 17 groups (as previously defined), 11 were clearly associated with the start of some activity in Hα. Five others occurred while Hα activity was in progress, but could not be associated with any specific phenomenon. Only one rather weak pair of bursts (2214) may have occurred during the absence of Hα activity, although even in that case there was a hint of some activity. Such a high degree of correlation could not have been detected without the resolution of the Big Bear observations. This may explain the lower correlation reported by previous workers. Further, the radio positions were isolated by use of an interferometer.

The occurrence of type III bursts was a necessary but not a sufficient condition for flaring in this active region. It is difficult to analyze this quantitatively because the Hα phenomenology is so complicated. Yet we have clear instance of Hα events for which no type III bursts were seen. We do not know of difference between type III-associated Hα events and those events which do not have type III's but shall investigate this point in subsequent studies. It is possible that, in the latter cases, no energetic

particles were produced, or alternately that they were produced but trapped. Analysis of X-ray and centimeter-wavelength data may clarify this point.

It is not possible to generalize from a single day's observations. Yet it is interesting that there are apparently some conditions under which the correlation of type III bursts with Hα events is high. In the majority of these cases, the events have a clearly impulsive character. The analysis of other periods of activity will determine whether this is a general property of type III bursts.

Acknowledgements

Our appreciation is due to Drs William C. Erickson and Harold Zirin, who initiated the collaboration between the Clark Lake Radio Observatory and the Big Bear Solar Observatory, and whose assistance and criticisms were invaluable to this work. We thank Drs E. v. P. Smith, R. G. Stone and D. Wentzel for their comments. Nancy Roth and Geoffrey Pressman assisted with the reduction of the radio activity records. Susan Mellerup, Robert V. Webber, and Robert Hippard aided with the Big Bear films in Pasadena.

The log-periodic array at Clark Lake is operated as a joint project between the Laboratory for Extraterrestrial Physics of Goddard Space Flight Center and the Astronomy Program of the University of Maryland under National Aeronautics and Space Administration Grant NGR 21-002-029. The Clark Lake Radio Observatory is supported by the National Science Foundation under Grant GP 19401. The Big Bear Solar Observatory is operated on NASA Grant NGR 05-002-034 and NSF Grant Ga. 24015. The computer time for the radio burst analysis was supported by NASA Grant NsG 398 to the Computer Science Center of the University of Maryland. One of us (T.B.H.K.) thanks the Graduate School of the University of Maryland for permission to publish this part of his thesis.

References

Big Bear Solar Observatory: 1971, *Solar Phys.* **18**, 340.
Kundu, M. R., Erikson, W. C., Jackson, P. D., and Fainberg, J: 1970, *Solar Phys.* **14**, 394.
Loughhead, R. E., Roberts, J. A., and McCabe, M. K.: 1957, *Australian J. Phys.* **10**, 483.
Pasachoff, Jay M.: 1972, *Proc. IAU Colloq. on Stellar Chromospheres* **19**, in press.
Sheridan, K. V.: 1963, *Proc. I.R.E. Australia* **24**, 174.
Swarup, G., Stone, P. H., and Maxwell, A.: 1960, *Astrophys. J.* **131**, 725.
Zirin, H.: 1971, *Solar Phys.* **18**, 194.
Zirin, H. and Werner, S.: 1967, *Solar Phys.* **1**, 66.

DETAILED COMPARISON OF TYPE III RADIO BURSTS WITH Hα ACTIVITY

II. *The Isolated Type III Activity of March and April, 1971*

T. B. H. KUIPER*

Clark Lake Radio Observatory, Astronomy Program, University of Maryland, College Park, Md. 20742, U.S.A.

(Received 16 April, 1973; Revised 29 June, 1973)

Abstract. Isolated type III radio burst activity was observed at Clark Lake Radio Observatory in March and the first part of April, 1971, to occur in discrete regions of the corona above certain active regions. When these regions were examined under high resolution in Hα all the type III events appeared to have associated activity in Hα. The potential coronal magnetic field in these regions appeared to be either open or diverging, whereas the field over a rather active region which did not have radio burst activity was closed in a magnetic arcade. The latter feature has been associated with streamers. Streamers have also been associated with dark filaments. The occurrence of a stable dark filament in an active region appeared to have an inhibiting effect on type III activity. It is suggested that a streamer field configuration is not favorable to the escape of isolated type III exciters.

1. Introduction

It has long been recognized that there is a relationship between type III bursts and flares (Loughhead *et al.*, 1957; Swarup *et al.*, 1960; Malville, 1961). Malville included the greatest number of subflares in his sample and found that 76% of the type III bursts occurred while a flare was in progress. In an analysis which used only isolated flares, he estimated that 44% of the bursts which occurred during the flare period are truly associated with the flare. Of the type III bursts which occurred between the start and the maximum of the flare 61% were truly associated. A similar conclusion had been drawn by Swarup *et al.* Thus, only some 35% of all type III bursts could be considered to be truly associated with flares or subflares, although there was a suggestion that this increased with the completeness of the flare sample. Malville suggested that, while many of the metric fast-drift bursts might result directly from flares, a sizeable fraction could be independent of flares or originate in some other form of solar activity not visible in Hα or with dimensions below the limits of resolution. In the preceding paper of this series (Kuiper and Pasachoff, 1973, hereafter referred to as Paper I) we gave an example of one active region in which nearly all the type III bursts had associated Hα activity.† In this paper several other regions are examined for type III-associated Hα activity, using the high-resolution Hα observations made at Big Bear Solar Observatory.

Loughhead *et al.* (1957) first suggested that type III bursts might be associated

* Current address: Jet Propulsion Laboratory, 183B–365, California Institute of Technology, Pasadena, Calif. 91103, U.S.A.

† In that paper we used the word 'correlation'. Since much Hα activity is not associated with type III bursts (with fluxes in excess of about 5×10^{-22} Wm^{-2} Hz^{-1}) the word 'association' seems more suitable.

Solar Physics **33** (1973) 461–474.

with particular active regions. They noted that the association between type III bursts and flares was higher than average in some regions, whereas other regions showed no association with type III bursts. Erickson (1963), by measuring the positions of type III bursts on a day-to-day basis, was able to show that the rotation of regions of type III activity was consistent with the rotation of active regions. His positional accuracy, however, did not allow him to conclude that all the bursts were associated with active regions. A method for removing most of the effect of ionospheric refraction (Kuiper, 1973a, b) permits, below, a re-examination of this question.

Flares and type III bursts are generally considered as two aspects of the same phenomenon, owing to the correlation, albeit partial, between them. If the suggestion of Loughhead *et al.* (1957) that some active regions have no type III activity is correct, then one would inquire what property of these regions inhibits type III activity. Since type III bursts result from particle streams ejected to great heights in the corona, open lines of magnetic field, or at least loop structures of very large dimensions, would seem to be a prerequisite.

The schematic configuration generally associated with type III bursts involves a magnetic field drawn out into a streamer configuration by the interplanetary wind (e.g. Wild and Smerd, 1972). The density determinations of Wild *et al.* (1959) and Weiss (1963), which suggested a value twice that of the Newkirk (1959) streamer model, appeared to necessitate such an explanation. The observations of McLean (1970) of type III bursts distributed along a line on the solar disk are also taken as suggestive of a neutral-sheet configuration. (See below for a discussion of the relationship between streamers and magnetic neutral sheets). The apparent heights of the radio bursts may, however, exceed the true heights. Scattering of radio waves in the corona would cause such an effect (Riddle, 1972). Also, it is often not clear whether the bursts are observed at the fundamental frequency or the harmonic. For limb bursts the latter is probably the case, so that the bursts would appear above their appropriate plasma levels (Kuiper, 1973a, b). In an attempt to clarify whether bursts occur in streamers or not, we will consider the magnetic field configuration in regions of type III activity.

Newkirk (1967) has suggested that a white-light coronal feature forms over a young active region initially as an *enhancement* of the lower corona, evolving to an *active streamer* as the region grows in importance. With further development, the photospheric magnetic field organizes itself into two extended areas of opposite sense and the streamer takes on a characteristic *helmet* configuration. It has been suggested that the streamer is a neutral sheet in the coronal field, formed over the boundary between two magnetic regions of opposite polarity (e.g. Sturrock and Smith, 1968). The magnetic configuration is like that proposed by Carmichael (1964) as a possible site for flares with a filament supported by the closed field lines near the base. Axisa *et al.* (1971) have suggested that, as in the case of helmet streamers, the presence of a filament is a necessary condition for the existence of active streamers, and that both have the same basic magnetic structure.

Newkirk and Altschuler (1970) have compared coronal structures observed during

an eclipse to the potential magnetic field of the corona. This field is calculated from line-of-sight observations of the photospheric field, made during one solar rotation, on the assumption that the corona is current-free (Altschuler and Newkirk, 1969). A number of magnetic structures were recognized. *Magnetic rays* (MR's) are open field lines by which particles can escape from the Sun. *Diverging fields* (DF's) occur over active regions, either because of a real excess of photospheric field of one polarity or because the photospheric field observations are not sufficiently accurate. Changes in the region during the two week period when it is observed could also contribute to an erroneous excess of photospheric field. *Magnetic arcades* are series of loops which form a corridor. MA's, which indicate a boundary between two rather extended regions of opposite polarity, correlate with streamers. (Altschuler and Newkirk did not distinguish between AR streamers and helmets in their paper.) In this paper we will consider the magnetic configurations in which type III bursts occur. Similar studies have already been reported for type II bursts (Dulk *et al.*, 1971) and for type IV bursts (Dulk and Altschuler, 1971).

2. Observations

Observations of the east-west positions of type III radio bursts were made between 20 and 65 MHz with the log-periodic array at Clark Lake Radio Observatory (Erickson and Kuiper, 1973). These positions were corrected for ionospheric refraction (Kuiper, 1973a, b). In many instances the radio data alone are sufficient to locate the active region (e.g. Kuiper, 1973b) even though we lack resolution in the north-south direction. In this paper, however, the occasional coincidences between type III's and flares are used to identify the active regions. It is then shown that the positions of the other bursts are consistent with these regions.

Figure 1 shows the east-west positions at 60 MHz of type III bursts observed in March and April of 1971 plotted as a function of the date. In cases when the data were of sufficient quality to correct for ionospheric refraction, only these corrected positions are shown. One can see discrete regions of type III activity co-rotating with the Sun. Also shown are the loci of points radially above the active regions, which are identified in the figure by the last three digits of their McMath number. These regions, with the exception of McMath 11249 and 11250, were chosen because they showed Hα activity coincident with type III bursts. Regions 11249 and 11250 were also plotted since the positions of bursts suggested these regions might be responsible. For the regions represented by solid lines, a height of 0.6 $R_\odot$ was assumed, corresponding to the apparent height of type III bursts at 60 MHz (Kuiper, 1973a, b). For the regions identified with dashed lines, a height of 1.0 $R_\odot$ was assumed. It is seen that the positions of the bursts are consistent with locations above the active regions.

3. The Association of Type III Bursts with Hα Activity

One five days Big Bear Solar Observatory covered the regions on the Sun above

which type III bursts appeared to occur. Big Bear films were examined for the period 3 March–4 April. In Table I are listed all those bursts or groups of bursts which occurred during times when Big Bear had Hα data. Below are given a description of Hα and radio burst activity which showed association with each other. Such a description cannot however substitute for an actual viewing of the films.

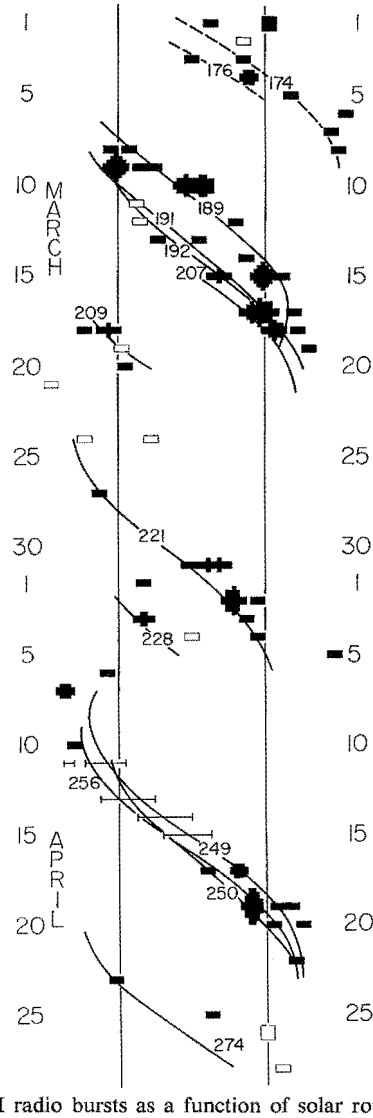

Fig. 1. Positions of type III radio bursts as a function of solar rotation. Positions corrected for ionospheric refraction are shown as solid blocks, those not corrected as open. The size of the block represents the number of groups measured. The approximate positions of continuum storms are shown by error bars. The loci of points 0.6 (solid lines) and 1.0 (broken lines) solar radii above certain active regions, identified in Table II, are also shown.

9 March. At 19:48:30 two bright features formed on either side of a dark fibril connecting the major sunspot with a newly emerging spot. The features brightened and moved in opposite directions, one towards the main spot, the other to the new spot. At approximately the time when the brightenings reached the two spots, a series of type III bursts occurred.

18 March. At 18:09 there occurred a type III burst whose position line coincided with the west limb of the Sun. At about this time a very small faint flare occurred near a region of emerging flux which followed the main spot in McMath 11207.

From 19:47:00 to 19:48:30, from 19:50:10 to 19:50:45, and from 19:53:00 to 19:53:20 there occurred groups of type III bursts with position lines on the east limb of the Sun. Very small Hα events, possibly surges, were seen at these times in McMath 209. The frames in which they were most apparent were taken at 19:48:15, 19:51:03 and 19:53:48, respectively.

At 20:19 a small bright bridge was seen to connect two plage regions southeast of the spot in 207. A type III burst occurred on the west limb at 20:19:55. Another group of type III's occurred from 20:33:05 to 20:33:20. At 20:36 a small bright bridge in a different position convected the two plages.

At 21:35:25 a sequence of faint type III bursts started near the east limb of the Sun coincident with the start of a small flare near the EFR in McMath 207 (near the Sun's west limb) which reached its maximum at 21:36:25 and had subsided two minutes later. Another type III burst occurred at the east limb at 21:37. This is one of the rare instances of simultaneous activity at two very well separated locations on the Sun. It is not possible to say whether there is a genuine association between these events.

At 23:28 a group of III's occurred a half solar radius beyond the west limb with another burst at 23:29. At this time Big Bear was patrolling McMath 207 but poor seeing and transparency made a close study of the Hα phenomena impossible.

20 March. A group of type III's occurred between 20:14:30 and 20:16:40 near the east limb of the Sun. At 20:19:25 a brightening became visible along a long thin plage, reaching a maximum at 20:21:02.

2 April. It is difficult to make a clear case for detailed association of activity between type III bursts and the Hα activity for this day. During our period of observation a filament immediately west of the region was continuously active. Tlamicha and Takakura (1963) have suggested a possible association between type III bursts and active dark filaments. In addition, there were two subflares in the region which may have had associated type III bursts.

At 19:09 a subflare began east of the NW spot. The activity continued to be visible until 19:23. A group of strong type III bursts occurred from 19:16:15 to 19:20:45. Another type III burst occurred at 19:23:25.

At 20:05:10 on-band Hα coverage was resumed following a wavelength scan. This appeared to coincide with the start of a flare at the end of the filament nearest the sunspots. At this time also a group of type III bursts occurred, lasting from 20:05:07 to 20:07:30. The most active phase of this Hα event ended at 20:25.

TABLE I

Association of type III events with activity in BBSO patrol films

Date/UT	Burst position	Suspected region	SGD flare data		BBSO patrol	
			Region	Times	Region	Activity
3 Mar. 1938	0	176			173	
1943	0.7	174	174	1943–2004	173	
6 Mar. 2259	2.1	?			174	
9 Mar. 1956	−1.1	191 or 192			191	yes
2253	−0.6	189			191	
10 Mar. 1751	0	189			191	
1955	0.2	189	189	1951–2005	191	
2014	0.1	189			191	
12 Mar. 2014	−0.7[a]	191 or 192			191	
14 Mar. 2016	0.7	189			195	
15 Mar. 1945	0.7[a]	?			196	
2006	0.4[a]	191/192/207			196	
2016	0.6[a]	?			196	
2019	0.9	189			196	
2026	0.6[a]	?			196	
2038	0.5[a]	?			196	
2052	1.2	189			196	
2202	1.0	189			196	
2220	1.0	189	192	2117–2222	196	
2230	0.4	191/192/207			196	
17 Mar. 2133	1.1	191/192/207			196	
2142	0.7[a]	?			196	
2208	0.9	191/192/207			196	
18 Mar. 1809	1.2	191/192/207			207	yes
1948	−1.0	209			209	yes
1950	−1.2	209			209	yes
1953	−1.5	209			209	yes
2020	1.4	191/192/207			207	yes
2033	1.1	191/192/207			207	yes
2135	−1.0[a]	209			207	yes
2137	−0.9[a]	209			207	yes
2328	1.6	191/192/207			207	
2334	−1.1	209			207	
20 Mar. 2015	−0.9	209			209	yes
21 Mar. 1644	2.3[a]	?			209	
1 Apr. 1916	−0.3[a]	221	221	1847–1941	west limb	
2 Apr. 1734	0.5	221			221	yes
1736	0.5	221			221	yes
1800	0.5	221	221	1758–1810	221	yes
1833	0.6	221	221	1829–1849	221	yes
1904	0.8	221	221	1907–1956	221	yes
1919	0.7	221	221	1910–1938	221	yes
1923	0.7	221	221	1919–1930	221	yes
1950	1.3[a]	221			221	yes
2002	0.7	221	221	2015–2022	221	yes
2006	0.8	221			221	yes
3 Apr. 1925	0.8	221			221	yes
1938	−0.6	228	228	1937–1946	221	
4 Apr. 1900	0[a]	?	228	1900–1919	221	yes
1908	0.9	221			221	yes

[a] Not corrected for refraction.

3 April. During the period of Big Bear's patrol McMath 221 was very quiet. A group of type III bursts occurred from 19:24:18 to 19:25:35. At about this time there was a fast faint subflare running in a thin line north of the SE spot. Because of poor seeing, it was not possible to time it precisely, but its most visible phase occured at 19:27:32.

4 April. During this day McMath 221 was again very active. The filament, which had been almost non-existent the previous day, was even more substantial this day than it had been on April 2. The activity in this filament was very violent on this day. It was not possible to associate the radio bursts with any specific events. The most interesting thing about the radio burst activity on this day was its mildness considering the activity visible in Hα.

We see that type III bursts can be attributed to specific active regions, not only in the sense that the bursts originate over these regions as was shown in the previous section, but in that bursts are associated with Hα events in these regions. Hα activity was seen in all of the 21 bursts or groups of bursts which occurred over active regions patrolled by Big Bear Solar Observatory. In twelve cases specific Hα events could be identified as being associated with the bursts on the basis of temporal coincidence. In one additional instance (20:15, 20 March) the timing is less convincing. For eight radio events the Hα phenomenology was to complicated to make such an association.

Although further study is in progress on the detailed association of type III bursts with Hα phenomena, it appears that the following assertion can be made on the strength of these results and those of Paper I: Nearly all (>95%) type III bursts or groups of bursts with fluxes in excess of about 5×10^{-22} Wm^{-2} Hz^{-1} occurring in isolation of other radio activity and not in extended storms of type III bursts are associated with activity in Hα.

We find that the distinction suggested by Loughhead *et al.* (1957) between active regions which have type III bursts and those which do not is real. McMath 11196 was a particularly active region which showed no type III activity. McMath 11221 had days when it showed type III activity and days when it showed little or none, in spite of flare activity. In the next section this will be related to the large-scale coronal magnetic field associated with the region.

4. The Coronal Magnetic Field in Regions of Type III Activity

In Figure 2 the plage drawings (*Solar Geophysical Data*, 1971a) and calculated coronal fields (Altschuler, private communication, 1972) are shown for the regions which were associated exclusively with isolated type III activity. In each instance the field is either diverging or, in the cases of the more active of the regions, open. It would appear, therefore, that type III bursts occur in regions of open or at least diverging field, rather than coronal streamers, which are associated with magnetic arcades. In order to confirm the occurrence of open field lines the records of RAE-1, which recorded radio emissions above the ionosphere in the frequency range 0.2–5 MHz, were examined. By the coincidence of type III bursts measured at Clark Lake

with those measured in interplanetary space by the satellite, it was seen that energetic particles escaped each of the active regions, with the exception of McMath 165 for which there was sufficient data.

A particularly active region which did not show any type III activity was McMath 11196. This region is represented in Figure 3. It is seen that the calculated coronal

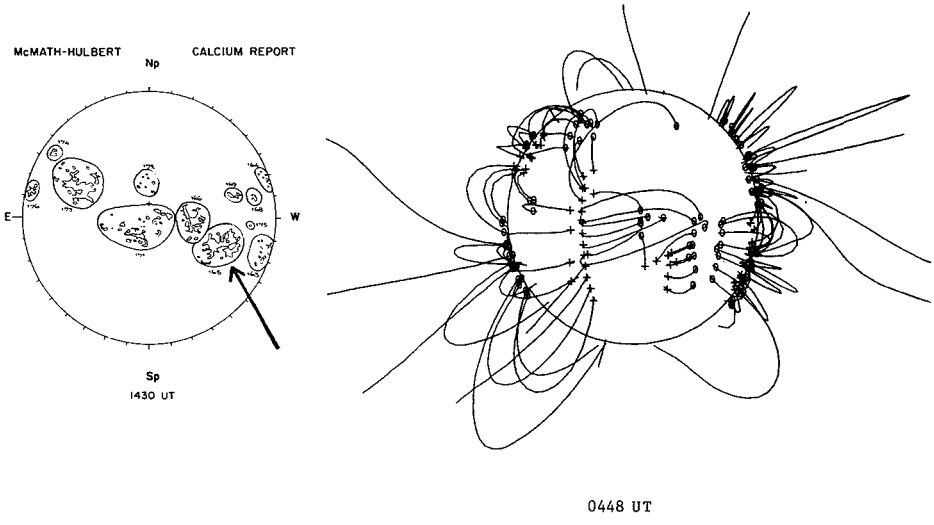

Fig. 2a. Plage drawings and calculated coronal fields for 26 February, 1971; active region McMath 11165.

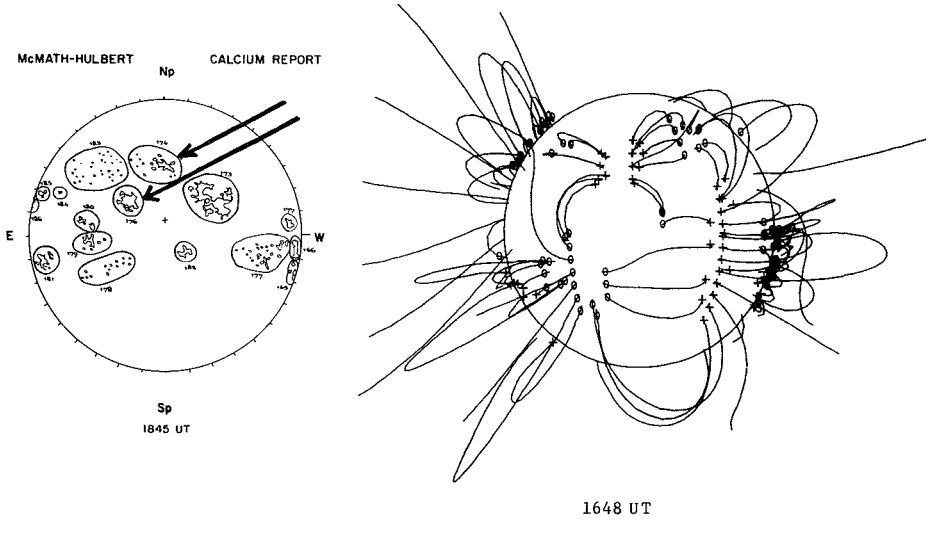

Fig. 2b. Plage drawings and calculated coronal fields for 2 March, 1971; active regions McMath 11174 and 11176.

field is characterized by a tightly closed structure, known as LMA (Low Magnetic Arcade), a feature which is associated with streamers. A filament did occur adjacent to this region, aligned more or less in the direction of the LMA. There were no type III bursts in this region, in spite of all the flare activity so that it would appear that the magnetic configuration was unfavorable.

The behavior of McMath 221 may shed further light on the relationship of the coronal field to type III activity. This region appeared on the east limb on March 25, and was relatively quiet with one reported flare during the Clark Lake observing period on the 26th, and three more flares and two type III groups on the 27th. A large filament was looped around the north of this region. The low level of activity continued on the 28th. On March 29, however, this region was extremely active. Six

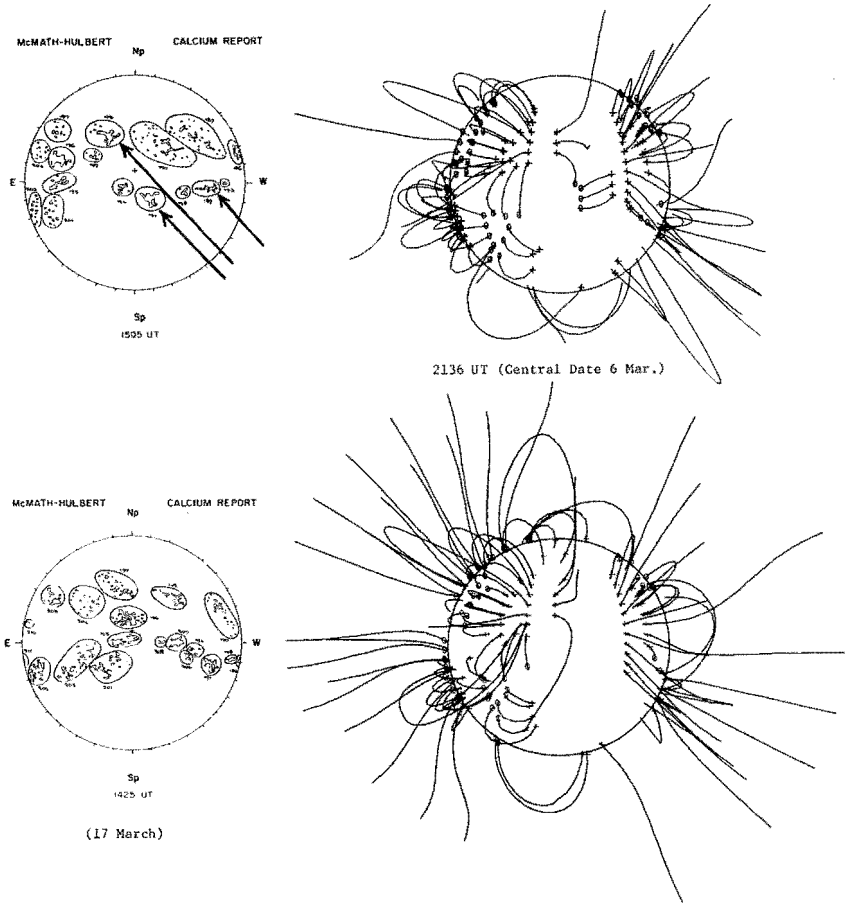

Fig. 2c. Plage drawings for 14 March (upper left) and 17 March (lower left) and calculated coronal fields for 14 March for observations having central dates of 6 March (upper right) and 20 March (lower right); active regions McMath 11189, 191, 192 and 207. Note the emergence of 207 and associated regions between 14 and 17 March.

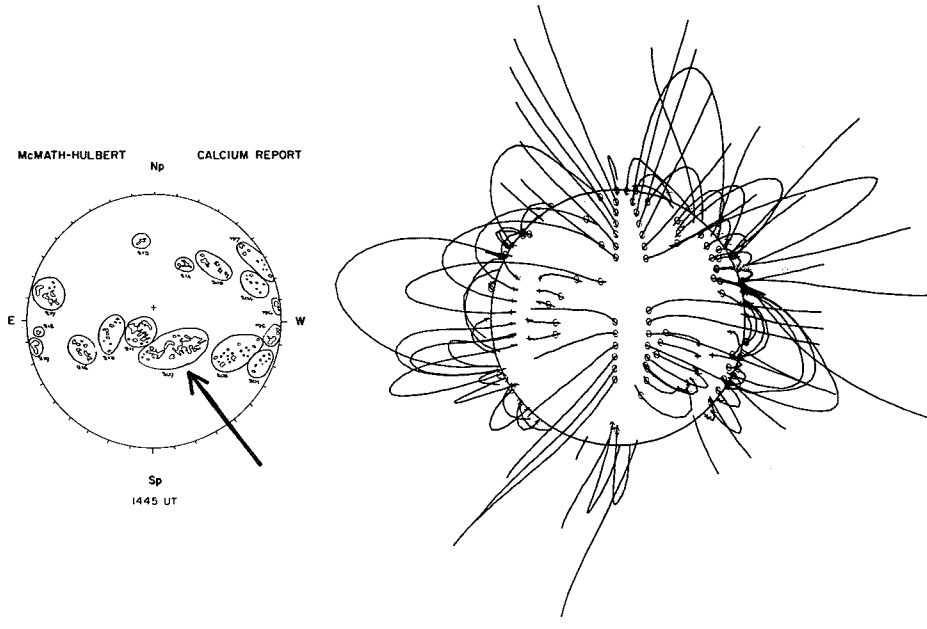

Fig. 2d. Plage drawings and calculated coronal fields for 23 March, 1971; active region McMath 11209.

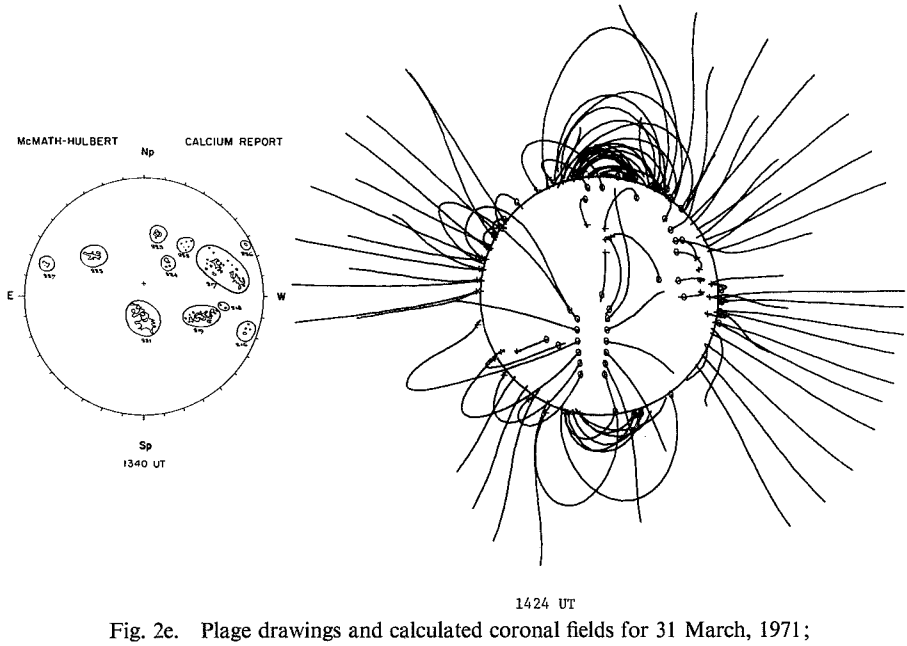

Fig. 2e. Plage drawings and calculated coronal fields for 31 March, 1971; active region McMath 11221.

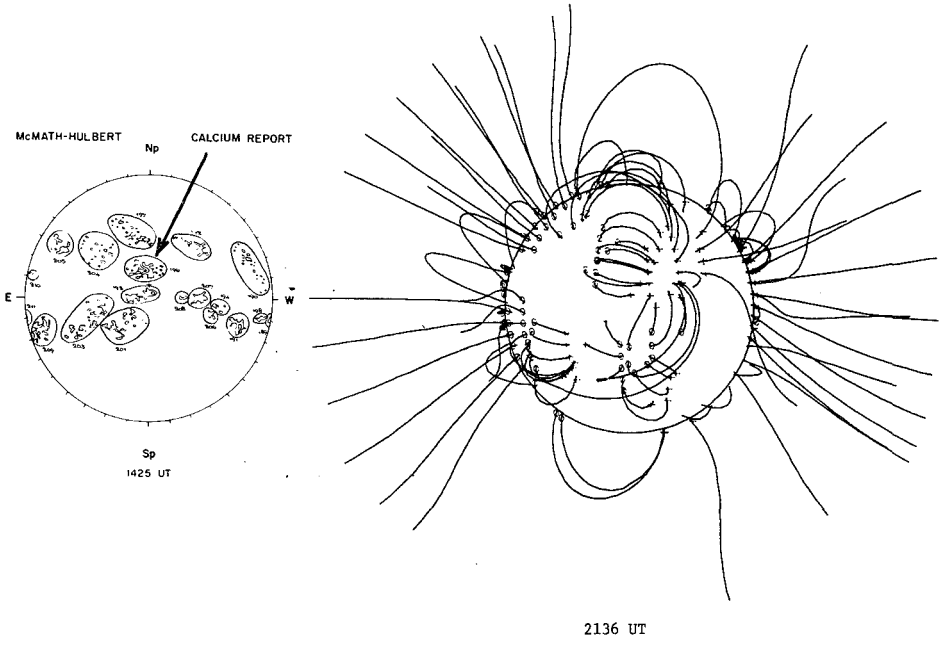

Fig. 3. Plage drawings and calculated coronal fields for 17 March, 1971, showing McMath 11196, an active plage which did not exhibit type III radio bursts.

flares were reported during Clark Lake's normal observing period. The Big Bear Hα patrol of this region showed the filament to be highly agitated. Although Clark Lake did not observe this day, other observatories reported no radio activity. On March 30 the filament disappeared. Although three flares were reported, only one extremely faint group was observed at 19:14. The group was too weak to get a reliable position measurement, but it appears to have occurred on the western half of the Sun, away from 221. Lack of any activity in 221 at this time also suggests the burst was not related to this region.

On March 31 six flares were reported. Eleven type III groups occurred, at least eight of which were positionally related to McMath 221. Three of these were coincident with the published flares. On April 1 six flares were reported in this region, but no radio bursts occurred there. By this time a new small filament had formed, running westward from the center of the plage. April 2 was extremely active. The Big Bear patrol shows almost continuous activity, both flares and turbulence in the new filament, accompanied by strong type III activity. On April 3 the region was quiet. The filament which ran west and then north from the plage was barely visible. The only group of type III bursts from this region during Big Bear's patrol period was visible in Hα. On April 4 the region was extremely active again in Hα, but relatively quiet in the radio. The filament had grown in importance and was more prominent than it had been on April 2. It was also extremely active. The region

thereafter remained relatively quiet in the radio until its disappearance over the west limits after April 6.

It would appear from the behavior of the filaments, that the field underwent significant changes during the period 27 March–4 April. The calculated coronal field using photospheric data for the rotation having a central date of 20 March is significantly different from the field calculated from data with a central date of 2 April, also indicating that there were changes in the coronal field. This was accompanied by considerable flare activity. Type III bursts, however, were prevented until the field configuration associated with the large filament which existed before April 30 was destroyed. On and after April 4, when a new filament was established in the region, radio burst activity was again inhibited.

5. Conclusion

The positions of type III radio bursts occurring between approx 16:00 and 24:00 UT from 1 March to 5 April, 1971, were determined and corrected for ionospheric refraction wherever possible. It was found that these bursts occurred over active regions whose calculated potential coronal fields were characteristically diverging and generally open. This magnetic field of configuration is not characteristic of streamers. In observations at Culgoora, Dulk (private communication, 1972) has also found that the bursts occur in regions of open field, with or without a streamer nearby. It appears, therefore, that type III bursts need not occur preferentially in streamers, as was first suggested by Wild *et al.* (1959) on the basis of the heights of the bursts.

The type III radio bursts were intimately related to activity in Hα. Out of 21 cases for which Big Bear Solar Observatory had coverage of the region responsible for the bursts, Hα activity was seen in each instance. In 12 cases the activity was either brief or began at the time of the burst, suggesting that the two phenomena were related. One case was uncertain. In the other eight cases there was continuous and complex activity so that no such identification could be made. A similar result was obtained in the detailed analyses of other periods of activity (Zirin and Werner, 1967; Paper I). It is suggested that almost all, if not all, isolated type III bursts have associated activity in Hα.

The Hα phenomena associated with type III bursts are not always flares. Martres *et al.* (1972) have shown that in some instances the associated phenomena are seen as small transient absorbing features. In other cases disturbances in filaments seem to be related to type III bursts (Tlamicha and Takakura, 1963; this paper).

The existence of a stable filament in a region represents an unfavorable magnetic field configuration for type III bursts. Active filaments, however, indicate that the field is changing. During this time particles may escape to cause type III bursts. Tlamicha and Takakura (1963) have also noted an association between type III bursts and active filaments. The confinement of fast particles is not in any sense absolute. Some type III activity was seen on March 27 and April 4. Similarly, when a region is open, not all flares yield radio bursts (e.g. Zirin and Werner, 1967; also Paper I).

In all likelihood confinement by small-scale magnetic structures near the chromosphere is also important (e.g. Lazareff and Zirin, 1973).

The type III bursts on which this work is based occurred in isolation of any other radio activity or of flares greater than subflares. For bursts of this kind the following interpretation is believed to be consistent with the observations. Isolated type III bursts or groups of bursts are generally associated with active regions in early stages of development. These regions are characterized by an open field. The acceleration occurs low in the corona or in the chromosphere, since all the bursts have associated Hα activity. As the region develops the magnetic field configuration closes, inhibiting the escape of these particles. Only when a major reorganization of the field occurs will paths be temporarily opened for particles to escape.

Acknowledgments

I would like to acknowledge discussions with, suggestions from, and criticisms by M. D. Altschuler, William C. Erickson, T. E. Gergely, R. T. Hansen, M. R. Kundu, J. M. Pasachoff, E. V. P. Smith, R. G. Stone, and H. Zirin. I am particularly grateful to Big Bear Solar Observatory for access to the Hα patrol films, to the High Altitude Observatory for coronal potential field maps, and the Radio Astronomy Section at Goddard Space Flight Center for use of the Radio Astronomy Explorer-I data. My thanks go also to J. Pressman and N. Roth who reduced the Clark Lake radio data. Clark Lake Radio Observatory is supported by National Science Foundation grant NSF GP 19411 and National Aeronautics and Space Administration grant NGR 21-002-367. The photospheric magnetic field measurements used to compute the coronal maps were made by R. Howard of the Hale Observatories with the support of the Office of Naval Research.

References

Altschuler, Martin D. and Gordon Newkirk, Jr.: 1969, *Solar Phys.* **9**, 131.
Axisa, F., Avignon, Y., Martres, M. J., Pick M., and Simon, P.: 1971, *Solar Phys.* **19**, 110.
Billings, Donald E.: 1966, *A Guide to the Solar Corona*, Academic Press, New York.
Carmichael, Hugh: 1964, in W. N. Hess (ed.), *AAS-NASA Symposium on the Physics of Solar Flares*, NASA, Washington, p. 451.
Dulk, G. A. and Altschuler, M. D.: 1971, *Solar Phys.* **20**, 438.
Dulk, G. A., Altschuler, M. D., and Smerd, S. F.: 1971, *Astrophys. Let.* **8**, 235.
Erickson, W. C.: 1963, *J. Geophys. Res.* **68**, 3169.
Erickson, W. C. and Kuiper, T. B. H.: 1973, *Radio Science* **8**, 845.
Kuiper, T. B. H.: 1973a, in R. Ramaty and R. G. Stone (eds.), *High Energy Phenomena on the Sun*, Symposium Proceedings, NASA, Washington, p. 540.
Kuiper, T. B. H.: 1973b, Thesis, University of Maryland.
Kuiper, T. B. H. and Pasachoff, Jay: 1973, *Solar Phys.* **28**, 187.
Lazareff, B. and Zirin, H.: 1973, Big Bear Solar Observatory preprint, No. 0130.
Loughhead, R. E., Roberts, J. A., and McCabe, Marie K.: 1957, *Australian J. Phys.* **10**, 483.
Malville, J. M.: 1961, Thesis, University of Colorado.
Martres, M. J., Pick, M., Soru-Escaut, I., and Axisa, F.: 1972, *Nature Phys. Sci.* **236**, 25.
McLean, D. J.: 1970, *Proc. Astron. Soc. Aust.* **1**, 315.
Newkirk, Gordon J., Jr.: 1959, Paris Symposium on Radio Astronomy, (ed. by R. N. Bracewell), Stanford.

Newkirk, Gordon J., Jr.: 1967, *ARAA* **5**, 213.
Newkirk, Gordon Jr. and Altschuler, Martin D.: 1970: *Solar Phys.* **13**, 131.
Riddle, A. C.: 1972, *Proc. Astron. Soc. Aust.* **2**, 148.
Solar Geophysical Data: 1971a, No. 321 Part I, 33–63.
Solar Geophysical Data: 1971b, No. 325 Part II, 5–22.
Solar Geophysical Data: 1971c, No. 326 Part II, 4–31.
Sturrock, P. A. and Smith, Sheldon M.: 1968, *Solar Phys.* **5**, 87.
Swarup, G., Stone, P. H., and Maxwell, A.: 1960, *Astrophys J.* **131**, 725.
Tlamicha, A. and Takakura, T.: 1963, *Nature* **200**, 999.
Weiss, A. A.: 1963, *Australian J. Phys.* **16**, 2401.
Wild, J. P. and Smerd, S. F.: 1972, *ARAA* **10**, 159.
Wild, J. P., Sheridan, K. V., and Neylan, A. A.: 1959, *Australian J. Phys.* **12**, 369.
Zirin, Harold and Werner, Susan: 1967, *Solar Phys.* **1**, 66.

Reprinted from THE ASTROPHYSICAL JOURNAL
Vol. 177, No. 1, Part 1, October 1972

THE ASTROPHYSICAL JOURNAL, 177:101–114, 1972 October 1

VERY LONG BASELINE INTERFEROMETER OBSERVATIONS OF TAURUS A AND OTHER SOURCES AT 121.6 MHz

W. C. ERICKSON AND T. B. H. KUIPER
Astronomy Program, University of Maryland, College Park, Maryland
T. A. CLARK
Radio Astronomy Branch, Goddard Space Flight Center, Greenbelt, Md.
S. H. KNOWLES
Naval Research Laboratory, Washington, D.C.
AND
J. J. BRODERICK*
National Radio Astronomy Observatory, Charlottesville, Virginia
Received 1971 October 18: revised 1972 April 17

ABSTRACT

VLBI observations with an antenna spacing of 92,000 λ (2".2 lobe separation) were made on a number of small-angular-diameter sources at a frequency of 121.6 MHz. Through positional and spectral coincidence, these observations confirm the physical association of the compact source in Tau A with the pulsar NP 0532; in the east-west direction, the two objects agree in position to an accuracy of ±0".1. The fluxes of the small-angular-diameter components of 3C 48, 3C 84, 3C 144, 3C 147, 3C 273, 3C 274, 3C 298, 3C 405, 3C 459, and 3C 461 are estimated.

I. INTRODUCTION

On 1970 January 8–12, a very long baseline interferometer (VLBI) was operated between the National Radio Observatory's 300-foot (91.4-m) antenna at Greenbank, West Virginia and the Naval Research Laboratory's 84-foot (25.6-m) antenna at Riverside, Maryland. The NRAO MK-I terminals were employed. Our 230-km (92,000 λ) east-west baseline yielded a fringe separation of 2".2. One purpose of the experiment was to make an accurate determination of the relative positions of the compact source in Tau A and the pulsar NP 0532. We also wished to observe the small-angular-diameter components of a number of radio sources and to demonstrate the technical feasibility of VLBI observations in the 100-MHz frequency range. This was important because several VLBI observations in the 100-MHz frequency range had been attempted with larger antenna spacings. None of these programs produced interferometer fringes, and we feared that these failures might be due to some unrecognized propagation effect in the interstellar, interplanetary, or ionospheric medium. Before undertaking more ambitious programs of longer-baseline observations, we wanted to be certain that the VLBI technique could be successfully applied over a relatively short baseline. We also observed a number of pulsars. The signal-to-noise ratios for all pulsars except Tau A were not adequate to yield useful information.

II. ANALYSIS OF TAURUS A OBSERVATIONS

It is well known that the pulses from NP 0532 show strong dispersion in frequency. We are dealing with a series of periodic pulses which drift from high to low frequencies.

* Present address: Arecibo Observatory, Arecibo, P.R.

Usually we consider the pulse profile as a function of time at a constant frequency. Alternatively, we can consider the pulse train as a function of frequency at a single instant of time. In doing this, we find that several pulses are present within the 330-kHz bandpass of the MK-1 terminal at any instant of time. This fact greatly reduces the output fluctuations due to the pulses. However, the system sensitivity was such that the full bandpass was required to obtain an adequate signal-to-noise ratio.

In MK-1 VLBI observations the data are sampled and recorded on digital computer tapes at each end of the interferometer. The output tapes are correlated later. We can easily impose a real-time delay in one arm of the interferometer merely by slipping one tape with respect to the other during the cross-correlation processing. A local-oscillator frequency shift in one arm can also be imposed during processing by applying a progressive phase rotation to the correlation coefficient. This is accomplished in a manner similar to that described by Bare *et al.* (1967).

A time delay τ in one arm of an interferometer creates a phase gradient $\nu\tau$ across the bandpass. Suppose that a large time delay is imposed so that exactly one cycle of phase shift is produced over one pulse interval in frequency (see fig. 1). The phase progresses linearly with frequency across the band and thus, as shown analytically below, integration over the passband yields the first Fourier component of the pulse shape. As a function of time, this component goes through one cycle of phase in one pulse period. Therefore, this component appears at the pulsar repetition frequency F. Just as a time delay τ produces a progressive phase shift in the frequency domain, so a local oscillator (LO) offset f produces a progressive phase shift in the time domain. If a LO offset of $f = -F$ is imposed, this first Fourier component will appear at constant phase, i.e., zero frequency, during the observing period. Integration over the observing period yields sufficient signal-to-noise to observe one component of the pulse shape. The standard VLBI reduction programs compensate for phase shifts generated by Earth rotation, and these terms are omitted in the following discussion.

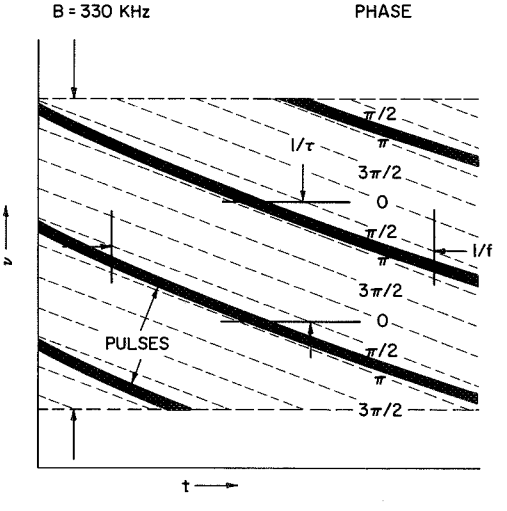

FIG. 1.—This diagram illustrates the pulses from NP 0532 as they cross our system's 330 kHz bandpass. A frequency offset, f, causes an instrumental phase rotation of 2π in a period $1/f$ while a time delay offset, τ, produces a phase rotation of 2π in a frequency interval $1/\tau$. Lines of constant phase are given by $ft + \tau\nu$ = constant. Thus, the dotted lines of constant instrumental phase are by appropriate adjustment of f and τ made parallel to the pulses.

If time delay and LO frequency shifts of $(2\tau, -2F)$ are imposed, the second Fourier component of the average pulse shape is determined. Similarly, the higher components can be found. In this experiment, the first four components were observed.

The method will now be developed analytically. An idealized interferometer is shown in figure 2. Radiation of amplitude $E(\nu, t)$ is incident on the two antennas, having collecting areas A_1 and A_2, respectively. The signals at the two antennas differ by a phase $\phi(t)$ due to the orientation of the baseline with respect to the source, the path difference through the intervening plasma to the two antennas, and other effects. When the geometrical phase is removed, a residual phase, ϕ_0, remains. If a time delay τ and a frequency offset f are applied to the signal from one of the antennas, then the two signals E_1 and E_2 arriving at the correlator may be written as

$$E_1(\nu, t) \propto g(\nu, t + \tau) \exp\{i2\pi[(\nu - \nu_0)(t + \tau) + ft + \phi_0]\}$$

$$E_2(\nu, t) \propto g(\nu, t) \exp\{i2\pi[(\nu - \nu_0)t]\},$$

where $g(\nu, t)$ is a random function of time which describes the variation of signal amplitude at frequency ν. The signals are converted to a video band through multiplication by the LO frequency ν_0 as shown in figure 2. They are delayed by a relative delay $\tau = \tau' - \tau_g$ and offset in frequency through multiplication by $\Delta f'$ and $\Delta f''$. If the geometrical fringe frequency is f_g, then $f_g + \Delta f' + \Delta f'' = f$. Due to the delay offset, the signals are translated in time relative to each other by the delay offset τ. In practice, $\tau \approx 10^{-5}$ s and is very much less than the time interval, $(30 \text{ Hz})^{-1} \approx 10^{-2}$ s over which $g(\nu, t)$ varies. Thus $g(\nu, t + \tau) \approx g(\nu, t)$. The flux density of the source is $S(\nu, t) = g(\nu t)g^*(\nu, t)$.

Neglecting random noise terms for clarity, the correlator output is $E_1(\nu t)E_2^*(\nu, t)$

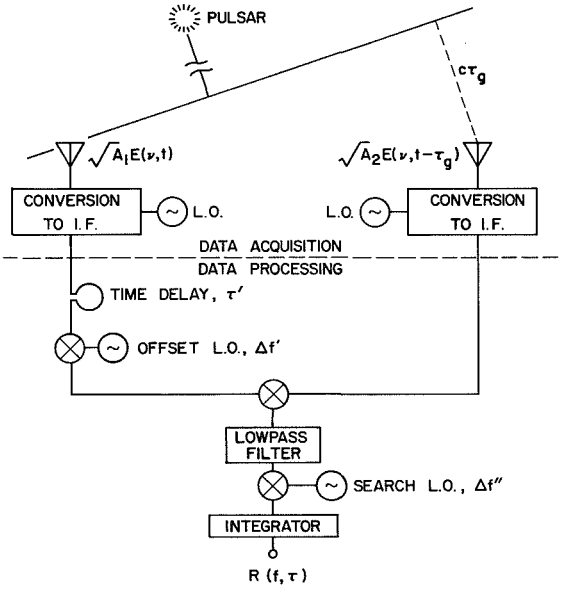

FIG. 2.—An idealized interferometer consisting of antennas with effective areas A_1 and A_2, data recording systems, and data processing systems. τg is the geometrical time delay and f_g is the geometrical fringe rate. $\tau = \tau - \tau_g$; $f = \Delta f + \Delta f'' + f_g$.

averaged over a uniform bandpass B and an integration time T. The system output is thus

$$R(f, \tau) \propto \frac{(A_1A_2)^{1/2}}{TB} \int_T \int_B E_1(\nu, t)E_2^*(\nu, t)d\nu dt$$

$$\propto \frac{(A_1A_2)^{1/2}}{TB} \int_T \int_B g(\nu, t)g^*(\nu, t) \exp \{i2\pi[(\nu - \nu_0)\tau + ft + \phi_0]\}d\nu dt$$

$$\propto \frac{(A_1A_2)^{1/2}}{TB} \int_T \int_B S(\nu, t) \exp \{i2\pi[(\nu - \nu_0)\tau + ft + \phi_0]\}d\nu dt . \quad (1)$$

In analyzing the radiation from the Crab Nebula, we assume that the source flux $S(\nu, t)$ may be generated by two components, I_s and I_p. I_s is the steady component and I_p is the pulsating component. Since these components may be positionally distinct, the signals from each component may arrive at the correlator with different relative phases, ϕ_{0s} and ϕ_{0p} respectively. Therefore,

$$R(f, \tau) \propto \frac{(A_1A_2)^{1/2}}{TB} \int_T \int_B [I_s(\nu) \exp (i2\pi\phi_{0s}) + I_p(\nu, t) \exp (i2\pi\phi_{0p})]$$
$$\times \exp \{i2\pi[(\nu - \nu_0)\tau + ft]\}d\nu dt . \quad (2)$$

If F is the pulse repetition frequency and $1/G$ is the pulse spacing in the frequency domain, then for a given pulse, $Ft + G\nu$ = constant (fig. 1). The dispersion is given by

$$\frac{d\nu}{dt} = -\frac{\nu^3}{2D} \approx -\frac{F}{G}, \quad (3)$$

where D = dispersion constant. Over our bandpass $d\nu/dt$ varies by less than 1 percent. A more complicated analysis which includes frequency-time curvature due to this variation as well as other small effects results in conclusions that are identical to those derived here. The A_n are the set of real Fourier coefficients which describe the average pulse shape,

$$I_p(\nu, t) = \sum_{n=-\infty}^{+\infty} A_n \exp [i2\pi n(Ft + G\nu) + i2\pi\phi_n] . \quad (4)$$

Inserting this expression into equation (2), we have

$$R(f, \tau) \propto \int_T \int_B [I_s(\nu) \exp (i2\pi\phi_{0s}) + A_0] \exp (i2\pi\phi_{0p}) \exp [i2\pi(\nu\tau - \nu_0\tau + ft)]d\nu dt$$
$$+ \sum_{\substack{n=-\infty \\ n\neq 0}}^{+\infty} \int_T \int_B A_n \exp [i2\pi(\phi_{0p} + \phi_n + \nu\tau - \nu_0\tau + ft + nFt + nG\nu)]d\nu . \quad (5)$$

Suppose that we adjust the τ' and $\Delta f'$ in figure 2 such that

$$\tau = -NG$$

and

$$f = -NF; \qquad N = 0, \pm 1, \pm 2, \ldots . \quad (6)$$

The dispersion constant for NP 0532 is given by Goldstein and James (1969) as 23.575×10^{-16} Hz. Combined with an apparent pulse repetition rate of 30.2042 Hz, we find $G = 7.92\ \mu$s and thus $BG \approx$ (330 kHz)(7.92) $\approx 3 > 1$. Therefore, each term for which $n \neq N$ involves integration over several cycles of phase of the exponential

factor and is negligible compared with the $n = N$ term. Thus, for a rectangular bandpass, with $I_s(\nu) \approx$ constant over the passband,

$$R(0, 0) \propto I_s \exp(i2\pi\phi_{0s}) + A_0 \exp(i2\pi\phi_{0p}) \tag{7}$$

and

$$R(-NF, -NG) \propto A_N \exp[i2\pi(\phi_{0p} + \phi_N + NG\nu_0)], \tag{8}$$

where $R(0, 0)$ is the nonfluctuating component normally associated with the compact source. Terms in $N = \pm 1, \pm 2, \pm 3, \ldots$, determine the various Fourier components of the pulse shape of NP 0532. The observed values of $R(\pm NF, \pm NG)$ also contain noise contributions which are uncorrelated between the $\pm N$th sidebands.

It is now necessary to define what is meant by the terms "compact source" and "pulsar," and to relate the intensities of these components to the observed quantities. As illustrated in figure 3, suppose that we observe an object which emits a steady component plus a pulsating component, with the two not necessarily coincident in the sky. Then A_0 is the average flux of the pulsating component. The total intensity which would be observed with any system that has a low pass or d.c. response is $I = I_s + A_0$. This is the component which has been called the "compact source" by all observers (even though I includes A_0), since pulsations would have been smeared out by the large time constants and/or bandwidths employed in "compact source" observations. It would be far better to call I_s the "compact source," but most observers could not distinguish between I_s and I. To avoid confusion, we will not use the term "compact source" and will simply refer to I, I_s, and A_0. The average flux of the pulsating component, A_0, is the component which would be observed with a high-pass response and a sufficiently narrow passband. It is the component normally referred to as the "pulsar."

In this experiment, also, we cannot distinguish directly between A_0 and I_s. The function $R(0, 0)$ gives us I. However, A_0 can be independently evaluated because it can be related to the sideband intensities A_n, $n \neq 0$, which are independently observable.

Rewriting equation (4),

$$I_p(\nu, t) = A_0 + \sum_{n=1}^{\infty} \{A_n \exp[i2\pi n(Ft + G\nu) + i2\pi\phi_n] + A_{-n} \exp[-i2\pi n(Ft + G\nu) + i2\pi\phi_{-n}]\}.$$

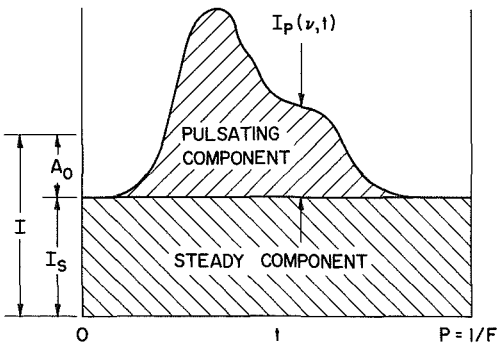

FIG. 3.—A simple pulse superposed on a steady "d.c." bias illustrating the relation of the steady (I_s), and pulsating (I_p) intensities to the average pulsating (A_0) intensity and the total (I) intensity.

Since $I_p(\nu, t)$ is real, its spectrum is Hermitian. Thus $A_n = A_{-n}$, $\phi_n = -\phi_{-n}$, and

$$I_p(\nu, t) = A_0 + \sum_{n=1}^{\infty} 2A_n \cos 2\pi[n(Ft + G\nu) + \phi_n] . \tag{9}$$

By definition, $I_p(\nu, t)$ must be zero at some point in its period, $P = 1/F$. Suppose that for some (ν', t'), $I(\nu', t') = 0$. Then

$$A_0 = -\sum_{n=1}^{\infty} 2A_n \cos 2\pi[n(Ft' + G\nu') + \phi_n] . \tag{10}$$

In these observations we did not independently determine the epoch of the pulses, so we have no *a priori* knowledge of (ν', t'). However, from the observed values of $R(\pm NF, \pm NG)$, $N \neq 0$, we can determine the A_n and the $[n(FT + G\nu) + \phi_n]$ for some arbitrary (ν, t). Since $I(\nu, t) \geq 0$,

$$A_0 \geq -\sum_{n=1}^{\infty} 2A_n \cos 2\pi[n(Ft + G\nu) + \phi_n]$$

for arbitrary (ν, t). We can insert various values of (ν, t) into this expression until we find those values, (ν', t'), which maximize the summation. When that is accomplished, A_0 may be found from equation (10) and, since $R(0, 0)$ gives us I, the flux of the steady component is found, $I_s = I - A_0$.

It will next be shown that the relative phases of the various components can be measured to determine the relative positions of the objects which emit them. I must be real. Thus the relative phase of $R(0, 0)$ and I is ϕ_0, the average phase of the I component in the interferometer pattern.

Since $I_p(\nu, \tau)$ is real and its spectrum is Hermitian with $A_N = A_{-N}$ and $\phi_N = -\phi_{-N}$, from equation (8) the average phase of R_{+N} and R_{-N} is

$$\phi_{0p} = \tfrac{1}{2}(\phi_{0p} + \phi_N + NG\nu_0) + \tfrac{1}{2}(\phi_{0p} - \phi_N - NG\nu_0) . \tag{11}$$

Differences between ϕ_{0p} and ϕ_0 would indicate positional shifts in the interferometer pattern between the I_s and I_{0p} components. If the compact source and the pulsar are physically identical, ϕ_{0p} will equal ϕ_0. The radiation generating each component will follow essentially identical paths through the medium between the source and the antennas. This method of analysis effectively eliminates practically all effects of refraction in the interstellar, interplanetary, and ionospheric media. Positional shifts of less than 0".1 can be determined even though the radiation is refracted irregularly through angles several orders of magnitude larger than this.

All of the $(\phi_N + NG\nu_0)$ can obviously be found, and the pulse shapes and epochs can be derived by summation of the Fourier series for $I_p(\nu, \tau)$.

III. OBSERVATIONAL RESULTS ON TAURUS A

When our method of analysis was applied to the data, many problems arose with the standard VLBI reduction programs. VLBI reductions do not normally require that one keep track of phase under time delay and LO offsets. To do this, epochs must be defined carefully and consistently throughout the reduction programs. For the pulsar reductions, we utilized the MIT–GSFC reduction program on the IBM 360-91 computer at NASA–Goddard Space Flight Center.

The flux scale was calibrated through observation of 3C 48 and 3C 147. The total fluxes at 121.6 MHz of these sources were taken to be 68 and 62 f.u., respectively, and they were assumed to be unresolved. The average correlation coefficient of the I component of Tau A was $37.4 \pm 2.5 \times 10^{-4}$. After correcting for the fact that the

system noise level was raised by the presence of Tau A in the antenna response patterns, this correlation coefficient corresponds to a flux of 29 ± 6 f.u. (see fig. 4).

The observations of the sidebands generated by NP 0532 are summarized in table 1. Unfortunately, with only an 84-foot dish as one end of the interferometer, the signal-to-noise ratios of the sidebands are marginal. The rms noise level corresponds to a correlation coefficient of 2.13×10^{-4}. Since the sidebands were only a few times this noise level, their identification was often doubtful. The output fringe-rate spectrum was examined within a region of ±0.1 Hz centered upon *NF*, and the time-delay spectrum was examined over ±4 μs in the vicinity of *NG*. If the largest deflection in these regions occurred within ±0.01 Hz and ±0.5 μs of the proper fringe rate and time delay, it was accepted as "real" and used in table 1. When no fringes were detected with this criterion, the true correlation was assumed to be in the range $(0–5) \times 10^{-4}$. The amplitudes given for the sidebands are obviously crude, and the missing sidebands complicate the analyses of the pulse amplitude and shape. The noise level is too high for accurate measurement, and the sideband deflections are systematically overestimated because of random noise contributions. This overestimation occurs because, by definition, a fringe amplitude less than or equal to zero is impossible. This leads to a fringe-amplitude probability distribution function which, for weak fringes, follows a Rice distribution rather than a Gaussian. In the limit of zero correlation, this becomes a Rayleigh distribution with a positive, nonzero expectation value. If a correction is made for this overestimation and the total sideband power, A_0, is estimated, this power equals 65 ± 15 percent of the $N = 0$ flux. If the compact source and the pulsar are assumed to be distinct, then the spectrum of the I_s component must be exceedingly steep and this component's flux at 121.6 MHz must be ~10 f.u.

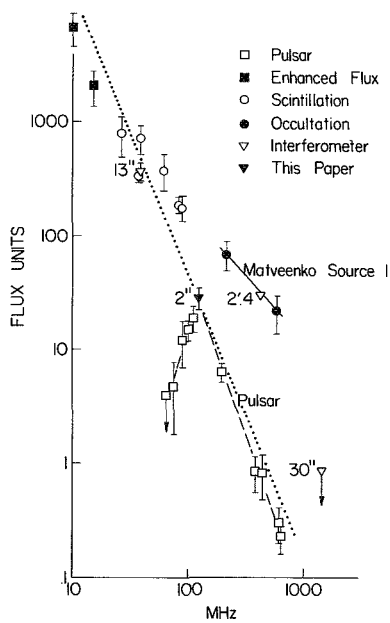

FIG. 4.—The spectra of the small components of Tau A. The spectrum of NP 0532 given by Rankin *et al.* (1970) is shown by the dashed line. A spectrum with an index of −2.5 fits all of the data concerning the ≈1″ source reasonably well. Matveenko's Source I must be resolved by long-baseline interferometer and interplanetary-scintillation techniques.

TABLE 1

AMPLITUDES AND PHASES OF THE SIDEBANDS GENERATED BY NP 0532

Date	Time (UT)	I Correlation Coefficient $\times 10^4$	$(A_1 + A_{-1})/I$	$(A_2 + A_{-2})/I$	$(A_3 + A_{-3})/I$	$(A_4 + A_{-4})/I$	Average Phase of Sideband Relative to $N = 0$		Remarks
							± 1	± 2	
1970 Jan 10..	0305	38.0	0.50	0.19–0.32	0–0.26	0–0.26	+34°3	...	
	0328	31.1	0.57	0.37	0.15–0.31	0.14–0.30	+51.2	+13°6	
	0410	23.3	0.50	0.29–0.51	0.35	0.42	+18.6	...	
1970 Jan 11..	0305	40.7	0.49	0.48	0.15–0.27	0.14–0.26	−16.8	−9.0	
	0405	31.5	0.49	0–0.32	0–0.32	0–0.32	−22.3	...	
1970 Jan 12..	0300	42.3	...	...	...	...	...	...	Interference
	0325	44.7	0.51	0.20–0.32	0–0.22	0.15–0.26	−10	...	
	0400	41.7	0.48	0.38	0.10–0.20	0–0.20	+3.8	+25.6	
Average (min-max).		37.4 ± 2.5	0.51	(0.26–0.39)	(0.11–0.27)	(0.12–0.29)	+8°4	+10°1	
Mean.....		37.4 ± 2.5	0.51	0.32	19	0.21	+8°9 ± 7°2	...	

NOTE.—The phases are given only when both sidebands were present. The $N = \pm 3$ and ± 4 sidebands were too weak for reliable phase determinations. When a range of amplitudes is specified, one or both pulsar sidebands were not detected, and the range is indicative of the possible amplitudes of the undetected sidebands.

The relative phases of the sidebands and the $N = 0$ component are shown in table 1 to agree to 8°.9 ± 7°.2. The rather large scatter in the relative phases is consistent with the poor signal-to-noise ratios, and the small disagreement in phase is probably not significant. Therefore, the I component agrees in position with the A_0 component to an accuracy of (8°.9/360°) × 2″.2 ≈ 0″.05.

Gower (1967) has shown that the position of the compact source agrees with that of the pulsar to an accuracy of 10″ E-W and 1′ N-S. Matveenko and Pynzar (1969) find that they agree to ± 7″ E-W. Our measurement tightens the E-W agreement to about ± 0″.1. Of course, our data would allow a few ambiguities at the 2″.2 fringe spacing. The absence of phase residuals that are systematic in hour angle indicates that the components are coincident in declination to a few seconds of arc.

The observations were spaced at roughly 30^m intervals. It does not appear possible to average the sideband signals coherently over these long intervals to increase the signal-to-noise ratio. For better accuracy, it will be necessary to employ larger telescopes, wider bandwidths, and/or longer integration times.

Cronyn (1970*a*, *b*) and Rankin *et al.* (1970) have asserted that the compact source and NP 0532 are identical and that below 100 MHz the pulses are scattered and delayed in the interstellar medium by more than one period to form the compact source. Our experiment confirms this assertion, and our observations of the fluxes of the fluctuating and steady components at 121.6 MHz agree with Cronyn's calculation.

Considerable confusion concerning the spectrum of the compact source has existed. This is caused by the fact that the Crab Nebula apparently contains several localized sources with various angular diameters and spectra (Matveenko 1968*a*, *b*; Wilson 1971). Occultation observations and moderate-baseline interferometer observations indicate a localized source with a spectral index ≈ -1.2 (Minkowski 1968); this is probably Matveenko's Source I. It must have an angular diameter of at least a few seconds of arc and be resolved by long-baseline interferometer and interplanetary-scintillation techniques. Determinations of the position of the scintillating source have ruled out its coincidence with Source I which is located ≈1′ southeast of the pulsar (Matveenko 1968*b*). The spectral index of −1.2 for the compact source seems to have arisen because of a confusion between Source I and the small angular diameter (< 1″) source associated with the pulsar. The interpretation of enhancements of the spectrum of Tau A in the 10–20 MHz range (Bridle 1970; Braude *et al.* 1969; Clark 1967) will be uncertain until the structure of the source region is determined.

Our observation proves that the Crab Nebula contains no source with dimensions $\lesssim 1''$ and flux greater than ≈30 f.u. at 121.6 MHz. The source that we observed agrees with the pulsar NP 0532 both in position and in flux. This source must be the same object that is observed by the interplanetary-scintillation methods (Matveenko and Pynzar 1969; Cronyn 1970*a*; Bell and Hewish 1967; Gower 1967; Antonova, Panajian, and Pynzar 1971) and by long-baseline interferometry at 38 MHz (Slee and Wraith 1967) since these techniques would discriminate against a larger-angular-diameter object. From figure 4 we see that the spectral index of the small-angular-diameter component associated with the pulsar is about −2.5 from 26.3 to 121.6 MHz. This agrees with the spectral index of NP 0532 above 100 MHz for which Rankin *et al.* (1970) give 2.9 ± 0.4. Some curvature in the spectrum may exist. This spectrum also fits the enhanced low-frequency flux estimates given by Bridle (1970), but, as noted above, no certain identification of the 10–20 MHz source can yet be made.

The electromagnetic spectrum of the nebula and the pulsar are shown in figure 5. We have shown that there is very little continuum radiation associated with NP 0532. Our estimated $\nu^{-2.5}$ spectrum of the total emission from the pulsar disagrees violently with its optical and X-ray spectra. The pulsar flux rises sharply in the radio region and has a second broad peak in the optical or ultraviolet range.

Simultaneous observations over long and short baselines should prove interesting.

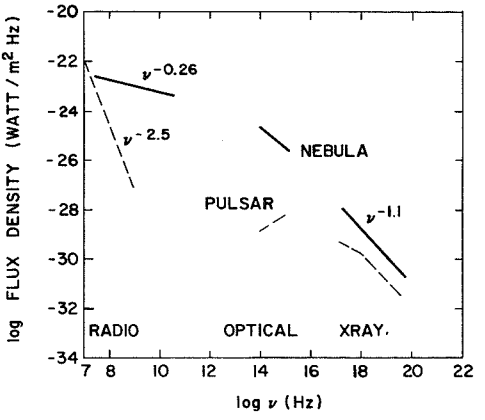

FIG. 5.—The electromagnetic spectrum of the Crab Nebula and the pulsar NP 0532

Even when most of the flux has been scattered by the interstellar medium to form a nonfluctuating compact source of moderate angular size, a smaller-angular-diameter fluctuating source should still be observable. The radiation which follows a nearly direct path from the source to the observer will appear in a small-angular-diameter component; it should undergo less excess multipath delay in the interstellar medium than the larger-angle component. Therefore, measurements of the modification of pulse shapes by the interstellar medium should be possible by observing the correlated signals over long and short baselines.

IV. OTHER SOURCE OBSERVATIONS

Our results on other sources are summarized in table 2. The ratio of the total fluxes of 3C 48 and 3C 147 at 121.6 MHz are essentially equal to the ratio of their correlation coefficients. Therefore, these sources were assumed to have unit visibility and were used to establish the constant of proportionality between correlation and flux after normalization by the single-dish antenna temperatures. The antenna temperatures are variable since they contain the total flux from the sources plus the galactic background. These data were processed on the NRAO 360-50 computer.

TABLE 2

THE UNRESOLVED FLUXES AND APPROXIMATE VISIBILITIES OF SEVERAL SOURCES OBSERVED AT 121.6 MHz WITH A 92,000 λ INTERFEROMETER

Source	Assumed Total Flux	Unresolved Flux	Number of Observations	Approximate Visibility
	(fu)			
3C 48	68 ± 5	68 ± 6	2	Assumed 1.0
3C 84	95	6 ± 2	3	0.06
3C 144 (Tau A)	1,560	29 ± 6	9	0.02
3C 147	62 ± 5	62 ± 7	9	Assumed 1.0
3C 273	74	12 ± 5	3	0.16
3C 274 (Vir A)	1,400	7 ± 4	4	0.005
3C 298	73	30 ± 5	3	0.4
3C 405 (Cyg A)	12,600	<15	2	<0.002
3C 459	32	14 ± 4	3	0.44
3C 461 (Cas A)	15,500	<20	3	<0.002

Each source will be discussed individually below.

a) 3C 48

There is no evidence that this source should be resolved at 92,000 λ, and it is the primary calibrator of our flux scale. Anderson and Donaldson (1967) find that it is 0".35 by ≤0".23 at 408 MHz. The source was unresolved at 158 MHz by Allen *et al.* (1962) and at 38 MHz by Slee and Wraith (1967).

b) 3C 84

The compact source, 3C 84A has been separated into three components with angular sizes ~0".001, 0".1, and 5′ by Ryle and Windram (1968). We have apparently observed the second component, and this is also the B component for which Clarke *et al.* (1969) find a flux of 11 f.u. at 448 MHz. This component is apparently undergoing self-absorbtion in the 100–400 MHz range, and its spectral index in this frequency range is about +0.5. The spectrum of 3C 84 is shown in figure 6.

c) 3C 147

Anderson and Donaldson (1967) give dimensions of 0".52 by ≤0".21 for this object at 408 MHz. As seen from table 2, a flux scale derived from the assumption that 3C 147 is unresolved by our 2".2 fringes agrees excellently with a scale using 3C 48 as a calibrator. Therefore, we assume that 3C 147 is unresolved in spite of the fact that Allen *et al.* (1962) give a fringe visibility of only 0.5 at 61,000 λ for this source at 158 MHz. This present results would also seem to agree with the complex source structure at scales ≲0".1 found by Donaldson and Smith (1971) at 1422 and 2694 MHz.

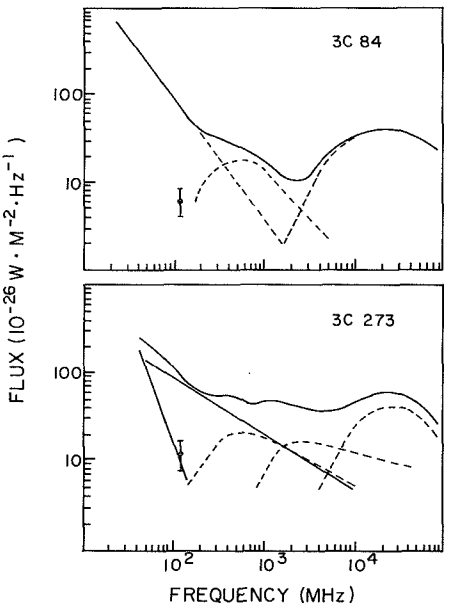

FIG. 6.—The fluxes of the small-angular-diameter components of 3C 84 and 3C 273B at 121.6 MHz compared with those given by Kellermann and Pauliny-Toth (1969).

d) 3C 273

The A component of this source (Bailey *et al.* 1964) is probably well resolved by our interferometer, and we are observing the B component discussed by Kellermann *et al.* (1968). The spectrum of this component is shown in figure 6. Assuming that this is the same component that Clarke *et al.* (1969) observed at 448 MHz, its spectrum is practically flat in the 100–500 MHz range. Remnants of the complex structure observed at 408 MHz by Anderson and Donaldson (1967) may make a simple interpretation of our observation impossible.

e) 3C 274 (Virgo A)

We are apparently observing the "jet" component of Vir A for which Donaldson, Miley, and Palmer (1971) give a flux of ≈ 2.5 f.u. at 1422 MHz. Combining our observations with those of Allen *et al.* (1962), Vir A appears to have a constant visibility of about 0.005 over baselines from 9700 λ to 92,200 λ. These observations agree with the model suggested by Graham (1970). The small nuclear component is probably weak at our frequency.

f) 3C 298

We find a visibility of 0.4 for this source while at 158 MHz Allen *et al.* (1962) give 0.1 at 61,100 λ and 0.6 at 32,000 λ. It is tempting to combine the data since both baselines are oriented nearly E-W. If the visibility function has a null near 61,100 λ and then rises again, a double-source model with a component separation of $\approx 1''.6$ would fit the data. Anderson and Donaldson (1967) interpret their 408-MHz data as indicating a double source with components separated by $1''.2$ at a position angle of 78°.

g) 3C 405 (Cygnus A)

The high system-noise level produced by Cyg A prevents the detection of weak fringes. We confirm the suggestion of Miley and Wade (1971) that the fine structure in Cyg A has a low-frequency cutoff.

h) 3C 459

This faint N galaxy (Wyndham 1966) apparently has structure on the $1''$ scale. Our results agree with Allen *et al.* (1962). Smaller-scale structure does not appear to have been observed.

i) 3C 461 (Cassiopeia A)

We find no evidence of fine structure in Cas A.

V. TECHNICAL RESULTS

As shown in figure 7, the short-term phase stability of our fringes is excellent. At 121.6 MHz, some 6 μs of excess group delay may be encountered by a wave as it traverses the ionosphere, yet the relative phases of the waves at the two antennas are stable to a small fraction of a nanosecond. Essentially no difference in the phase stability was found for daytime, early-evening, or late-night observations.

The bandwidth of the VLBI terminal yields a coherence time ~ 3 μs. Under ideal conditions, this allows determination of the point of maximum coherence between the two signals arriving at the antennas to an accuracy of a few hundred nanoseconds. To this accuracy, the point of maximum coherence was stable and independent of local time. No differential ionospheric delays were observed over our 230-km baseline.

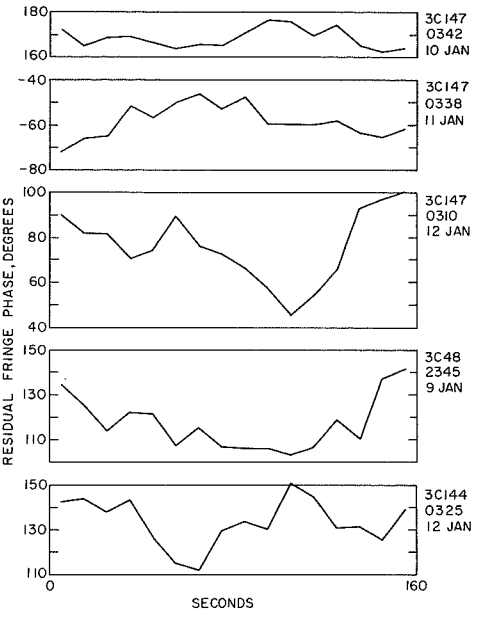

FIG. 7.—Examples of the residual phase stability achieved during 160-s VLBI observations at 121.6 MHz. Each point represents a 10-s integration.

This work was supported by the National Aeronautics and Space Administration under grant NGL-21-002-029 and by the National Science Foundation under grant GP-19401. The National Radio Astronomy Observatory is operated by Associated Universities, Inc., under contract with the National Science Foundation.

We wish to acknowledge the invaluable assistance of Mr. Allen Whitney of MIT for development and modification of the MIT/GSFC data reduction programs to permit the Tau A processing. The NRAO data processing programs that we utilized were developed by B. Clark.

REFERENCES

Allen, L. R., Anderson, B., Conway, R. G. Palmer, H. P., Reddish, V. C., and Rowson, B. 1962, *M.N.R.A.S.*, **124**, 477.
Anderson, B., and Donaldson, W., 1967, *M.N.R.A.S.*, **137**, 81.
Antonova, T. D., Panajian, V. G., and Pynzar, A. V., 1971, *Astr. Zh.*, **48**, 19.
Bailey, J. A., Branson, N. J. B. A., Elsmore, B., and Scheuer, P. A. G. 1964, *Nature*, **201**, 755.
Bare, C., Clark, B. G., Kellermann, K. I., Cohen, N. H., and Jauncey, E. L. 1967, *Science*, **157**, 189.
Bell, S. J., and Hewish, A. 1967, *Nature*, **213**, 1214.
Braude, S. Ya., Lebedeva, O. M., Megne, A. V., Ryatov, B. P., and Zhouch, I. N. 1969, *M.N.R.A.S.*, **143**, 289.
Bridle, A. H. 1970, *Nature*, **225**, 1035.
Clark, T. A. 1967, Ph.D. thesis, University of Colorado.
Clarke, R. W., Broten, N. W., Legg, T. H., Locke, J. L., and Yen, J. L. 1969, *M.N.R.A.S.*, **146**, 381.
Counselman, C. C., III, and Rankin, J. M. 1971, *Ap. J.*, **166**, 513.
Cronyn, W. M. 1970*a*, Ph.D. thesis, University of Maryland.
———. 1970*b*, *Science*, **168**, 1453.
Donaldson, W., Miley, G. K., and Palmer, H. P. 1971, *M.N.R.A.S.*, **152**, 145.
Donaldson, W., and Smith, H. 1971, *M.N.R.A.S.*, **151**, 253.

Goldstein, S. J., Jr., and James, J. T. 1969, *Ap. J.* (*Letters*), **158**, L179.
Gower, J. F. R. 1967, *Nature*, **213**, 1213.
Graham, I. 1970, *M.N.R.A.S.*, **149**, 319.
Kellermann, K. I., Clark, B. G., Bare, C. C., Rydbeck, O., Elldér, J., Hansson, B., Kollberg, E., Höglund, B., Cohen, M. H., and Jauncey, D. L. 1968, *Ap. J.* (*Letters*), **153**, L209.
Kellermann, K. I., and Pauliny-Toth, I. I. K. 1969, *Ap. J.* (*Letters*), **155**, L71.
Matveenko, L. I. 1968*a*, *Soviet Astr.—AJ*, **12**, 128.
———. 1968*b*, *ibid.*, 552.
Matveenko, L. I., and Pynzar, A. V. 1969, *Soviet Astr.—AJ*, **13**, 433.
Miley, G. K., and Wade, C. M. 1971, *Ap. Letters*, **8**, 11.
Minkowski, R. 1968, in *Stars and Stellar Systems*, Vol. 7, ed. B. M. Middlehurst and L. H. Aller (Chicago: University of Chicago Press), p. 623.
Rankin, J. M., Comella, J. N., Craft, H. D., Jr., Richards, D. W., Campbell, D. B., and Counselman, C. C., III. 1970, *Ap. J.*, **162**, 708.
Ryle, M., and Windram, M. D. 1968, *M.N.R.A.S.*, **138**, 1.
Slee, O. B., and Wraith, P. K. 1967, *Nature*, **214**, 971.
Wilson, A. S. 1971, in *The Crab Nebula*, ed. R. D. Davies and F. G. Smith (Dordrecht: D. Reidel Publishing Co.), p. 67.
Wyndham, J. D. 1966, *Ap. J.*, **144**, 459.

Reprinted from PROCEEDINGS OF THE IEEE
VOL. 61, NO. 9, SEPTEMBER, 1973
pp. 1230-1233

Long Wavelength VLBI

T. A. CLARK AND WILLIAM C. ERICKSON

Abstract—**The application of very-long baseline interferometry (VLBI) techniques at meter and decameter wavelengths has proven to be a unique tool for studying a number of different phenomena. Because of the high angular resolution which we achieve with VLBI, candidate objects for study include the compact nuclei and "jets" associated with quasars and radio galaxies, pulsars, small knots in galactic supernova remnants, and nonthermal planetary sources. Our investigations have been aimed at determining the emission spectra of these objects, measuring their apparent angular size, and mapping their structure. We expect that these properties will be interrelated, particularly at or below the frequencies at which their spectra peak. As various components of a radio source become self-absorbed the apparent angular structure must change quite radically. Concomitant investigations of transmission properties of the various media which intervene between the source and the observer must be carried out. Often these investigations of the interstellar, interplanetary, and ionospheric media are as interesting as the study of the radio sources themselves.**

Manuscript received February 15, 1973. This work was supported in part by the National Science Foundation under Grant GP 19401, and in part by the National Aeronautics and Space Administration under Grants NGL-21-002-029 and NGL-21-002-033. The National Astronomy and Ionospheric Center is operated by Cornell University under Contract with the National Science Foundation. The National Radio Astronomy Observatory is operated by Associated Universities, Inc., under Contract with the National Science Foundation.

T. A. Clark is with the Radio Astronomy Branch, Goddard Space Flight Center, Greenbelt, Md. 20771.

W. C. Erickson is with the Astronomy Program at the University of Maryland, College Park, Md. 20742.

I. INTRODUCTION

THE very-long baseline interferometry (VLBI) observations reported here are among the more sensitive measurements of discrete radio sources which have been made at long wavelengths. This high sensitivity is due to a number of factors. The large "dc" signal due to the galactic background and the "ac" confusion noise due, primarily, to structure in the background, are suppressed since they arise from regions larger than the fringe spacing; the coarsest fringes of any experiment reported herein are ~20″. Since the VLBI sensitivity is set by the achievable bandwidth, integration time, and telescope collecting area, rather than by confusion, it behooves us to maximize each of these quantities. The maximum bandwidth we have been able to employ is about 1 MHz, but more typically about 300 kHz, as dictated by terrestrial interference. The ionospheric phase stability has been found to limit our coherent integration time to about 50–200 s. The limits on these two parameters have caused us to use the NRAO Mark I VLBI recording systems [1] which record digital clipped data at a rate of 720 kb/s on conventional computer tape. At this recording rate a roll of tape holds about 3 min of data. The meter-wavelength experiments have utilized large-dish telecopes such as the 1000′ Arecibo, 300′ NRAO, and 150′ NRL instruments, while the 26.3-MHz observations were made with large (10^4 m^2

TABLE I

THE LONG WAVELENGTH VLBI EXPERIMENTS

Experiment Number	Dates	Frequency (MHz)	Stations and Location	Telescope Size and Type
1	Jan. 70	121.6	NRAO, Green Bank, W. Va. NRL, Maryland Point, Md.	300′ dish 84′ dish
2	Aug. 70	26.3	NOAA, Boulder, Colo. NOAA, Haswell, Colo.	10^4 m² arrays
3	Mar. 71	144.5 and 114.5	NRL, Sugar Grove, W. Va. U. of Ill., Vermillion River Observ. (VRO) Caltech, Owens Valley Observ. (OVRO)	150′ dish 120′ dish 130′ dish
4	Aug. 71	26.3	(same as 2) + Ames, Iowa	(same as 2)
5	Nov. 71–Mar. 72 (5 separate runs)	196.5 and 111.5	NRAO, Green Bank, W. Va. NRL, Sugar Grove, W. Va. Cornell, Arecibo, P. R.	300′ dish 150′ dish 1000′ dish
6	Dec. 72 and Mar. 73	111.5 and 73.8	(same as 5)	(same as 5)

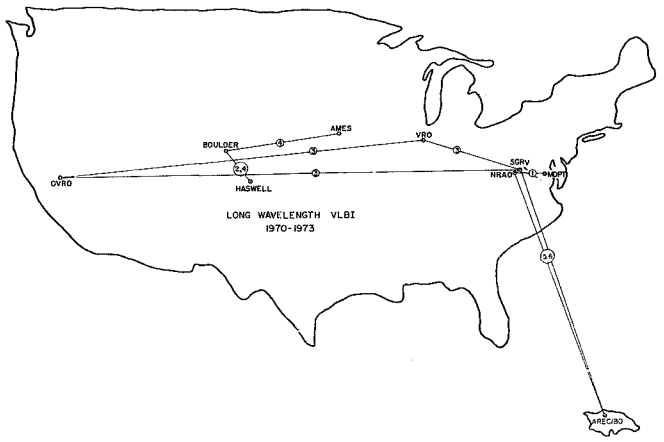

Fig. 1. The baselines utilized in the various long wavelength VLBI experiments. The numbers on the baselines refer to entries in Table I.

collecting area) phased arrays. With these instruments we have been able to achieve sensitivities of 1–10 flux units (fu) (1 fu = 10^{-26} W·m^{-2} Hz^{-1}) on each 3-min tape.

Although the primary beamwidths of the telescopes are necessarily large at these long wavelengths, a small region of sky within the primary beamwidths can be isolated by accepting only those signals which have a proper interferometer fringe frequency and time delay. By reprocessing the original data tapes, the signals from various points within the primary beamwidth of the telescope can be measured.

Since January 1970, groups with which the authors are affiliated have performed a series of six successful experiments utilizing a number of different telescopes and involving a large number of participants from the various observatories. These six sessions are summarized in Table I and Fig. 1. In addition to the authors, those who have been most intimately involved in the planning and organization of these experiments have included J. J. Broderick, W. M. Cronyn, S. H. Knowles, S. D. Shawhan, G. M. Resch, and N. R. Vandenberg. Many others, too numerous to name, have been involved. In addition to our efforts at these wavelengths, we should also note that the Jodrell Bank RF link interferometer has been used at 38 and 158 MHz with baselines up to 127 km [2], [3]. The Canadian VLBI team has carried out a number of successful 2000–6000-km experiments at 408 MHz [4]. Several groups, including ones at the University of Florida and at the University of Colorado have used VLBI techniques at decameter wavelengths to observe Jupiter.

II. VLBI Observations Within the Solar System

Jupiter's decametric radiation arises from a small diameter source. The Jovian decametric radiation has been detected at several frequencies in the 18–24-MHz range by various groups [5], [6] and by us at 26.3 MHz. The radiation seems to arise from a source which is unresolved on all baselines employed and, hence, appears smaller than about 0″.1. An alternative explanation is that the emission mechanism is phase coherent and antenna-like. If this is the case, the emission would seem to come from a single point regardless of the physical size of the aperture. We have unsuccessfully attempted to detect small diameter sources on the sun, but we would expect such sources to be heavily scattered by the solar corona. Scattering associated with irregularities in the solar wind has been observed on signals from sources outside the solar system.

III. VLBI Observations of Galactic Objects

The most intensively studied object has been the small angular diameter component of the Crab Nebula. It generally provides the largest unresolved flux at the longer baselines and it is of great intrinsic interest. The dispersion of the Crab Nebula pulsar is so large that several pulses are in the passband of the system simultaneously. For observing this pulsar, a novel method of coherently dedispersing the pulses was developed [7]. The two data tapes are displaced in such a fashion that the instrumental dispersion of the interferometer compensates for the dispersion in the interstellar medium. In this fashion both the steady and the pulsating components of the small angular diameter source in the Crab Nebula have been observed. Here we find that the steady and pulsating components are identical in position to an accuracy of about 0″.01. Therefore, the physical association of the low-frequency compact source with the pulsar is confirmed. The apparent angular size of the source is consistent with that to be expected for a point source that has undergone scattering in the interstellar medium. In Table II our measurements of the

TABLE II

THE APPARENT ANGULAR SIZE OF THE SMALL COMPONENT IN THE CRAB NEBULA AS MEASURED BY VLBI TECHNIQUES

Baseline	Frequency (MHz)	Apparent Angular Size (seconds of arc)	Interstellar Scattering (seconds of arc)
Sugar Grove–NRAO Arecibo	196.5	<0.04	0.03
Sugar Grove–VRO OVRO	144.5	0.055±0.01	0.05
Sugar Grove–NRAO Arecibo	111.5	0.07±0.01	0.08
Boulder–Haswell Ames	26.3	~1–2	1.45

Note: A Gaussian brightness distribution is assumed. The interstellar scattering sizes are those predicted by Harris *et al.* [8] assuming a distance of 2000 parsecs to the Crab Nebula.

apparent angular size are compared with the predictions based on interstellar scattering by Harris, Zeissig, and Lovelace [8]. The data in Table II are in good agreement with the angular sizes expected from interstellar scattering and are at least consistent with the expected wavelength-squared dependence of the scattering.

More detailed observations lead to a number of intriguing results [9]. The total flux from the small angular diameter component appears to remain constant while the ratio between the pulsating and steady fluxes varies by factors of 2 over periods of 1 h. This would indicate that the power output of the pulsar is constant while the multipath scattering that produces the steady component is highly time variable. The pulsating component displays strong linear polarization while the steady component is unpolarized. If the depolarization of the steady component resulted from differential Faraday rotation around multiple paths through the interstellar medium, impossible electron densities and magnetic fields would be required. This indicates that the multipath scattering that presumably smears out the pulsations and produces the steady component occurs near the pulsar, probably well within the nebula. Finally, the pulse profiles under high and low angular resolutions are remarkably similar. If multipath time delays in the interstellar medium smeared out the pulses to produce the steady component, one would expect the pulse profile to be resolution-dependent. Under high resolution the scattered component should be partly eliminated and the pulse profile should sharpen. These observations indicate that the source distribution is certainly time- and polarization-dependent. The assumption of a Gaussian brightness distribution in Table II is an oversimplification and the agreement between our data and simple model of interstellar scattering is probably quite fortuitous.

A number of other pulsars have been observed. They are *nearby* and of *low dispersion* so they have undergone little interstellar scattering. They all appear to be point sources to the limit of our resolution. Small angular diameter components in several supernova remnants, including Cas-A (3C461) and Tycho (3C10), have been found at 26.3, 73.8, and 111.5 MHz. We have not yet shown that any of these are central sources like the small angular component in the Crab Nebula. They seem to be an accumulation of sharp edges and knots in a complex distribution quite similar to that seen at centimeter wavelengths.

TABLE III

EXAMPLES OF THE RESULTS OBTAINED ON THE ARECIBO–NRAO BASELINE

Source	111.5 MHz Approximate Unresolved Flux	111.5 MHz Total Flux (fu)	196.5 MHz Approximate Unresolved Flux	196.5 MHz Total Flux (fu)	Optical ID
0106+01	2.4	5			Quasar
0C328	2.8	2	1.0	2.5	
3C48	5.5	67	~1	5.3	Quasar
3C49	4.5	13	1.8	10	
NRAO 91	3.0	6.5	2.4	6.0	
CTA 21	2.5	6.3			
3C120	1.7	8.5			Seyfert Galaxy
3C138			1.1	18	Quasar
0736+01	1.1	3	1.2	3	Quasar
1055+01	2.8	3	2.7	4.7	Quasar
1148−00	2.5	2	2.1	2.6	Quasar
3C273B	~5	140	~8	70	Quasar
3C274	0.8	1580	0.6	988	Elliptical Galaxy
3C287	17.8	20	8	16	Quasar
3C286	29.2	28	24.9	26	Quasar
1345+12	3.3	3 (19)	6.7	4 (14)	Spiral Galaxy
3C298	4.4	60	2.8	50	N Galaxy
3C459	1.4	35	1	20	N Galaxy

Note: The values of unresolved flux are based upon measured aperture efficiencies, and the cases where the unresolved flux exceeds the estimated total flux are simply caused by small measurement errors. The apparently unresolved sources, 1148−00, 3C286, 3C287, and 1345+12, are all above 55° galactic latitude.

IV. VLBI OBSERVATIONS OF EXTRAGALACTIC SOURCES

About 100 compact extragalactic sources have been observed during the various meter-wavelength experiments and about 25 have been detected at 26.3 MHz. One of the main goals of these observations has been to use these sources as probes of the interplanetary, interstellar, and possibly intergalactic ionized media by studying the variation of apparent angular sizes with solar elongation, galactic latitude, frequency, and distance. If the scattering effects can be separated, then we can also hope to gain additional data on the variation of intrinsic source size and structure with frequency. Although these analyses are still in progress, we find that sources near the galactic pole appear smaller than those near the galactic plane, and find evidence for the wavelength squared dependence of the scattering.

The angular resolution obtained on even a single baseline obviously varies with frequency. Therefore, each experiment listed in Table I yields a different angular resolution, and at the present time the intrinsic and scattering effects are still being separated. In Table III we present some examples of the data. One can see that most sources are heavily resolved, but that fringe visibilities increase at the higher frequencies as would be expected if the apparent angular size is mostly a result of scattering.

Another major goal has been to utilize the shorter baselines, in particular the 50-km baseline between Green Bank and Sugar Grove, to provide just enough angular resolution to filter out the larger components (such as haloes) and permit us to measure the fluxes of the nuclear components and "jets" in these objects. If small diameter sources radiate by the synchrotron process, we should observe a peak in their power spectrum at a frequency which is a function of the size of the source and physical properties within the source; many sources are known to have such peaks in the 0.5–10-GHz region. At frequencies below this synchrotron self-absorption

cutoff, simple models would predict a power low spectrum proportional to $f^{+2.5}$. The shorter baseline experiments at 73.8, 111.5, and 196.5 MHz have made use of the excellent sensitivity and suppression of large angular features to test such models. These data are also still being analyzed but very few, if any, of the sources fit the simple model. One possible interpretation of this discrepancy is that the sources do not consist of a single small diameter component, but rather of a series of more-or-less concentric shell components showing evidence of earlier nuclear activity and subsequent expansion.

V. Conclusion

VLBI techniques find a number of applications at meter wavelengths. Since scattering in the interplanetary medium is known to bias the data, we have planned most of our observations in the antisolar direction. Scattering in the interstellar medium complicates the observation of intrinsic source properties and vice-versa. In the immediate future we will be concerned with analyzing and interpreting the data we have acquired. Once we have a firm understanding of interstellar scattering phenomena and intrinsic source structure in this wavelength region, it will be interesting to turn our attention to interplanetary scattering and to study the phase fluctuations impressed by the interplanetary medium at various baseline lengths and solar elongation angles.

References

[1] C. C. Bare *et al.*, "Interferometer experiment with independent local oscillators," *Science*, vol. 157, pp. 189–191, July 1967.
[2] L. R. Allen *et al.*, "Observations of 384 radio sources at a frequency 158 Mc/s with a long baseline interferometer," *Mon. Notices Roy. Astron. Soc.*, vol. 124, pp. 477–499, 1962.
[3] O. B. Slee and P. K. Wraith, "Discrete radio sources at 38 Mc/s," *Nature*, vol. 214, pp. 971–974, June 1967.
[4] N. W. Broten *et al.*, "Long baseline interferometer observations at 408 and 448 MHz—I. The observations," *Mon. Notices Roy. Astron. Soc.*, vol. 146, pp. 313–327, 1969.
[5] G. W. Brown, T. D. Carr, and W. F. Block, "Long-baseline interferometry of S-bursts from Jupiter," *Astrophys. Lett.*, vol. 1, pp. 89–94, 1968.
[6] G. A. Dulk, "Characteristics of Jupiter's decametric radio source measured with arc-second resolution," *Astrophys. J.*, vol. 159, pp. 671–684, Feb. 1970.
[7] W. C. Erickson *et al.*, "Very long baseline interferometer observations of Taurus A and other sources at 121.6 MHz," *Astrophys. J.*, vol. 177, pp. 110–114, Oct. 1972.
[8] D. E. Harris, G. A. Zeissig, and R. V. Lovelace, "The minimum observable diameter of radio sources," *Astron. Astrophys.*, vol. 8, pp. 98–104, 1970.
[9] N. R. Vandenberg *et al.*, "VLBI observations of the Crab Nebula pulsar," *Astrophys. J. Lett.*, vol. 180, pp. L27–L29, Feb. 1973.

Radio Science, Volume 8, Number 10, pages 845–853, October 1973

The log-periodic array at the Clark Lake Radio Observatory

W. C. Erickson and T. B. H. Kuiper

Clark Lake Radio Observatory, Astronomy Program, University of Maryland, College Park, Maryland 20742

(Received April 18, 1973; revised July 20, 1973.)

A log-periodic array, three km in length, is operating at Clark Lake Radio Observatory. It makes one-dimensional sweeps of the solar brightness distribution in the frequency range 20 to 65 MHz once per sec. The phasing of the array and the receiving system are described, as well as how the dynamic spectra are analyzed for the positions of solar radio sources. Simultaneous measurements at many frequencies enable the observer to remove the effects of ionospheric refraction and to obtain fundamental positions to an accuracy of about one arc min at decametric wavelengths. Fundamental positions are given for Cassiopeia A.

INTRODUCTION

In order to obtain decametric wavelength observations, a swept frequency array [*Sheridan,* 1963; *Begovich,* 1966] has been designed, constructed, and is now in operation at the Clark Lake Radio Observatory near Borrego Springs, California. In all phases, this is a cooperative program between the Laboratory for Extraterrestrial Physics at NASA Goddard Space Flight Center and the Astronomy Program at the University of Maryland. The array was designed to be a useful solar instrument in its own right, and also to provide decametric observations of the positions of solar emission regions to complement hectometric observations made from satellites.

The observing frequency of the array is swept from 20 to 60 MHz once per sec. This causes the array's response pattern to be swept many times across the sun to determine one-dimensional brightness distributions and positions of solar emission regions. The time evolution of solar bursts may thus be studied in both angular and frequency coordinates. Data concerning the brightness distributions and positions of solar emission regions are being obtained each day between 16 and 24 hr UT. The data are being analyzed both at the University of Maryland and at Goddard Space Flight Center [*Kundu et al.,* 1970; *Kuiper and Pasachoff,* 1973]. At the former the analysis emphasizes the study of the radio sun at decametric wavelengths and at the latter the analysis emphasizes the complementary aspects of decametric and hectometric emission.

THE ANTENNAS

The antennas are equatorially-mounted log-periodic elements identical to those built at Stanford University by *Howard* [1965] (Figure 1). The primary beamwidth of each element is 60° in both the *E* and *H* planes, and each element gives a gain of 9 db with respect to an isotropic radiator. Each element is fed at its apex and presents a 450–ohm balanced impedance with a VSWR of less than 2 to 1 over the frequency range from 20 to 65 MHz. A wide-band balun is placed at the apex to match this impedance to a 50-ohm coaxial cable and a pair of General Electric IN916 diodes are soldered across the balanced antenna terminals to protect the system from excessive signal levels.

The equatorial mounts have polar axes which can be driven electrically in increments of 4° under control from the observatory. Because of the large amount of maintenance required for the tracking system, it is not normally used with the wide beamwidth of the elements. This does not seriously detract from the normal operation. For special observations, however, tracking is accomplished by stepping in rapid succession. Declination adjustment is accomplished manually.

THE ARRAY

Sixteen antennas are spaced at equal intervals of 220 m on an east-west baseline (Figures 2, 3). Con-

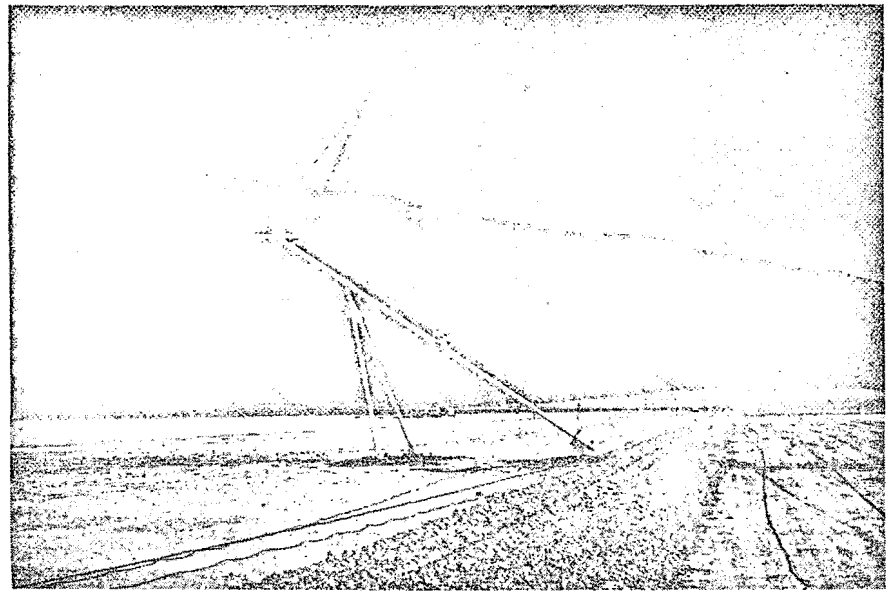

Fig. 1. A log-periodic element of the array.

sequently the voltage pattern is given by the Fraunhofer diffraction pattern of a 16-slit grating [*Kraus*, 1966],

$$E(\psi) = \sin(n\psi/2)/n \sin(\psi/2)$$
$$\psi = (2\pi l/\lambda) \sin\theta + \delta \qquad (1)$$

where

n = 16,
l = average antenna separation, 220.000 ± .003 m,
θ = complement of the angle between the interferometer axis and the radius vector in the direction of radiation (the "interferometer angle"),
$\lambda = c/f$, f = frequency at which the antenna is being operated,
δ = progressive phase difference between antennas.

The pattern has nulls when the numerator of equation 1 is zero, that is, when $16\psi = 2\pi k$, except when k is a multiple of sixteen. In that case, the denominator is also zero, and $E(\psi)$ achieves a maximum value of unity.

In a conventional grating array the observing fre-

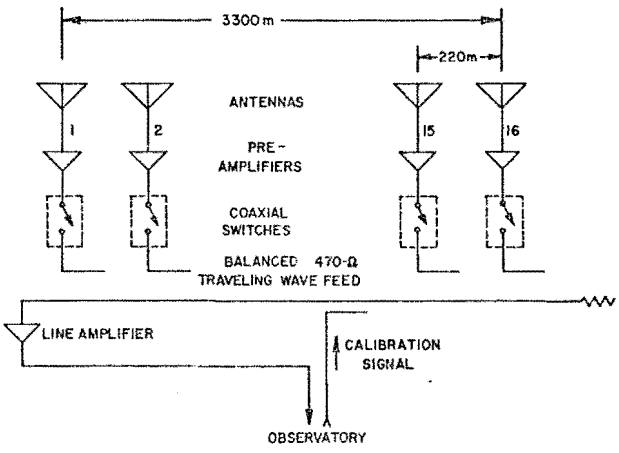

Fig. 2. Schematic of the log-periodic array and its feed system.

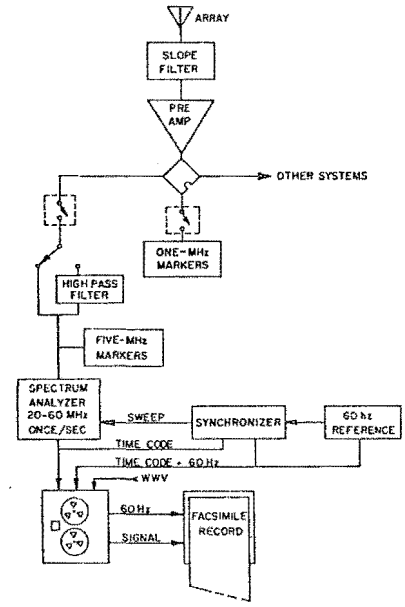

Fig. 3. Schematic of the electronics.

quency, f, is fixed. Equation 1 then gives the voltage pattern as a function of the angular coordinate, θ. If we decrease the observing frequency (increase the wavelength), the diffraction pattern will broaden; the fringes will move away from the white-light fringe and become correspondingly fatter. Thus, by smoothly altering the observing frequency, we can sweep a fringe (or several adjacent fringes) across a source which we want to observe.

There is another way to look at the operation of this array. Equation 1 achieves a maximum whenever

$$(l/\lambda) \sin \theta + (\delta/2\pi) = k \qquad k = \text{integer} \qquad (2)$$

In conventional arrays, λ is kept fixed. The earth's rotation moves the antenna pattern across the celestial sphere and the telescope shows a maximum response whenever the interferometer angle of the source, θ, is such that equation 2 is satisfied. This scanning process is far too slow for the highly transient solar events, so for rapid scanning we alter λ. By noting the wavelengths at which the response of the array is maximized, we can deduce the position, θ, of the source.

From (2) it is easily shown that the beamspacing and beamwidth are given by

$$\Delta\theta = \lambda/l \cos \theta \qquad (3)$$

and

$$\delta\theta = \lambda/16l \cos \theta \qquad (4)$$

respectively. Near transit, $\theta \simeq 0°$, so that at 20 MHz $\Delta\theta \simeq 4°$ and $\delta\theta \simeq 15$ arc min; at 60 MHz, $\Delta\theta \simeq 1.3°$ and $\delta\theta \simeq 5$ arc min. The spacing of the fringes is such that the position of a solar radio burst can be unambiguously identified.

ARRAY FEED SYSTEM

The array is fed from the western end of an east-west, open-wire, traveling-wave transmission line 3.3 km in length (Figure 2). The line is built of two strands of 1/4-in. diameter copperweld wire at 6-in. spacing, giving a characteristic impedance of 470 ohm. These wires are placed under approximately 1,000 lb tension and are fixed mechanically to the earth at each end, thus minimizing the thermal variation of the length of the line since variations in temperature cause only a change in tension, not physical length. They are supported by 1/4-in. phenolic hangers at random intervals of about 35 m. After preamplification, the signals are lightly coupled to this transmission line by means of directional couplers [*Oliver,* 1954]. The attachment points for the couplers were determined through SWR measurements with the east end of the feed line short-circuited. Two measurements, made independently several months apart, agreed within 6 cm at each coupling point. The velocity factor of the line is 0.99932 $\pm$ 0.00003 with respect to free space. The spacing of the coupling points, l_{line}, was found to be 0.9999415 $\pm$ 0.000003 of the antenna separation, l. Consequently the increment of phase introduced between antennas by the transmission line is

$$\delta = 2\pi l_{line}/\lambda_{line} \qquad \begin{matrix} l_{line} = (0.9999415 \pm 0.000003)l \\ \lambda_{line} = (0.99932 \pm 0.00003)\lambda \end{matrix}$$

and thus equation 2 takes the form

$$\sin \theta + (1.00062 \pm 0.00003) = k\lambda/l \qquad k = \text{integer} \qquad (5)$$

The effect of the velocity factor of the transmission line is to shift the antenna pattern eastward by $(2.14' \pm 0.1') \cos \theta$ with respect to the pattern expected for a velocity factor of unity and a coupler spacing of exactly 220 m.

In order to find the frequency difference between fringes centered on the same angle, θ, we differentiate (5) and find that for $\Delta k = 1$

$$\Delta f = c/l(\sin \theta + 1.00062) \qquad (6)$$

The ratio $c/l = 1.362695$.

One property of the transmission line which is not understood is that the attenuation of the line is proportional to frequency, rather than $f^{1/2}$, in spite of the fact that dielectric losses are negligible [*King et al.,* 1965]. The degree of coupling at each antenna was adjusted so that each antenna delivers approximately equal power at the line amplifier (Figure 2) in spite of the attenuation on the line. This cannot be achieved exactly for all frequencies so the coupling was designed to achieve uniform illumination at 35 MHz. The illumination deviates from uniform by less than 25% at 20 or 60 MHz.

A serious problem in decametric observations at our site are very strong shortwave broadcast signals in the 19, 25, and 31 m bands. Intermodulation of these signals in the preamplifiers must be avoided. Accordingly, the preamplifiers were chosen for their high linearity, and they incorporate filters to attenuate signals outside the frequency range of 20 to 60 MHz. They have a measured noise temperature of 950 K. After preamplification, coupling losses, and line losses, each antenna delivers 450 to 500 K of

noise power at the west end of the transmission line. Thus, a total noise power at 7000 to 8000 K from all sixteen antennas is delivered to the amplifier at the end of the line. This amplifier also has a noise temperature of 950 K and thus contributes 13 to 14% to the total noise. The gain in this amplifier exceeds subsequent losses in the transmission to the observatory by 8 to 13 db, depending on the frequency. The signal level at this point is so high that no further degradation of the noise figure occurs.

We should note that any deviation from uniform aperture illumination does not affect the pointing of the antenna, but only the resolution and side-lobe level. If the phases have been accurately adjusted, then the aperture illumination of the array is purely real, except for the linear phase gradient which affects only the pointing of the beam. The voltage pattern, the Fourier transform of the aperture illumination, is therefore Hermitian and the power pattern is consequently symmetrical [*Bracewell,* 1965]. Any variation in the illumination, which might be caused by gain variations in the preamplifiers or changes in the coupling coefficients, will affect the beam in a symmetrical way and have no serious influence on determinations of source positions.

ELECTRONICS SYSTEM

Figure 3 is a schematic diagram of the receiving system. The galactic background temperature varies approximately as $f^{-2.5}$ across our operating band. In addition, transmission line attenuation increases with frequency. These effects result in a decrease of nearly 20 db in output noise level from 20 to 60 MHz. This is undesirable because it greatly reduces the dynamic range of solar signals which can be accommodated by the detectors and recording apparatus. Therefore, a slope filter is introduced which attenuates the low frequency portion of the band and results in an approximately uniform noise level. It also weakens the strong signals below 20 MHz which tend to cause intermodulation. The slope filter overcompensates slightly for the fact that the collecting area of the constant gain log-periodic elements varies as f^{-2}. Thus a source of constant flux will result in an output deflection which is slightly larger at 60 MHz than at 20 MHz.

One-MHz frequency calibration markers are injected into the system for a brief period every six min. The antenna is disconnected during the retrace of the sweep receiver in order to separate the sweeps clearly. This facilitates digital processing of the data.

In addition to the part of the system shown, a variety of other systems is available. For a two-year period ending September 1971, four additional spectrum analyzers swept each 10-MHz segment of the 20 to 60 MHz range four times per sec. These analyzers are now devoted to new arrays.

Signal path lengths through various elements of the array differ by as much as 6600 m and these differences depend upon the position of the source. The coherence bandwidth of the array is therefore narrow and dependent upon source position. In order to insure coherence at all positions, a receiver bandwidth of 10 kHz is employed. This does result in somewhat less than optimum sensitivity, but the narrow bandwidth has the advantage of discriminating against terrestrial interference. The effective integration time can be computed from the frequency sweep rate.

For the purpose of determining the total solar flux without the angular resolution of the array, one additional receiver records the signal received by a single element.

RECORDING AND DISPLAY OF SIGNAL

The output from the receiver is amplified, and the baseline adjusted as required. The signal is then recorded on an FM analog tape recorder which has a bandwidth of approximately 1-1/2 kHz at 1-7/8 in. sec^{-1} recording speed. The Fourier transform of such a frequency response is a function in the time domain having a width of approximately 0.4 msec. Since the receiver is sweeping at a rate of about 50 MHz sec^{-1}, this corresponds to an RF bandwidth of 20kHz. Only late in the afternoon when the coherence bandwidth is very narrow in frequency will there be a broadening of the fringes due to the bandwidth limitation of the tape recorder.

One channel of the tape records a 60-Hz reference signal from the observatory's frequency standard. It also contains timing information. This channel is used to synchronize a facsimile recorder (see Figure 3).

The facsimile recorder is a fathometer recorder adapted to this purpose because of its high resolution and wide dynamic range. The recording paper is 19 in. wide and the effective resolution is $\lesssim$0.001 in. Its dynamic range is about 12 db. The dynamic range of the receivers and the tape recorder is about 30 db. This dynamic range can only be utilized by digital processing of the tape-recorded data or by redisplaying the data on the facsimile recorder at

different levels. Figure 4 shows a solar radio event seen on the facsimile records. The pen of the recorder is drawn across the paper at the rate of once per sweep. The pen is driven by the recorded 60-Hz reference signal and synchronized to time marks on the data channel (see Figure 3). The signal modulates the intensity of the pen trace so that the intensity as a function of frequency is displayed by each trace. The paper moves continuously so that the time evolution of the spectrum is recorded.

CALIBRATION

Proper calibration of the array would require that coherent signals of known strength be injected at each of the elements. This would require an independent feed system. Instead, great care was taken to insure the gain and phase stability of the feed system and the electronics from the line amplifier onward are calibrated daily. An underground coaxial cable from the observatory couples signals to the center of the transmission line (Figure 2). Noise calibration signals are inserted on the transmission line at the beginning of each observing day, resulting in a series of gray shades on the facsimile record. These can be compared to the density of the fringes to provide a flux calibration to within 3 db for bursts on the linear portion of the facsimile record's density scale.

In order to establish the flux scale, the calibration noise source was compared to Cassiopeia A at three discrete frequencies using fixed frequency receivers. The fringes and calibrations were recorded on a chart recorder and compared. It was found that the calibration noise source provided a signal equivalent to about $3 \pm 1 \times 10^{-20}$ Wbm^{-2} Hz^{-1}. The flux densities of Cassiopeia A were taken from a spectum compiled by *Parker* [1968] and corrected for secular variation. By calibrating the calibration noise source in terms of antenna temperature, the collecting area is found. The collecting area as a function of frequency is given in Table 1. Pattern measurements of a single log-periodic element yielded an estimated collecting area of about one square wavelength.

It appears that the array performs as expected at the higher frequencies where the sixteen elements give a combined collecting area of about sixteen square wavelengths, but that the collecting area fails below the predicted area at lower frequencies. As the wavelength increases, the radiating region moves down the log-periodic antenna structure. The decrease in collecting area at longer wavelengths may be caused by a partially reflected wave from the ends of the antenna booms, or by radiation from the booms themselves.

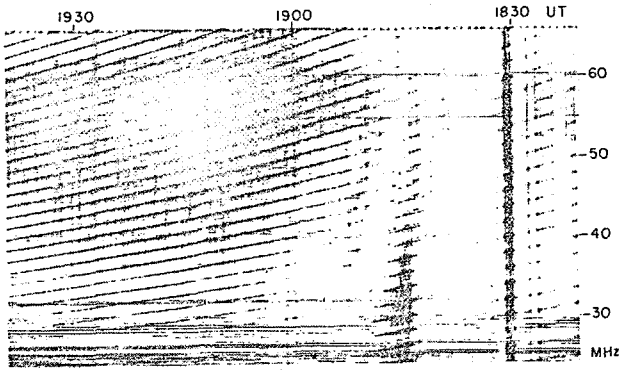

Fig. 4. A typical fascimile record.

DATA REDUCTION

In Figure 4 we show a record of solar activity in which the spectrum is modulated by a periodic pattern $E^2(\psi)$ of the grating array (see equation 1). Thus by measuring f at the maxima of the pattern, the position of the source, θ, can be known. Any uncertainty in the fringe order can usually be resolved. It is our concern, at this point, to see how f and t may be accurately determined.

Actual measurement of the facsimile record is done on an x, y coordinate digital converter. This has a table top surface on which a pointer can move along two orthogonal axes, x and y. The facsimile record is aligned as accurately as possible on this surface. The axis parallel to the flow of time is the x axis and the axis parallel to the frequency scale the y axis. We are concerned, then, with converting the coordinate (x, y) to the coordinate (t, f). If t is linear with x and f is linear with y, the calibration is easy and the conversion trivial.

It has been our experience that t is a very linear function of x. We find that we are generally able to calibrate the time scale on our charts to one sec (or 0.007 in.). There is a variety of effects which complicates the calibration of the frequency scale. The

TABLE 1. The collecting area as a function of frequency.

Frequency (MHz)	Collecting area (m^2)	(λ^2)
31	890 ± 80	9.5 ± 0.9
38	880 ± 440	14 ± 7
48	610 ± 110	15.5 ± 3

receiver is tuned over the frequency range, 20 to 60 MHz, in response to a sawtooth sweep voltage (see Figure 3). Although this sweep is highly linear, our criteria are extremely severe and the response of the receiver to the sweep voltage is not perfectly linear. Another effect which is important is phase jitter in the synchronization between the pen drive and the reference signal, which causes tiny displacements of the frequency scale. We must be able to establish the frequency of a fringe to about 15 kHz, which amounts to an accuracy of 0.005 in.

To the first order, the frequency of a point on the facsimile record is given by $f = a_1 + a_2 y$. The center frequency to which the receiver is tuned affects a_1. The sweep range of the receiver affects both a_1 and a_2. Drifts in the local oscillators, lateral motion of the paper during recording, and changes in the sawtooth voltage will result in changes in a_1 and a_2. Consequently, in calibrating the frequency scale of the facsimile records, allowance must be made for variations of a_1 and a_2 with time.

The frequency versus voltage response of the sweep circuit of the receiver is slightly nonlinear, so that

$$f = a_1 + a_2 y + \text{voltage-dependent correction term}$$

Since the frequency of the receiver has a one-to-one correspondence with the voltage applied to the sweep circuit, the correction term can also be expressed as a function of frequency. We have found that the calibration function can best be written as

$$f = a_1 + a_2 y + a_3 \cos [(f - a_4)/a_5] + a_6 \cos [(f - a_7)/a_8] + a_9 \cos [(f - a_{10})/a_{11}] \quad (7)$$

The coefficients a_3 to a_{11} are characteristic of the receiver and thus do not vary during the day. Since the correction terms are small, we can approximate the calibration function by

$$f \simeq a_1 + a_2 y + a_3 \cos [(a_1 + a_2 y - a_4)/a_5] + a_6 \cos [(a_1 + a_2 y - a_7)/a_8] + a_9 \cos [(a_1 + a_2 y - a_{10})/a_{11}] \quad (8)$$

The coefficients a_3 to a_{11} are determined once for the day under reduction. Coefficients a_1 and a_2 are determined periodically and interpolated as required.

Having established the frequency of a series of fringes at some instant of time we can deduce the position angle θ. The antenna pattern (see equation 6) has many lobes and so the position, θ, of radiation observed at some frequency, f, will always be ambiguous in the order of the lobe, n. There are, however, two possibilities for removing this ambiguity.

Since we are concerned mostly with radiation from sources whose position is known with sufficient accuracy (i.e., in the immediate vicinity of the sun), we can use this information to find the fringe order, k. We compute, for a measurement of frequency f,

$$k^* = (\sin \theta + 1.00062)f/1.362695 \quad (9)$$

where k^* is, in general, nonintegral. The fringe order is almost always the integer nearest to the value k^*. This is the approach we normally use. It is not possible to confuse radiation from the sun (or the source being observed) with radiation from a source elsewhere in the sky. Radiation associated with a given source will always have approximately the same value of θ, regardless of frequency. The fringe spacing in frequency (equation 6) can therefore be used to evaluate θ approximately as a check that the radiation is coming from the solar vicinity.

If we wish to localize the position of unknown radiation, we can use equation 6 to find the approximate value of θ. We would then use the procedure outlined in the above paragraph to find the fringe orders.

We compute $\theta - \theta_S$ in solar radii for each fringe, θ_S being the position of the center of the sun,

$$\sin \theta_S = \cos \delta_S \sin HA_S$$

The position angle of the fringes with respect to celestial north is also noted,

$$\cos (90^\circ - \phi_S) = \tan \theta_S \tan \delta_S$$

In order to improve the accuracy of position measurements, we generally measure three points on each fringe: the high frequency edge, the center, and the low frequency edge. The edges are defined as the points where the intensity gradient is steepest, and for fringes which are not so intense as to saturate the record, they might be expected to correspond to the half-power points. All three measured points are converted to positions (in solar radii) and plotted (see Figure 5). The center measurement is plotted as a one-digit number representing the nearest sec in time. The upper and lower edges are plotted as the symbol $\triangle$. The position of the source is then taken to be the mean of these three positions. Analysis of all the fringes at one time thus results in measurements of position as a function of frequency.

It should be noted that this method of finding the

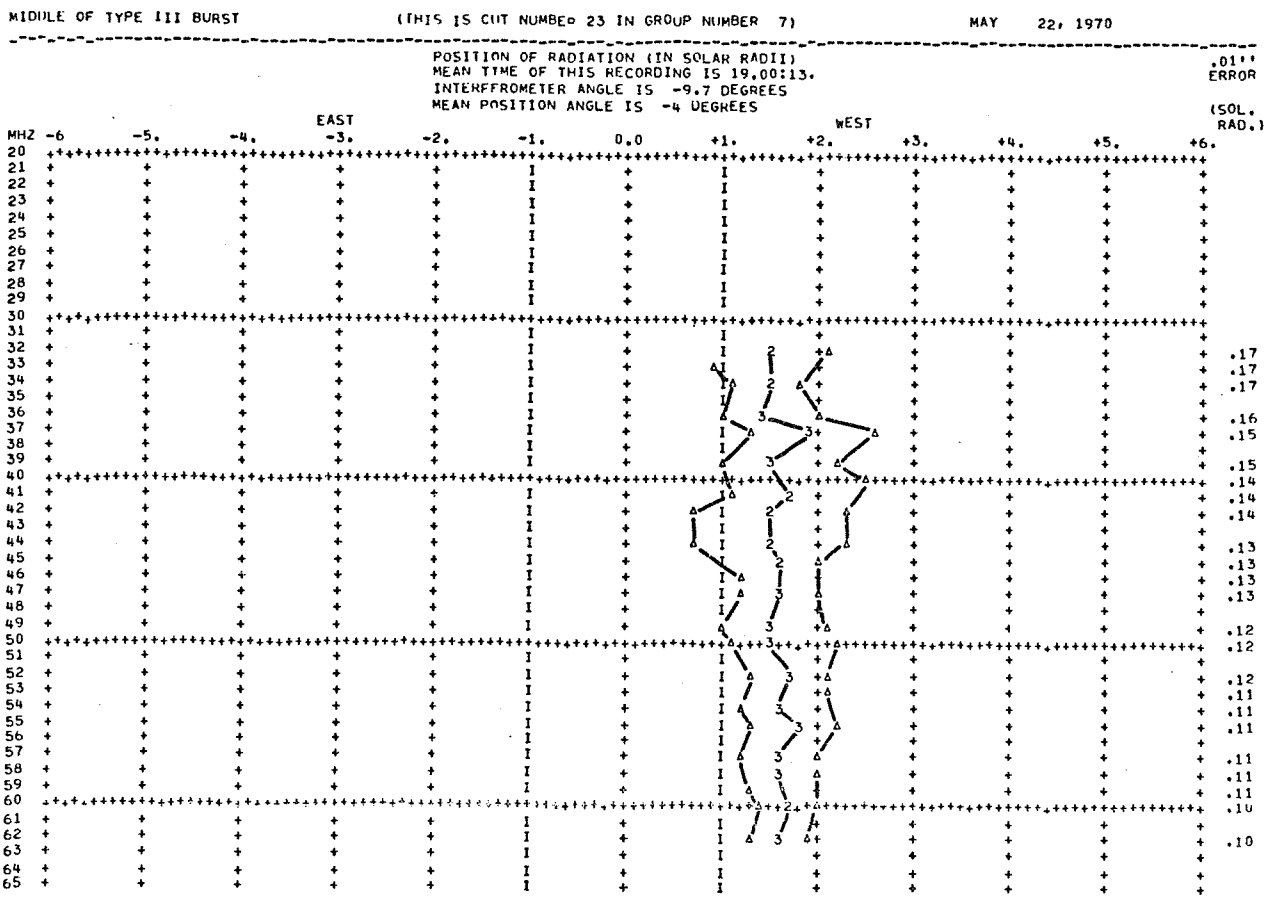

Fig. 5. Position of a type III burst as a function of frequency. Triangles give the positions corresponding to the high and low frequency edges of the fringes. The numbers give the positions corresponding to the peaks or centers of the fringes, the number representing the time to the nearest sec. On the right-hand side of the plot is given the uncertainty in position (in solar radii) if the measurement error on the *xy* coordinate converter is .01 in.

position of a source generally assumes that both the antenna beam and the source are symmetrical. Consider a fringe which is saturated on the record. (Because of the limited dynamic range of the facsimile record, this is often the case.) The sides of the fringes are taken to be those frequencies at which the density of the record appears to fall off most sharply. These frequencies will not represent, then, the half-power points but some lower, often significantly lower, power level. The person scanning the fringe will take the peak to be some frequency which is an average of the two side frequencies. When these frequencies are converted to positions and averaged together to yield the position of the fringe, we end up with a position which is defined by some power level near the base of the fringe. If the source or the beam is significantly asymmetrical the position defined by the peak-power or half-power points may be quite different.

RESULTS

A full-scale analysis of solar type III and IV events is under way, the results of which will be reported in later papers [e.g., *Kuiper,* 1973].

As a check on both the array and the data reduction program, observations were made of Cassiopeia A for about two hours around transit on November 10 and 11, 1970, and on March 16, 1972. The position lines of the source were measured at 45 MHz relative to an assumed right ascension of 23h 21m 10s and declination of +58°32′30″ (epoch 1950.0). Because of the rotation of the earth, the position angle of the antenna fringes projected on the source varied from about −20° to +30°. The

best intersection of the position lines was found to be

November 10 and 11, 1970:
23h 20m 58.7s ± 1.9s +58°37.0′ ± 0.8′

March 16, 1972:
23h 20m 41.4s ± 1.9s +58°24.3′ ± 0.8′

The effect of stellar aberration has been taken into account, but no correction for ionospheric refraction was made. Refractive effects cause most of the discrepancy between these positions.

The position of Cassiopeia A was measured simultaneously at frequencies from 25 to 50 MHz. Assuming that the centroid of the source's intensity distribution at these frequencies is the same, we can correct for ionospheric refraction by fitting each set of measurements at a given time to the function

$$\rho = A + Bf^{-2}$$

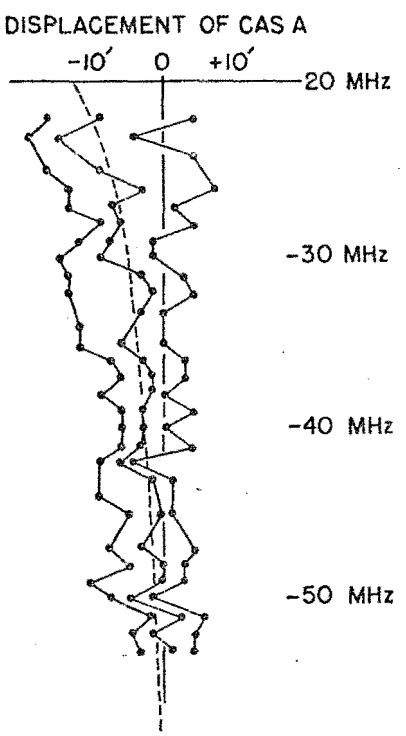

Fig. 6. Observed position as a function of frequency of Cassiopeia A. Measurements of the high frequency edge, middle, and low frequency edge (dots) are connected respectively with solid lines. The dashed line represents the function $\rho = (1.0' \pm 0.9') + (5.83' \pm 1.2') \times 10^3 \times f^{-2}$ where frequency is given in MHz. The refraction is thus determined to be 6.5′ at 30 MHz.

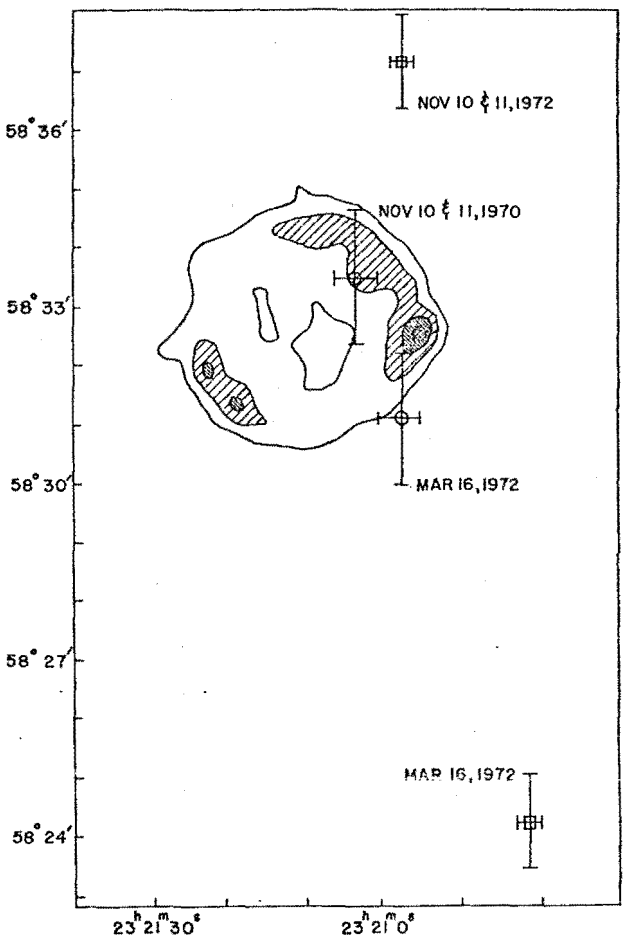

Fig. 7. The positions of Cassiopeia A at decametric wavelengths, uncorrected for refraction (□), and corrected for refraction (○), superimposed on a 1.4 GHz contour map based on the results of *Ryle et al.* [1965]. The contour interval is 15,000 K. Unless all parts of Cassiopeia A have identical spectra, the centroids of the brightness distributions need not necessarily coincide at centimeter and decameter wavelengths.

where A represents the position of the centroid in the absence of ionospheric refraction (Figure 6). We found that the uncertainty in determining A for any given set of measurements was comparable to the scatter in position at 45 MHz. Consequently, for the measurements at any given time, the position represented by the parameter A is not any more reliable than the measured position at 45 MHz. However, when we solve for the best intersection of all the position lines which have been corrected for refraction, we find that the data are much more consistent:

November 10 and 11, 1972:
23h 21m 3.7s ± 2.5s +58°33.5′ ± 1.1′

March 16, 1972:

23h 20m 57.5s ± 2.5s +58°31.1′ ± 1.1′

These positions, as well as the positions obtained when the effect of refraction is neglected, are plotted in Figure 7 on a contour map of Cassiopeia A based on the Cambridge observations at 1.4 GHz [*Ryle et al.*, 1965]. These results demonstrate the potential of simultaneous multifrequency observations to obtain accurate fundamental positions at decametric wavelengths. Our two position measurements agree to 0.8 arc min in right ascension, the direction in which the array has high angular resolution. Better agreement could not be expected because 0.8 arc min is approximately one-tenth of a beamwidth.

CONCLUSION

We have described an instrument which has been on solar patrol since March 1969. Dynamic spectra are recorded daily from 1600 to 2400 UT. From the fringe pattern on the dynamic spectra one can obtain the position of radio sources as a function of frequency in the range 20 to 65 MHz. The pointing of the array is known to an accuracy of 0.1 arc min. Positions can usually be measured to an accuracy of about 1 arc min.

It has been suggested that ionospheric refraction can be measured by simultaneous observations at two or more frequencies [*Lawrence et al.*, 1964], but that refractive effects might not behave in the expected way below 50 MHz. We have made observations of Cassiopeia A in the range 25 to 55 MHz and find that the inverse square dependence on frequency is followed in this frequency range. We have used this dependence to correct the observations and have found that we are able to determine the position of Cassiopeia A to within 1.0 arc min in right ascension. More sensitive arrays, such as the one now being built at Clark Lake, will be able to use this principle to obtain accurate fundamental positions of radio sources in the decametric wavelength range.

Acknowledgments. We wish to acknowledge the work of J. Fainberg and J. Hubbard who played major roles in the design and construction of this instrument. R. Stone has enthusiastically supported the work at Goddard Space Flight Center. Most of the daily operation is conducted by P. Dooley. We are especially grateful to T. Gergely for many helpful discussions and constant feedback on the behavior and misbehavior of the data reduction programs, and to N. Roth, who cheerfully repeated again and again the measurements of the Cas A calibration data, as the reduction procedure was being developed. Clark Lake Radio Observatory is supported by the National Science Foundation under grant NSF GP 19411, and the National Aeronautics and Space Administration under grant NGR 21-002-367.

REFERENCES

Begovich, N. A. (1966), Frequency scanning, in *Microwave Scanning Antennas*, vol. 3, edited by R. C. Hansen, pp. 35–215, Academic, New York.

Bracewell, R. (1965), *The Fourier Transform and its Applications*, p. 15, McGraw-Hill, New York.

Howard, H. T. (1965), An antenna array for radar astronomy studies in the 20 to 55 Mc range, *IEEE Trans. Antennas Propagat., AP-13*, 365.

King, R. W. P., H. R. Mimno, and A. H. Wing (1965), *Transmission Lines, Antennas, and Wave Guides*, p. 14, Dover, New York.

Kraus, J. D. (1966), *Radio Astronomy*, pp. 162–165, McGraw-Hill, New York.

Kuiper, T. B. H. (1973), On the density of the corona in regions of type III activity, in High Energy Phenomena on the Sun, Symposium Proceedings, edited by R. Ramaty and R. G. Stone, *NASA X-693-73-193*, pp. 540–551, Washington, D. C.

Kuiper, T. B. H., and J. Pasachoff (1973), Detailed correlation of type III radio bursts with *Hα* activity, 1, Active region of 22 May 1970, *Solar Phys., 28*, 187–196.

Kundu, M. R., W. C. Erickson, P. D. Jackson, and J. Fainberg (1970), Positions and motions of solar bursts at decameter wavelengths, *Solar Phys., 14*, 394–403.

Lawrence, R. S., C. G. Little, and H. J. A. Chivers (1964), A survey of ionospheric effects upon earth-space radio propagation, *Proc. IEEE, 52*, 4–27.

Oliver, B. M. (1954), Directional electromagnetic couples, *Proc. IRE, 42*, 1686–1692.

Parker, E. A. (1968), Precise measurements of the flux densities of the radio sources Cas A and Cyg A at metre wavelengths, *Mon. Notic. Roy. Astron. Soc., 138*, 407–422.

Ryle, M., B. Elsmore, and A. C. Neville (1965), High-resolution observations of the radio sources in Cygnus and Cassiopeia, *Nature, 205*, 1259–1262.

Sheridan, K. V. (1963), Techniques for the investigation of solar radio bursts at metre wavelengths, *Proc. IRE Aust., 24*, 174.

Reprinted from PROCEEDINGS OF THE IEEE
VOL. 61, NO. 9, SEPTEMBER, 1973
pp. 1276-1277

The Clark Lake Array

WILLIAM C. ERICKSON

Abstract—**A powerful new instrument for meter and dekameter wavelength radio astronomy is described. It will soon be available for both solar and sidereal studies.**

A FULLY STEERABLE array of 720 conical log spiral antennas is near completion at the University of Maryland's Clark Lake Radio Observatory in southern California. It is capable of operation at any frequency between 15 and 130 MHz with an instantaneous bandwidth of 3 MHz. The array is a pencil-beam instrument with a beamwidth proportional to the wavelength; it varies from 3′ to 27′ across the frequency range. Both the beam position and operating frequency will be computer controlled on a time scale of much less than 1 ms. The array will be used for solar studies and discrete radio source studies. For the radioheliograph application, 49 simultaneous beams will be formed.

The array is described in more detail elsewhere [1], [2]. The antennas are arranged in a T with an east–west arm of 480 elements, 3000 m in length, and a north–south arm of 240 elements, 1800 m in length. The elements are fixed in a vertical direction with a primary frequency-independent beamwidth of 100°. This limits the sky coverage of the instrument to zenith distances of approximately 50°. Each element is a teepee-shaped structure of 8 wires and is 7.8 m tall. (For this reason the array has been called the TPT.) Fig. 1 is a photo of the east–west arm of the instrument. This arm is now complete and in operation.

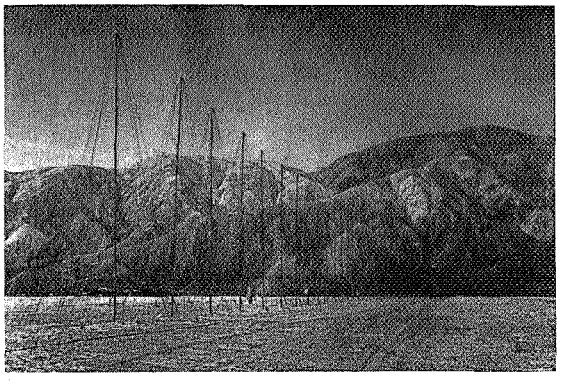

Fig. 1. This is a photograph of the east–west arm of the instrument. It consists of 480 log spiral elements.

Beam positioning is accomplished entirely by adjustment of the relative phases between the elements. No physical motion is involved. The primary phasing scheme employs electrical rotation of the left circularly polarized elements. Since a properly designed log spiral antenna maintains circular polarization well off axis, this scheme can be used at zenith distances of 50° or greater. The excitation of each multifilar spiral antenna is rotated by means of a diode switch installed

Manuscript received February 2, 1973. This work was supported by the National Science Foundation under Grant GP 19401 and by the National Aeronautics and Space Administration under Grant NGR 21-002-367.

The author is with the Astronomy Program at the University of Maryland, College Park, Md. 20742.

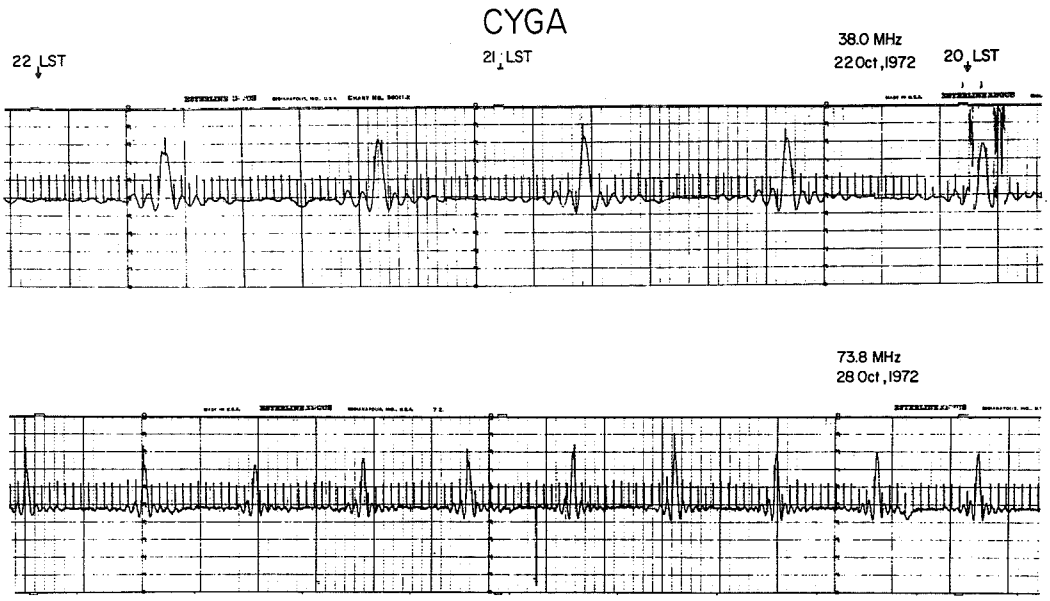

Fig. 2. Drift scans of Cyg A at two frequencies. To make these recordings, a 32-element grating array consisting of each fifteenth element was used. This grating array was correlated with an element at the center of the array to form a sin $32x/32$ sin x pattern for testing purposes. The spikes which occur on the record each minute are noise calibrations.

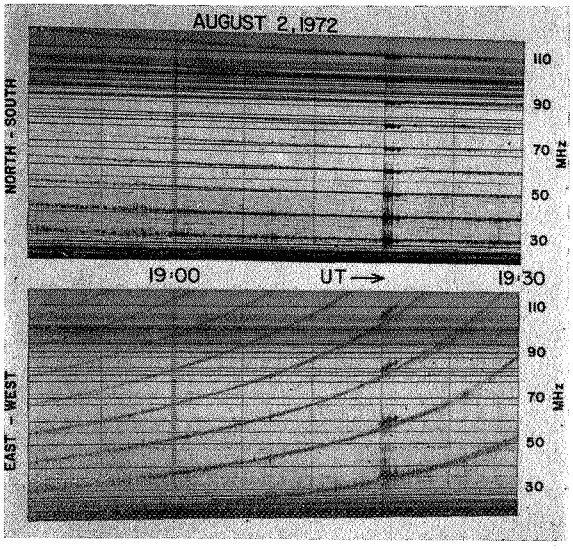

Fig. 3. Radio spectrograms of solar continuum obtained shortly before the great flares of August 1972. These recordings were taken with swept frequency receivers attached to the output of north–south and east–west grating arrays consisting of each fifteenth element. The receivers sweep the 20–120-MHz spectrum twice per second; as they sweep, lobes of the grating array's response cross the sun. Determination of time and frequency gives the position of the source. The rather steady sloping bands of continuum originate 9′ east and 3′ south of the sun's center. The Type III bursts at 1918–1920 UT are 10′ west and 20′ south of the sun's center. A second continuum region develops in the 80–120-MHz range between 1918 and 1927 UT. Interference below 30 MHz and FM transmissions in the 88–108-MHz band are plainly visible.

at its apex. The arms of the T are operated in banks which consist of 15 elements each. Each bank of elements is phased identically by means of 60 control wires which run down the length of the arms. The signal from each bank of elements is preamplified and brought back to the observatory on a separate coaxial feed line. At the observatory the signals from the banks are delayed and combined to form the pencil beams.

Fig. 2 illustrates some sample drift scans obtained with the east–west arm of the instrument. Since the east–west arm can track a source across the sky, it is being used in a supersynthesis mode to synthesize a pencil-beam response on high declination sources. Fig. 3 illustrates sample fan beam scans of the sun obtained with completed portions of the east–west and north–south arrays.

When completed, the instrument will be used during the day as a multifrequency radioheliograph and at night for radio source studies. "Pictures" of the sun will be obtained at several discrete frequencies every second. Swept frequency fan beam records in the east–west and north–south directions will be simultaneously obtained at intermediate frequencies. These will allow interpolation between the frequencies at which solar "pictures" are obtained.

The sensitivity limit and the resolution limit of the instrument are approximately equal at about 1 flux unit at all frequencies [2]. The instrument can be employed for radio source survey work, detailed studies of radio source spectra, and various other spectral studies. It can also be applied to pulsars, planets, or other dynamic sources. Because of its rapid beam positioning it can be used in a time-share mode between various observers or between calibrators and unknown sources on a 1-s time scale. Obviously, the data-acquisition capability of the instrument far exceeds the analysis capability of our small group. We will invite guest investigators to make use of the instrument.

References

[1] W. C. Erickson and J. R. Fisher, "A new wideband, fully steerable, dekametric array at Clark Lake," submitted to *Radio Sci.*, 1973.
[2] J. R. Fisher, "Design tests of the fully steerable, wideband, dekametric array at Clark Lake," Ph.D. dissertation, Univ. of Maryland, College Park, Md., 1972.

Astronomy Program
University of Maryland

Research in Radio Astronomy

at Meter and Decameter Wavelengths

1969-1973

W. C. Erickson and

M. R. Kundu

I. Research in Solar Radio Astronomy

A. Publications

1. "Positions and Motions of Solar Bursts at Decameter Wavelengths," M. R. Kundu, W. C. Erickson, P. D. Jackson and J. Fainberg, Solar Physics, 14, 394, 1970.

2. "Radio Astronomical Studies with 1500-meter Diameter Low-Frequency Telescope," NASA CR-1506, January 1970, M. R. Kundu.

3. "Solar Bursts at Decameter and Hectometer Wavelengths," Physics of the Solar Corona, (ed. C. Macris; D. Reidel Publishing Company), p. 287, 1971, M. R. Kundu.

4. "Meter and Decameter Wavelength Position of Solar Bursts of July 31-August 7, 1972," M. R. Kundu and W. C. Erickson, IAU Symp. No. 57 "Coronal Disturbances," Sept. 8-11, 1973.

5. "Decameter Type IV Bursts Associated with Coronal Transients," T. E. Gergely and M. R. Kundu, Solar Phys. (in press).

6. "Meter and Decameter Wavelength Positions of Solar Bursts of July 31-August 7, 1972," M. R. Kundu and W. C. Erickson, Solar Phys. (in press).

7. "Type III Burst Positions," T.B.H. Kuiper, Ph.D. Thesis, University of Maryland, 1973.

8. "Decameter Storm and Type IV Radiation," T. E. Gergely, Ph.D. Thesis, University of Maryland, 1974.

9. "Decameter Storm Radiation, I," T. E. Gergely and W. C. Erickson, Solar Phys. (submitted).

10. "Decameter Storm Radiation, II," T. E. Gergely and M. R. Kundu, Solar Phys. (submitted).

11. "Observations of Coronal Disturbances from 1 to 9 $R_{\odot}$ II - Second Event of January 11, 1973," R. T. Stewart, R. Howard, S. F. Hansen, T. E. Gergely and M. R. Kundu, Solar Phys. (in press).

12. "Detailed Correlation of Type III Radio Bursts with Hα Activity, I: Active Region of May 22, 1970," T.B.H. Kuiper, Solar Phys., 28, 187, 1973.

13. "On the Density of the Corona in Regions of Type III Activity," T.B.H. Kuiper, Proc. of NASA Symp. on "High Energy Phenomena on the Sun," p. 540, 1973.

14. "Detailed Comparison of Type III Radio Bursts with Hα Activity, II: The Isolated Type III Activity of March and April, 1971," T.B.H. Kuiper, Solar Phys., 33, 461, 1973.

15. "On the Probability of Occurrence of the Type IIIb Burst as a Precursor" J. de la Noe, Solar Phys. (submitted).

16. "The Decameter Activity of July and August 1970," J. de la Noe and T. E. Gergely, 1974 (in preparation).

17. "Study of a Radio Type II Burst," J. de la Noe, Y. Leblanc, R. T. and S. Hansen, 1974 (in preparation).

18. "The Type II Event of May 17, 1973, J. de la Noe, M. R. Kundu and W. C. Erickson, 1974 (in preparation).

19. "Coronal Density Structures in Regions of Type III Activity," S. F. Hansen, T.B.H. Kuiper and Y. Leblanc (in preparation).

B. Papers Presented at Meetings

1. AAS MEETINGS

"Decameter Type IV Bursts Associated with Coronal Transients," 142nd Meeting, Lincoln, Nebraska, March 26-29, 1974, T. E. Gergely and M. R. Kundu.

2. THE SOLAR TERRESTRIAL PHYSICS SYMPOSIUM IN LENINGRAD, MAY 1970

"Positions and Motions of Solar Bursts at Decameter Wavelengths," M. R. Kundu, W. C. Erickson, P. D. Jackson and J. E. Fainberg.

AT THE IAU GENERAL ASSEMBLY, BRIGHTON, AUGUST 1970

"Moving Type III Bursts," M. R. Kundu.

3. INVITED PAPER

At the NATO Summer School in Greece, Sept. 9-15, 1970, "Solar Bursts at Decameter and Hectometer Wavelengths," M. R. Kundu.

4. THE IAU SYMP. NO 57 "CORONAL DISTURBANCES," SURFERS PARADISE, Sept, 7-11, 1973

"Meter and Decameter Wavelength Positions of Solar Bursts of July 31-August 7, 1972," M. R. Kundu and W. C. Erickson.

5. URSI MEETINGS

"Ionospheric Refraction Corrections to Decametric Observations of Solar Type III Bursts," T.B.H. Kuiper, URSI-Spring Meeting, 1972.

6. NASA SYMPOSIUM ON HIGH ENERGY PHENOMENA ON THE SUN, GODDARD SPACE FLIGHT CENTER, Sept. 28-30, 1972

"On the Density of the Corona in Regions of Type III Activity," T.B.H. Kuiper.

II. Research in Cosmic Radio Astronomy

A. Publications

1. "A 26.3 MHz Radio Source Survey with an Absolute Flux Scale," M. R. Viner, Ph.D. Thesis, University of Maryland, 1973.

2. "VLB Interferometer Observations of Tau A and Other Sources at 121.6 MHz," W. C. Erickson, T.B.H. Kuiper, T. A. Clark, S. H. Knowles and J. J. Broderick, Astrophys. J., 177, 101, 1972.

3. "VLBI Observations of the Crab Nebula Pulsar," N. R. Vandenberg, T. A. Clark, W. C. Erickson, G. M. Resch, J. J. Broderick, R. R. Payne, S. H. Knowles and A. B. Youmans, Astrophys. J., 180, L27, 1973.

4. "Long Wavelength VLBI," T. A. Clark and W. C. Erickson, Proc. IEEE, 61, 1230, 1973.

5. "A 26.3 MHz Radio Source Survey, I - The Absolute Flux Scale," M. R. Viner (in preparation).

6. "A 26.3 MHz Radio Source Survey, II - Source Fluxes and Positions," M. R. Viner and W. C. Erickson (in preparation).

7. "High Resolution Observations of Cassiopeia A at Meter Wavelengths," L. K. Hutton, T. A. Clark, G. M. Resch, N. R. Vandenberg, W. C. Erickson, and S. H. Knowles (to be submitted to the Astronomical Journal).

8. "VLBI Observations of the Crab Nebula Pulsar ," N. R. Vandenberg, Ph.D. Thesis, University of Maryland (expected completion - July, 1974).

9. "Meter Wavelength Observations of Compact Radio Sources," G. M. Resch, Ph.D. Thesis, Florida State University (expected completion - August, 1974).

B. Papers Presented at Meetings

1. AAS MEETINGS

"Precise Absolute Flux Density Measurements at 26.3 MHz," M. R. Viner, BAAS, 3, 239, 1971.

"Observations of the Crab Nebula Pulsar," N. R. Vandenberg, W. C. Erickson, G. M. Resch, T. A. Clark and J. J. Broderick, BAAS, 4, 320, 1972.

2. INVITED PAPERS

"High Angular Resolution Studies of Radio Sources Employing Very Long Baseline Interferometry at Meter Wavelengths," W. C. Erickson, URSI Combined Session, April 13, 1972.

3. URSI MEETINGS

"Meter Wavelength Spectral Observations of Compact Radio Sources by VLBI," G. M. Resch, W. C. Erickson, T. A. Clark and S. H. Knowles, URSI-Spring Meeting, 1972.

"Pulsar VLBI," N. R. Vandenberg, J. J. Broderick and S. H. Knowles, URSI-Spring Meeting, 1972.

4. SYMPOSIUM ON INTERSTELLAR SCATTERING OF RADIO WAVES, JET PROPULSION LABORATORY, PASADENA, CALIFORNIA, FEBRUARY 1, 1974

"Apparent Angular Size Limits for Five Pulsars," N. R. Vandenberg.

5. SYMPOSIUM ON VLBI, CALIFORNIA INSTITUTE OF TECHNOLOGY, PASADENA, CALIFORNIA, FEBRUARY 4-6, 1974

"Meter Wavelength Spectral Observations of Compact Radio Sources," G. M. Resch.

"Meter Wavelength Observations of Pulsars," N. R. Vandenberg.

"VLBI Observations of Casseopeia A at Meter Wavelengths," L. K. Hutton.

III. Research in Radio Astronomical Instrumentation

A. Publications

1. "Design Tests of the Fully Steerable, Wideband, Decametric Array at the Clark Lake Radio Observatory," J. R. Fisher, Ph.D. Thesis, University of Maryland, 1972.

2. "The Log Periodic Array at the Clark Lake Radio Observatory," W. C. Erickson and T.B.H. Kuiper, Radio Science, 8, 845, 1973.

3. "The Clark Lake Array," W. C. Erickson, Proc. IEEE, 61, 1276, 1973.

4. "A New Wideband, Fully Steerable, Decametric Array at Clark Lake," W. C. Erickson and J. R. Fisher, 9, 387, 1974.

5. "Sidelobe and Cross-Polarization Response Suppression by Error Averaging," W. C. Erickson (submitted to IEEE Trans. Ant. and Prop.) 1974.

B. Papers Presented at Meetings

1. AAS MEETINGS

"The New Fully Steerable Decametric Array at Clark Lake," W. C. Erickson and J. R. Fisher, BAAS, 3, 243, 1971.

2. URSI MEETINGS

"Estimating the Confusion Limit of a Radio Telescope with High Sidelobe Levels," J. R. Fisher, URSI-Spring Meeting, 1972.

"A New Fully Steerable Array for Radio Astronomy," W. C. Erickson and J. R. Fisher, URSI-Spring Meeting, 1972.

"Performance Tests of the Elements Used in the New Clark Lake Array," J. R. Fisher and W. C. Erickson, URSI-Spring Meeting, 1972.

C. Unpublished Reports

"The 10 to 110 MHz Correlation Receiver," J. R. Fisher, University of Maryland Technical Report, 1972.

"The Confusion Limits of Radio Telescopes with High Sidelobe Levels," J. R. Fisher, University of Maryland Technical Report, 1972.

"The Clark Lake Radio Observatory - Observer's Handbook," W. C. Erickson, University of Maryland Technical Report, 1974.

IV. Federal Grants Held

A. "A Design Study of a Multi-Frequency Radioheliograph"
Principle Investigators: Dr. M. R. Kundu and Dr. W. C. Erickson
NASA NAS 5 11353 (12/1/70 - 3/31/71)

$ 20,000

B. "Multi-Frequency Mapping of the Sun"
Principle Investigators: Dr. M. R. Kundu and Dr. W. C. Erickson
NASA NGR 21-002-367 (10/1/72 - 9/30/74)

$202,000

C. "Cooperative Research in Radio Astronomy
Principle Investigators: Dr. W. C. Erickson and Dr. M. R. Kundu
NASA NGL 21-002-029 (3/1/69 - 2/28/74)

$221,000

D. "Operation of the Clark Lake Radio Observatory
Principle Investigators: Dr. W. C. Erickson and Dr. M. R. Kundu
NSF GP 19401 (3/15/70 - 11/30/74)

$424,400